IOP Publishing Semiconductor Science and Technology
Semicond. Sci. Technol. 32 (2017) 093002 (52pp) https://doi.org/10.1088/1361-6641/aa7ade

Topical Review

Atomic layer deposition: an enabling technology for the growth of functional nanoscale semiconductors

Necmi Biyikli[1] **and Ali Haider**[2,3]

[1] University of Connecticut, Department of Electrical and Computer Engineering, 371 Fairfield Way; U-4157 Storrs, Connecticut 06269-4157, United States of America
[2] National Nanotechnology Research Center (UNAM), Bilkent University, Bilkent, Ankara 06800, Turkey
[3] Institute of Materials Science and Nanotechnology, Bilkent University, Bilkent, Ankara 06800, Turkey

E-mail: necmi.biyikli@uconn.edu

Received 7 January 2016, revised 15 June 2017
Accepted for publication 21 June 2017
Published 14 August 2017

Abstract

In this paper, we present the progress in the growth of nanoscale semiconductors grown via atomic layer deposition (ALD). After the adoption by semiconductor chip industry, ALD became a widespread tool to grow functional films and conformal ultra-thin coatings for various applications. Based on self-limiting and ligand-exchange-based surface reactions, ALD enabled the low-temperature growth of nanoscale dielectric, metal, and semiconductor materials. Being able to deposit wafer-scale uniform semiconductor films at relatively low-temperatures, with sub-monolayer thickness control and ultimate conformality, makes ALD attractive for semiconductor device applications. Towards this end, precursors and low-temperature growth recipes are developed to deposit crystalline thin films for compound and elemental semiconductors. Conventional thermal ALD as well as plasma-assisted and radical-enhanced techniques have been exploited to achieve device-compatible film quality. Metal-oxides, III-nitrides, sulfides, and selenides are among the most popular semiconductor material families studied via ALD technology. Besides thin films, ALD can grow nanostructured semiconductors as well using either template-assisted growth methods or bottom-up controlled nucleation mechanisms. Among the demonstrated semiconductor nanostructures are nanoparticles, nano/quantum-dots, nanowires, nanotubes, nanofibers, nanopillars, hollow and core–shell versions of the afore-mentioned nanostructures, and 2D materials including transition metal dichalcogenides and graphene. ALD-grown nanoscale semiconductor materials find applications in a vast amount of applications including functional coatings, catalysis and photocatalysis, renewable energy conversion and storage, chemical sensing, opto-electronics, and flexible electronics. In this review, we give an overview of the current state-of-the-art in ALD-based nanoscale semiconductor research including the already demonstrated and future applications.

Keywords: atomic layer deposition, semiconductor, nanoscale, nanostructured, metal-oxide, III-nitride, self-limiting

(Some figures may appear in colour only in the online journal)

1. Introduction

Information age, digital revolution, age of computers… No matter how we name it, the latest technology revolution which still continues and deeply impacts our daily life was triggered by a key enabling device technology, i.e., the transistor. Germanium (Ge) was the semiconductor used throughout the early development phase, which later was replaced by another group-IV elemental semiconductor, silicon (Si), mainly due to its superior native oxide. Si-based integrated circuit (IC) technology (CMOS) began its journey in 1959 with only a single transistor/chip and 30 μm linewidth. Nearly 60 years of continuous and successful miniaturization effort led to more than three orders of magnitude shrinkage of the transistor gate lengths and about ten orders of magnitude increase in transistor density. Atomic layer deposition (ALD) played a crucial role in keeping the pace of Moore's law, particularly for the sub-65 nm technology nodes by providing novel materials and processing solutions including but not limited to ALD-grown high-k gate dielectrics and spacer-defined double patterning.

ALD is a chemical vapor deposition (CVD) technique where conventional gas-phase reactions are eliminated either by temporally or spatially separated half-cycles. Instead, within the ALD growth window, film deposition proceeds via self-saturating ligand-exchange surface reactions only. The unique surface-chemistry driven self-limiting growth character of ALD enables precision atomic-scale thickness control, ultimate three-dimensional conformality, and large-area uniformity, all being highly critical features for current and future atomic-scale precision device engineering and nanomanufacturing needs.

Originally developed and named as atomic layer epitaxy and molecular layering, initial efforts focused on sulfide and oxide semiconductor thin-film synthesis for electro-luminescent displays, sensors, catalytic materials, and thin-film solar cells. Early history details of ALD research can be found in the recently completed 'Virtual Project on the History of ALD' work and publications pioneered by Puurunen *et al* [1, 2]. Since then, both materials and applications list of ALD has been enriched tremendously: oxide, metal, nitride, sulfide, selenide, carbide, fluoride, polymer, and biomaterial growth recipes have been developed for applications including moisture barriers for light emitting devices/displays, surface passivation of solar cells, diffusion barriers for Li-ion batteries, anti-tarnishing jewelry coatings, anti-corrosion coatings of electronic circuit-boards/LEDs/sensors, gate insulators and nano-patterning of CMOS transistors, flexible/wearable electronics, surface functionalization for implants, nano-catalysts for remediation, hydrogen generation, solid-oxide fuel-cells, and self-cleaning surfaces.

When compared with ALD-grown semiconductors, dielectric and metallic ALD-materials constitute the majority of ALD literature, mainly due to the intense research efforts in high-k dielectrics, passivation/protection coatings, and relatively easy forming metallic nanocatalysts. Semiconductors, on the other hand, suffer mainly from low-temperature self-limiting growth windows, resulting in poly-crystalline or amorphous-like films with high levels of impurities which are incompatible with high-performance devices. In this respect, ALD-grown semiconductors can hardly compete with the material quality of mainstream epitaxial films grown via high-temperature metal-organic chemical vapor deposition (MOCVD) or molecular beam epitaxy (MBE). Instead, ALD-grown semiconductors might find significant use in precision coating of low-temperature compatible and highly porous/high surface-area substrates/templates, as well as in fabricating highly controlled functional nanostructures. Already demonstrated device applications of such low-temperature grown nanoscale semiconductors include solar cells, catalysis, energy storage, photocatalysis, flexible electronics, and chemical gas sensors.

Although excellent review articles on general ALD overview [3–8], specific ALD methods [9–11], nano-materials [12–15], and application areas [16–19] exist in the literature, an effort focusing on ALD-grown nanoscale semiconductors and their applications is yet missing. The aim of this review is to present the status and summary of the ALD semiconductor research activity by covering critical findings and contributions in the field. First, thin-film semiconductor growth reports are reviewed, followed by the efforts for the ALD synthesis of 0D, 1D, 2D, and core–shell nanostructured semiconductors. Finally, reported device applications are summarized along with a future perspective on ALD semiconductor research outlining the important challenges and opportunities.

2. Semiconductor thin-film synthesis via ALD

Among the semiconductor thin films grown via ALD, oxides, nitrides, and sulfides constitute the vast majority of reported literature. In addition to these three compound semiconductor material families, ALD of selenides, tellurides, and arsenides have been studied as well to a lesser extent. Low-temperature ALD efforts of group-IV elemental semiconductors, Si and Ge, are rather scarce with very limited studies available. An overview of the literature on semiconductor thin films grown via ALD is summarized in table 1.

2.1. Oxides

ALD of ZnO has been studied quite extensively [12, 20–26]. While H_2O has been the predominant choice for oxygen precursor, the first Zn precursor used for ALD of ZnO was zinc acetate, however it required high substrate temperatures (lowest reported is 280 °C) [27]. The most common Zn precursor used for ZnO ALD growth is diethylzinc (DEZn), which significantly lowered the growth temperatures (typically 100 °C–200 °C) due to its high reactivity and exothermic reaction for the formation of ZnO [21–24, 26, 28–68]. Dimethylzinc is another precursor used for ZnO growth which produces slightly higher ZnO growth per cycle (GPC) values when compared with diethylzinc [69]. Besides these common precursors, elemental zinc and $ZnCl_2$ have also been used as Zn source for ZnO ALD, they however required

Table 1. Overview of the growth conditions employed to deposit semiconductor thin films using ALD. The materials deposited, precursors used, the temperature during ALD, substrate, and type of ALD are mentioned.

Material	Reactant A	Reactant B	Growth temperature	Substrate	Type of ALD	References
ZnO	Diethyl zinc ($(C_2H_5)_2Zn$)	H_2O	106 °C–165 °C	Glass	Thermal	[204]
	$(C_2H_5)_2Zn$	H_2O, O_3	170 °C–300 °C	SiO_2/Si	Thermal, ozone assisted	[67]
	$(C_2H_5)_2Zn$	H_2O	90 °C–200 °C	Glass and Si (100)	Thermal	[57]
	Zinc acetate	H_2O	280 °C–400 °C	Sapphire and lime glass	Thermal	[24]
	$Zn(CH_3)_2$ and $(C_2H_5)_2Zn$	H_2O	90 °C–270 °C	Glass	Thermal	[68]
	$(C_2H_5)_2Zn$	H_2O	150 °C–400 °C	SiO_2/Si and Si	Thermal	[28]
	$(C_2H_5)_2Zn$	H_2O	180 °C	Sapphire	Thermal	[205]
	$(C_2H_5)_2Zn$	H_2O	180 °C	Sapphire	Thermal	[206]
	$(C_2H_5)_2Zn$	H_2O and O_2	200 °C	Glass and Si (100)	Plasma assisted	[66]
	$Zn(CH_3)_2$,	H_2O	250 °C–300 °C	Si	Thermal	[207]
	$(C_2H_5)_2Zn$	H_2O_2	200 °C, 300 °C	Si (100) and SiO_2	Thermal	[208]
	$(C_2H_5)_2Zn$	H_2O	160 °C	Borosilicate glass	Thermal	[209]
	$(C_2H_5)_2Zn$	H_2O	150 °C–300 °C	GaN/sapphire	Thermal	[210]
	$(C_2H_5)_2Zn$	H_2O	115 °C–235 °C	Sapphire	Thermal	[211]
	$(C_2H_5)_2Zn$	H_2O	250 °C	M plane Sapphire	Thermal	[212]
	$(C_2H_5)_2Zn$	NH_4OH, H_2O	100 °C	Si (100)	Thermal	[213]
	$(C_2H_5)_2Zn$	H_2O	280 °C–325 °C	GaN/sapphire	Thermal	[214]
	$(C_2H_5)_2Zn$	H_2O	280 °C	GaN/sapphire	Thermal	[215]
	$(C_2H_5)_2Zn$	H_2O	200 °C	GaAs (100)	Thermal	[216]
	$(C_2H_5)_2Zn$	H_2O	180 °C and 240 °C	Si (100) and Si (111)	Thermal	[217]
	$(C_2H_5)_2Zn$	H_2O	70 °C–130 °C	Sapphire (001)	Thermal	[218]
	$(C_2H_5)_2Zn$	H_2O	150 °C	Glass	Thermal	[219]
	$(C_2H_5)_2Zn$	H_2O	100 °C–300 °C	Glass	Thermal	[220]
	$(C_2H_5)_2Zn$	H_2O	180 °C	Sapphire (0001)	Thermal	[221]
	$(C_2H_5)_2Zn$	H_2O	200 °C	Si (100)	Thermal	[222]
	$(C_2H_5)_2Zn$	H_2O	140 °C–220 °C	Si (100), borosilicate glass, and sapphire	Thermal	[223]
	$(C_2H_5)_2Zn$	H_2O	200 °C	SiO_2/Si and glass	Thermal	[224, 225]
	$(C_2H_5)_2Zn$	H_2O	120 °C–300 °C	Soda glass and Si (100)	Thermal	[226]
	$(C_2H_5)_2Zn$	O_3	250 °C	SiO_2/Si and Si (100)	Ozone assisted	[25]
	$(C_2H_5)_2Zn$	H_2O	110 °C, 250 °C	Polymer template and Si	Thermal	[227]
TiO_2	Titanium ethoxide ($Ti_4(OCH_2CH_3)_{16}$)	H_2O	110 °C–350 °C	Si (100) and fused silica	Thermal	[99]
	Titanium isopropoxide ($Ti\{OCH(CH_3)_2\}_4$)	H_2O, H_2O_2	100 °C–300 °C	Si (100) and fused silica	Thermal	[88]
	$TiCl_4$	H_2O	100 °C–400 °C	Si (100) and amorphous silica	Thermal	[89]
	TiI_4	H_2O	135 °C–375 °C	Si (100) and amorphous silica	Thermal	[90]
	Titanium tetramethoxide	H_2O	200 °C–400 °C	Glass	Thermal	[91]
	Titanium isopropoxide ($Ti\{OCH(CH_3)_2\}_4$)	O_2	50 °C–300 °C	Si, glass, Pt, and RuO_2	Plasma enhanced	[101]
	Tetrakis dimethyl-amidotitanium and Titanium isopropoxide	H_2O	50 °C–325 °C	Si (100)	Thermal	[100]
	Tetrakis dimethyl-amidotitanium	H_2O	150 °C	Si (100)	Thermal	[228]
	$TiCl_4$	H_2O	350 °C	Soda lime glass	Thermal	[103]
	$Cp^*Ti(OMe)_3$	Ozone	235 °C–350 °C	Si (100)	Ozone assisted	[92]
	$TiCl_4$	H_2O	80 °C–120 °C	Si and polycarbonate	Thermal	[97]
	$TiCl_4$	O_2	25 °C–200 °C	Si	Plasma enhanced	[94]
	$TiCl_4$	H_2O	100 °C	Si (100) and SiO_2	Thermal	[95]
	$TiCl_4$	Ammonium hydroxide water solution	350 °C	Soda lime glass	Thermal	[96]
	Titanium isopropoxide ($Ti\{OCH(CH_3)_2\}_4$)	H_2O	225 °C–250 °C	Strontium titanate/Si(001)	Thermal	[98]
	Tetrakis dimethyl-amidotitanium	H_2O	200 °C	Si, cooper	Thermal	[229]
	$TiCl_4$	O_3	225 °C–450 °C	RuO_2	Ozone assisted	[230]
	$TiCl_4$	O_3	225 °C–600 °C	Si (100)	Ozone assisted	[231]
	Titanium isopropoxide ($Ti\{OCH(CH_3)_2\}_4$)	O_2	50 °C–350 °C	Si (100)	Plasma assisted	[232]
	Titanium isopropoxide ($Ti\{OCH(CH_3)_2\}_4$)	Acetic acid and O_3	200 °C	Si (100)	Ozone assisted	[87]
	Titanium isopropoxide ($Ti\{OCH(CH_3)_2\}_4$)	O_2	Room temperature	Si and glass	Plasma assisted	[233]
	Star-Ti	O_2	150 °C–400 °C	Si (100)	Plasma assisted	[234]

Table 1. (Continued.)

Material	Reactant A	Reactant B	Growth temperature	Substrate	Type of ALD	References
	$TiCl_4$	O_2, H_2O	30 °C–180 °C	Si (111)	Plasma assisted	[235]
	Tetrakis dimethyl-amidotitanium	H_2O	200 °C–250 °C	Si	Thermal	[104]
	Tetrakis dimethyl-amidotitanium	O_3	75 °C–400 °C	Si	Ozone assisted	[236]
	Titanium tetraisopropoxide	O_2	70 °C–100 °C	Si (100) and fused silica	Plasma assisted	[237]
	$TiCl_4$	H_2O	150 °C–400 °C	Fluorine doped tin oxide glass (FTO) and Si (100)	Thermal	[238]
	Tris(dimethylamido)-(dimethylamino-2- propanolato)titanium(IV) (TDMADT).	O_2	60 °C	Polyethylene-terephthalate (PET) and Si	Plasma assisted	[239]
Ga_2O_3	Ga(acac), (acac = pentane-2,4-dionate)	H_2O, O_3	350 °C–400 °C	Si (100), soda lime glass, and corning glass	Thermal	[105]
	$Ga_2(NMe_2)_6$	H_2O	150 °C–300 °C	Si (100)	Thermal	[106]
	$[(CH_3)_2GaNH_2]_3$	O_2	200 °C	Si (100) and sapphire (001)	Plasma assisted	[240]
	$[(CH_3)_2GaNH_2]_3$	O_2	200 °C	Si (100)	Plasma assisted	[241]
	$[(CH_3)_2GaNH_2]_3$	O_2	50 °C, 150 °C, 250 °C	Si (100)	Plasma assisted	[242]
	$Ga(CH_3)_3$	O_3	200 °C–450 °C	Si (100) and SiO_2	Ozone assisted	[243]
	$Ga_2(NMe_2)_6$	H_2O	—	TiO_2	Thermal	[244]
	Gallium tri-isopropoxide	H_2O	150 °C–250 °C	Si, glass, and carbon	Thermal	[107]
	$Ga(CH_3)_3$	O_2	100 °C–400 °C	Si (111)	Plasma assisted	[108]
	$Ga(CH_3)_3$	O_3	150 °C–400 °C	Si (100)	Ozone assisted	[245]
	Tris (2,2,6,6-tetramethyl-3,5-heptanedionato) gallium(III)	O_2	100 °C–400 °C	SiO_2/Si	Plasma assisted	[246]
	$Ga(CH_3)_3$	O_2	250 °C	Si (111)	Plasma assisted	[247]
	$Ga(CH_3)_3$	O_2	50 °C–150 °C	Si (100)	Plasma assisted	[109]
	$Ga(CH_3)_3$	H_2O	550 °C	Sapphire, GaN, and (111)- and (001)-oriented 3C–SiC	Thermal	[248]
	$Ga(CH_3)_3$	O_2	250 °C	SiC	Plasma assisted	[249]
In_2O_3	$InCl_3$	H_2O	500 °C	Corning glass	Thermal	[250]
	Cyclopentadienyl indium	O_3	200 °C–450 °C	Si (100) and glass	Ozone assisted	[111]
	In (acac)$_3$ (acac = acetylacetonate, pentane-2,4-dione)	H_2O, O_3	160 °C–300 °C	Si (100), fused silica, and soda lime glass	Ozone assisted and thermal	[112]
	Cyclopentadienyl indium	H_2O, O_2	100 °C–250 °C	Si (100), fused silica, and quartz	Thermal	[114]
	$In(CH_3)_3$	H_2O	150 °C–325 °C	Si and SiO_2/Si	Thermal	[113]
	$[In[(iPr)_2CNR_2]_3]$ where R = Et (1) and Me (2), namely tris-(N,N′-diisopropyl-2-diethylamido-guanidinato)-indium(III)(1) and tris-(N,N′-diisopropyl-2-dimethylamido- guanidinato)-indium(III)	H_2O	160 °C–320 °C	Si (100), Al_2O_3 (0001), and glass	Thermal	[251]
	$Et_2InN(SiMe_3)_2$	H_2O	225 °C–250 °C	SiO_2/Si	Thermal	[115]
	Cyclopentadienyl indium	H_2O, O_2	100 °C	SiO_2/Si	Thermal	[252]
	Cyclopentadienyl indium	H_2O, O_2	100 °C	SiO_2/Si	Thermal	[253]
	[3-(dimethylamino)propyl] dimethyl indium	H_2O	275 °C	Si	Thermal	[254]
	Dimethylamino- dimethylindium	H_2O	300 °C	Si (100)	Thermal	[255]
	Dimethyl(N-ethoxy- 2,2-dimethylpropanamido)indium	O_2	70 °C–250 °C	Si and glass	Plasma assisted	[256]
	$In(CH_3)_3$	O_3, O_2, H_2O, H_2O_2	100 °C–250 °C	Si(100), fused quartz, and glass	Thermal, ozone assisted	[257]
	[1,1,1-trimethyl-N-(trimethylsilyl)silanaminato]- indium (InCA-1)	H_2O_2	150 °C	Polyimide	Thermal	[116]
NiO	$Ni(dmamp)_2$ (dmamp = 1-dimethylamino-2-methyl-2-propanolate)	H_2O	80 °C–240 °C	Si (001)	Thermal	[258]
	$Ni(Cp)_2$ (Cp = cyclopentadienyl, C_5H_5) or $Ni(EtCp)_2$ [EtCp = ethylcyclopentadienyl, $(C_2H_5)(C_5H_4)$]	O_3	150 °C–300 °C	Si (100)	Ozone assisted	[259]
	Bis(2,2,6,6-tetramethyl- 3,5-heptanedionato)Ni(II)	H_2O	205 °C–275 °C	MgO (100) and Al_2O_3 (00 l)	Thermal	[260]
	bis(2,2,6,6-tetramethylheptane-3,5- dionato)nickel(II) ($Ni(thd)_2$)	H_2O	205 °C–290 °C	SiO_2	Thermal	[261]
	$Ni(Cp)_2$	O_3	230 °C	Si (100)	Ozone assisted	[262]
	Bis- methylcyclopentadienyl-nickel ($[MeCp]_2Ni$)	O_2	150 °C–350 °C	Pt, Ru, and W	Plasma assisted	[263]
	Nickel amidinate	H_2O	175 °C	Fluorine-doped tin oxide-coated glass substrates (FTO)	Thermal	[264]
	Nickel bis(N,N′- di-tert-butylacetamidinate) $[Ni(tBu\text{-}MeAMD)_2]$	H_2O	200 °C	Si	Thermal	[265]
	$Ni(Cp)_2$	O_3	275 °C	FTO	Ozone assisted	[266]

Table 1. (Continued.)

Material	Reactant A	Reactant B	Growth temperature	Substrate	Type of ALD	References
Bi_2O_3	$Bi(thd)_3$ (thd: 2,2,6,6-tetramethyl-3,5- heptanedionato)	H_2O	200 °C–350 °C	Si	Thermal	[267]
SnO_2	SnI_4	O_2	400 °C–750 °C	SiO_2/Si (100)	Thermal	[118]
	$SnCl_4$	H_2O	400 °C–500 °C	Pyrex glass and sapphire	Thermal	[119]
	Dibutyl tin diacetate	O_2	200 °C–400 °C	Si (100)	Plasma enhanced	[126]
	Dibutyl tin diacetate	O_2	300 °C	(100), (110), and (111) yttria-stabilized zirconia (YSZ) substrates	Plasma enhanced	[125]
GaN	$GaCl_3$	NH_3	550 °C	(001) GaAs	Thermal	[268]
	$Ga(CH_3)_3$	NH_3	550 °C	(0001) Sapphire	Thermal	[127]
	$Ga(CH_3)_3$	NH_3	500 °C–650 °C	(001) GaAs	Thermal	[128]
	$GaCl_3$	NH_3	400 °C–750 °C	Si (100)	Thermal	[129]
	$Ga(CH_3)_3$	NH_3	100 °C–500 °C	Si	Plasma enhanced	[130]
	$Ga(C_2H_5)_3$	N_2/H_2	200 °C, 450 °C	Si (100) and quartz	Plasma enhanced	[133, 269]
	$Ga(CH_3)_3$, $Ga(C_2H_5)_3$	N_2/H_2	200 °C	Si (100) and quartz	Plasma enhanced	[69, 132, 133, 139–269]
	$Ga(C_2H_5)_3$	N_2/H_2	200 °C	Si (100), Si (111), and *c*-plane sapphire	Plasma enhanced	[138]
	$Ga(C_2H_5)_3$	N_2/H_2	200 °C	Si (100)	Plasma enhanced	[136]
	$Ga(CH_3)_3$ and H radicals	NH_3	100 °C and room temperature	Si (111)	Electron enhanced	[139]
	$Ga(CH_3)_3$	N_2/H_2 and NH_3	200 °C	Si (100), Si (111), and *c*-plane sapphire substrates	Plasma enhanced	[131]
	$Ga(C_2H_5)_3$	N_2/H_2 plasma	150 °C–425 °C	*C*-plane sapphire substrates	Plasma enhanced	[270]
	$Ga(C_2H_5)_3$	N_2/H_2 plasma	275 °C	*C*-plane sapphire	Plasma enhanced	[137]
	$Ga(C_2H_5)_3$	NH_3	200 °C–500 °C	Si (100)	Plasma enhanced	[271]
InN	$In(CH_3)_3$	N_2 plasma	150 °C–350 °C	Si (100) and quartz	Plasma enhanced	[157]
	$In(CH_3)_3$	N_2 plasma	160 °C–260 °C	*a*-plane sapphire, Si(111), and GaN/sapphire	Plasma enhanced	[158]
	$In(CH_3)_3$	N_2 plasma	200 °C–260 °C	Si (100), Si (111), and sapphire (0001)	Plasma enhanced	[272]
	C_5H_5In and $In(CH_3)_3$	N_2/H_2 plasma or N_2 plasma	200 °C	Si (100), Si (111), and AlN/Si (100)	Plasma enhanced	[154]
BN	BCl_3	NH_3	630 °C	SiO_2/Si (100)	Thermal	[273]
	BBr_3	NH_3	400 °C and 750 °C	SiO_2	Thermal	[159]
	BCl_3	NH_3	227 °C	ZrO_2 particles	Thermal	[160]
	$(C_2H_5)_3B$	NH_3	500 °C–900 °C	sapphire and Si (001)	Thermal	[274]
	$(C_2H_5)_3B$	N_2/H_2 plasma	250 °C–450 °C	Si (100)and quartz	Plasma enhanced	[162]
	BBr_3	NH_3	250 °C–750 °C	SiO_2	Laser assisted and thermal	[161]
	BBr_3	NH_3	327 °C	Ru (0001)	Thermal	[164]
	BCl_3	NH_3	327 °C	Co (0001)	Thermal	[163]
AlN	$AlCl_3$	NH_3/H_2	350 °C	Si (100)	Plasma enhanced	[146]
	$Al(CH_3)_3$	NH_3	325 °C–470 °C	Glass	Thermal	[147]
	$Al(CH_3)_3$	NH_3	240 °C–370 °C	Si (100)	UV-assisted	[148]
	$Al(CH_3)_3$	N_2/H_2	350 °C	Si (111)	Thermal and plasma enhanced	[144]
	$Al(CH_3)_3$	N_2/H_2	250 °C	Si (100), Si (111), and sapphire	Plasma enhanced	[152]
	$Al(CH_3)_3$	N_2/H_2	210 °C and 250 °C	Si (100), Si (111), and sapphire (001)	Plasma enhanced	[153]
	$Al(CH_3)_3$	N_2/H_2	150 °C–300 °C	Si (100) and SiO_2	Plasma enhanced	[275]
	$Al(CH_3)_3$	N_2	500 °C	$Pt/HfO_2/Si(100)$	Plasma enhanced	[276]

Table 1. (Continued.)

Material	Reactant A	Reactant B	Growth temperature	Substrate	Type of ALD	References
	$Al(CH_3)_3$	NH_3	100 °C–500 °C	Si (100), Si (111), *c*-plane sapphire, MOCVD-grown GaN on *c*-plane sapphire, and glass (Pyrex)	Thermal and plasma enhanced	[141]
	$Al(CH_3)_3$	N_2/H_2	200 °C	Si (100)	Plasma enhanced	[150]
	$AlCl_3$ or $Al(CH_3)_3$	NH_3	80 °C–260 °C	Si (111)	Plasma enhanced	[143]
	$Al(CH_3)_3$	N_2/H_2 or N_2 or NH_3	200 °C	Si (100), Si (111), and *c*-plane Sapphire	Plasma enhanced	[149]
	$Al(CH_3)_3$	N_2/H_2 or N_2 or NH_3	200 °C	Si (111)	Plasma enhanced	[140]
	$Al(CH_3)_3$	NH_3	280 °C	Ti/Si (100), Si (100), and glass	Plasma enhanced	[151]
	$Al(CH_3)_3$	NH_3	200 °C	Polytetrafluoroethylene (PTFE)/SiO_2	Plasma enhanced	[277]
	$Al(CH_3)_3$	N_2/H_2	250 °C	Si (111)	Plasma enhanced	[142]
	$Al(CH_3)_3$	N_2/H_2	200 °C	Si (100)	Plasma enhanced	[145]
ZnS	$(C_2H_5)_2Zn$	H_2S	200 °C–350 °C	Glass	Thermal	[173]
	$(C_2H_5)_2Zn$	H_2S	250 °C–400 °C	Al_2O_3	Thermal	[172]
	$(C_2H_5)_2Zn$	H_2S	60 °C–400 °C	Si (100)	Thermal	[171]
	$(C_2H_5)_2Zn$	H_2S	25 °C–160 °C	Au (111)	Thermal	[168]
	$(C_2H_5)_2Zn$	H_2S	100 °C–300 °C	Si (100)	Thermal	[169]
	Bis(2,2,6,6-tetramethyl-3,5-heptanedionato)zinc ($Zn(TMHD)_2$)	H_2S	150 °C–375 °C	Quartz glass	Thermal	[175]
	$(C_2H_5)_2Zn$	H_2S	100 °C	Soda lime glass and Si	Thermal	[167]
	Zn	S	100 °C–350 °C	Si (100), Si (110), and Si (111)	Thermal	[278]
	ZnI_2 or $ZnCl_2$	H2S	300 °C–490 °C	$Al_2O_3/In_xSn_yO_z/Al_xTi_yO_z$ covered soda lime glass	Thermal	[166]
	$Zn(CH_3)_2$ or $(C_2H_5)_2Zn$	H_2S	100 °C–200 °C	Si (100)	Thermal	[69]
	$(C_2H_5)_2Zn$	H_2S/Ar	60 °C–300 °C	SiO_2/Si(100)	Plasma enhanced	[246]
CdS	$Cd(CH_3)_2$	H_2S	Room temperature	ZnSe (100)	Thermal	[177]
	Cd	S	340 °C	(100)GaAs	Thermal	[176]
	$Cd(CH_3)_2$	H_2S	100 °C–400 °C	Si (100) and glass	Thermal	[178]
Cu_xS	Cu(thd)2 (thd = 2,2,6,6-tetramethyl-3,5-heptanedione)	H_2S	125 °C–250 °C	Soda lime glass and Si(100)	Thermal	[184]
	$Cu(thd)_2$	H_2S	160 °C–260 °C	Corning 7059 glass, SnO_2:F, and TiO_2 films on SnO_2:F glass.	Thermal	[183]
	Bis(N,N-di-sec-butylacetamidinato)dicopper(I) $Cu_2(DBA)_2$,	H_2S	130 °C	Si (100) and fused silica	Thermal	[182]
	$Cu_2(DBA)_2$,	H_2S	80 °C or 135 °C	Fused quartz and silicon substrates	Thermal	[181]
	$Cu(thd)_2$	H_2S	200 °C	Quartz glass	Thermal	[180]
	$Cu(acac)_2$ (acac = acetylacetonate = 2,4- pentanedionate)	H_2S	130 °C–220 °C	Borosilicate glass and Si	Thermal	[179]
PbS	$Pb(tmhd)_2$	H_2S	140 °C–220 °C	Si (100)	Thermal	[186]
	$Pb(tmhd)_2$	H_2S	160 °C	Si (100)	Thermal	[185]
	$Pb(tmhd)_2$	H_2S	160 °C	Si/SiO_2 substrates	Thermal	[187]
SnS	Tin(II) 2,4-pentanedionate ($Sn(acac)_2$)	H_2S	175 °C	Si and Al_2O_3	Thermal	[188]
	Bis(N,N′-diisopropylacetamidinato)tin(II) [$Sn(MeC(N\text{-}iPr)_2)_2$], $Sn(amd)_2$	H_2S	100 °C–200 °C	SiO_2 and Au	Thermal	[189]
	$Sn(amd)_2$	H_2S	200 °C	a-SiO_2	Thermal	[279]
	Tetrakis(dimethylamino)tin (TDMASn, $[(CH_3)_2N]_4Sn$)	H_2S	60 °C–180 °C	SiO_2, Si, and glass	Thermal	[190]
In_2S_3	Indium acetylacetonate	H_2S	150 °C–160 °C	Si	Thermal	[192]
	In(III) N,N′ Diisopropylacetamidinate [In-$(amd)_3$]	H_2S	140 °C–240 °C	Si (100)	Thermal	[191]
GaS_x	Hexakis(dimethylamido)digallium	H_2S	125 °C–225 °C	Si, Fused silica	Thermal	[193]
ZnSe	Zn	Se	430 °C	GaAs and lime glass	Thermal	[195]
	Zn	Se	430 °C	Quartz, glass, and GaAs	Thermal	[196]
	$ZnCl_2$	$(R_3Si)_2Se$	400 °C	SiO_2 and glass	Thermal	[194]
CdSe	Cd	Se	150 °C–350 °C	Si	Thermal	[197]
PbSe	Lead(II)bis(2,2,6,6-tetramethyl-3,5-heptanedionato) ($Pb(C_{11}H_{19}O_2)_2$)	Bis-(triethyl silyl) selane ($(Et_3Si)_2Se$)	150 °C–250 °C	Si (100)	Thermal	[280]
Cu_2Se, CuSe	CuCl, Cu(II) pivalate	$(R_3Si)_2Se$	165 °C and 400 °C	SiO_2 and glass	Thermal	[194]
In_2Se_3	$InCl_3$	$(R_3Si)_2Se$	295 °C	SiO_2 and glass	Thermal	[194]

Table 1. (Continued.)

Material	Reactant A	Reactant B	Growth temperature	Substrate	Type of ALD	References
ZnTe	Zn	Te	250 °C	GaAs (100)	Thermal	[281]
	$ZnCl_2$	$(Et_3Si)_2Te$	400 °C	SiO_2 and glass	Thermal	[194]
Bi_2Te_3	$BiCl_3$	$(Et_3Si)_2Te$	165 °C	SiO_2 and glass	Thermal	[194]
	$BiCl_3$	$(Et_3Si)_2Te$	160 °C–300 °C	SiO_2/Si and soda lime glass	Thermal	[282]
GaAs	$GaCl_3$	$(Et_3Si)_3As$	125 °C–250 °C	SiO_2/Si and soda lime glass substrate	Thermal	[198]
Si	Si_2H_6	$SiCl_4$	355 °C–385 °C	SiO_2	Thermal	[202]
Ge	$GeCl_4$	1,4-bis(trimethylsilyl)-1,4-dihydropyrazine	150 °C–300 °C	Pt	Thermal	[203]
	$GeCl_2$	Atomic hydrogen	300 °C, 420 °C	Si (100)	Thermal Epitaxy	[199]
	$GeCl_4$	Atomic hydrogen	300 °C	Si (100)	Thermal	[200]

significantly higher growth temperatures and resulted in relatively low GPC values [70]. The ALD window for a typical ZnO ALD process using DEZn and H_2O as precursors can nonetheless be estimated to be around 110 °C–170 °C. However, there are variations in ALD growth window even when using the same precursors in different reports [21–24, 26–70]. Although a rather 'forgiving' technique, it is quite possible that reactor design also affects the resulting ALD temperature window. Generally, as-grown ALD ZnO films showed intrinsic n-type conductivity which was originating from the presence of defects and impurities in the ZnO crystal. Elevated deposition temperature increased the conductivity of the films, however at high growth temperatures where CVD-growth regime takes over, film resistivity starts to increase again [21–24, 26–70]. Instead of H_2O, when O_2 plasma was used as oxygen source, ZnO films became more stoichiometric as O_2 plasma can oxidize Zn more effectively, confirming that plasma-enhanced ALD (PEALD) can be used to control the stoichiometry of ZnO films [12]. Reduction in oxygen vacancies and interstitial Zn decreases the intrinsic n-type carrier concentration of ZnO, yielding in films with higher resistivity. The growth of epitaxial ZnO films by atomic layer epitaxy is reported on *c*-plane sapphire substrate and GaN [71–85]. Despite the considerable lattice mismatch between sapphire and ZnO (∼18%), still no buffer layer was necessary to obtain epitaxial ZnO films. The lattice mismatch between ZnO and GaN is lower which makes deposition of epitaxial high quality ZnO on GaN possible as well [86].

ALD of TiO_2 has been reported using several different compounds of Ti as precursors [87–101]. $TiCl_4$ is the most commonly used precursor which allows deposition of high quality TiO_2 material (refractive index as high as 2.6) at substrate temperatures ranging from 27 °C to 600 °C [89, 99, 102]. However, $TiCl_4$ is corrosive and chlorine contamination has been observed in the films grown below 100 °C [102]. Titanium alkoxides (titanium isopropoxide and titanium ethoxide) have been utilized as alternative Ti precursors for ALD of TiO_2 [88, 99, 100, 102, 103]. TiO_2 grown using titanium ethoxide showed low GPCs (0.3–0.4 Å) at substrate temperatures below 300 °C. Lower GPC obtained using titanium ethoxide might be due to larger molecular size compared with $TiCl_4$. However, other reasons such as incomplete ligand exchange reactions and low number of activated absorption sites might also implicate low GPCs with titanium ethoxide [99]. Moreover, alkoxides start to self-decompose around 300 °C, losing the self-limiting deposition characteristic of ALD and entering CVD growth regime [92]. Among the organometallic Ti precursors, cyclopentadienyl group based precursors have the advantage of higher thermal stability. ALD of TiO_2 has been reported using $Cp^*Ti(OMe)_3$ and ozone reactants where ALD growth window was achieved at growth temperatures higher than 300 °C [92]. A comparative study of TiO_2 nucleation on SiO_2 and hydrogen terminated Si showed that higher GPC can be achieved mainly due to the presence of hydroxyl groups on SiO_2 surface which serve as reactive sites [95]. Tetrakis-(dimethylamido) titanium (TDMAT) and oxygen reactants were also used to grow TiO_2 and the deposited film showed p-type conductivity [104]. It was hypothesized that p-type conductivity of TiO_2 is a result of native excess of oxygen interstitials in the grown film.

There have been a fair amount of efforts to grow Ga_2O_3 via ALD, a wide bandgap oxide material attracting recent interest for potential power device applications. In the very first report, Ga_2O_3 was grown using gallium(III) acetylacetonate ($Ga(acac)_3$) and H_2O/O_3 reactants and growth was achieved at deposition temperatures higher than 370 °C [105]. The amine based ($Ga_2(NMe_2)_6$) precursors and isopropoxide precursors have also been utilized to grow Ga_2O_3 where ALD growth window was relatively narrow [106, 107]. Ga_2O_3 has been grown using $Ga(CH_3)_3$ in combination with H_2O, O_2 plasma, and ozone [108, 109]. A wide temperature window (100 °C–400 °C) was observed for Ga_2O_3 grown using $Ga(CH_3)_3$ and oxygen plasma with a GPC of ∼0.53 Å.

In_2O_3 growth has been performed initially using $InCl_3$ and H_2O [110]. $InCl_3$ chemistry required relatively high growth temperatures in the range of 300 °C–500 °C and yielded a GPC of 0.25–0.40 Å. It has also been reported that $InCl_3$ can etch the deposited In_2O_3 which is a limitation especially in case of coating nanoporous/3D surfaces where long precursor exposures are required [110, 111]. Nanocrystalline cubic phase In_2O_3 was grown using cyclopentadienyl indium and ozone reactants where growth temperatures were reported in the range of 200 °C–450 °C with GPCs of 1.3–2.0 Å [111]. It was reported that In_2O_3 films grown using ozone as oxygen precursor have film resistivity values higher than $10^{-2}\,\Omega\,cm$ due to the removal of native donors such as oxygen vacancies (Vo^{2+}) and In interstitials (In_i^{3+}) [111, 112]. In another study, $In(CH_3)_3$ and H_2O reactants were used to perform ALD of In_2O_3 in the temperature range between 200 °C and 250 °C, resulting in film resistivity values as low as $2.8 \times 10^{-3}\,\Omega\,cm$ along with significantly Hall mobility values reaching $84\,cm^2\,V^{-1}\,s^{-1}$ [113]. Yet in another interesting study, cyclopentadienyl indium and combinations of both molecular oxygen and water as co-reactants were used to grow In_2O_3 [114]. Relatively low GPC values were obtained in the temperature range of 100 °C–250 °C when oxygen or water were used individually as oxygen source. Measurements revealed that H_2O performs the function of releasing ligands from the surface while oxygen acts as an oxidizing agent and therefore a synergy between water and oxygen resulted in increased GPC (1.0−1.6 Å) values [114]. $Et_2InN(SiMe_3)_2$ precursor in combination with H_2O was used to perform ALD of In_2O_3 at substrate temperatures of 225 °C−250 °C where very low film resistivity (2.3×10^{-4}–$5.16 \times 10^{-5}\,\Omega\,cm$) values were obtained which was mainly attributed to the oxygen deficient InO_x phases [115]. More recently, In_2O_3 films were grown using [1,1,1-trimethyl-N-(trimethylsilyl)silanaminato]-indium (InCA-1) and hydrogen peroxide precursors; as grown films showed high conductivity ($\sim 10^{-4}\,\Omega\,cm$) however, it was shown that N_2O plasma treatment can be applied on films to control the conductivity of materials leading to oxidation of InO_x, where oxygen vacancies act as shallow electron donors at a relatively low temperature of 150 °C [116].

Another significant oxide semiconductor is SnO_2, particularly utilized in chemical/gas sensors. Thermal ALD of

SnO_2 thin films was performed using tin halide and H_2O/O_2 precursors combination which resulted in polycrystalline SnO_2 films with (100) and (120) orientations [117–124]. Epitaxial SnO_2 films were reported using PEALD in which dibutyl tin diacetate and O_2 plasma combination was utilized [125, 126].

2.2. Nitrides

GaN growth via thermal ALD was initially reported using organometallic precursors—either $Ga(CH_3)_3$ or $Ga(C_2H_5)_3$—and NH_3 as Group-III and Group-V reactants respectively, at relatively high growth temperatures ranging from 450 °C up to 900 °C [127, 128]. Thermal ALD of GaN films was also demonstrated using $GaCl_3$ and NH_3 within a temperature range of 500 °C–750 °C. Better thermal stability of $GaCl_3$ yielded a relatively wide ALD temperature window, while in addition to oxygen, Cl impurities were detected as well [129]. In order to decrease the substrate temperature substantially, PEALD of GaN was first demonstrated using $Ga(CH_3)_3$ and NH_3 plasma, resulting in a self-limiting growth character within 185 °C–385 °C, which produced amorphous films with high oxygen content [130]. In an effort to decrease the oxygen contamination, hollow-cathode plasma-assisted ALD (HCPEALD) of GaN was demonstrated using $Ga(CH_3)_3$ and N_2/H_2 or NH_3 plasma reactants at substrate temperatures as low as 200 °C. Deposited films on Si (100) were polycrystalline with hexagonal (002) preferred orientation, however, the same preferred orientation was not observed on *c*-plane sapphire substrates [131]. Use of HCPEALD was found to be quite effective in decreasing the oxygen impurity within GaN films by more than two orders of magnitude [131–136]. Motamedi *et al* reported PEALD of GaN with $Ga(C_2H_5)_3$ and forming gas mixture (95% N_2/5% H_2) plasma reactants at 275 °C. Transmission electron microscopy (TEM) images revealed that the GaN films were epitaxial at the sapphire substrate interface vicinity (5 nm), transforming to polycrystalline structure for higher thickness values [137]. Interestingly, electrical conductivity measurements showed that deposited GaN films were p-type with a resistivity of 0.033 Ω cm, 1.68×10^{18} cm^3 carrier concentration, and a quite striking hole mobility of 110 $cm^2\ V^{-1}s^{-1}$ [137]. Si(111) might be a better substrate for HCPEALD of GaN using $Ga(C_2H_5)_3$ and N_2/H_2 plasma reactants as better crystalline quality and higher film density were obtained from GaN grown on Si(111) as compared to films grown on Si(100) and sapphire, which is attributed to the lower lattice mismatch and hexagonal nature of Si(111) substrate surface [138]. Another study showed that $Ga(CH_3)_3$ might be a better gallium source in comparison with $Ga(C_2H_5)_3$ for HCPEALD of GaN at low substrate temperatures, yielding GaN films with higher crystalline quality and larger grain sizes [132]. Recently, electron-enhanced ALD of GaN is reported at 100 °C and room temperature using $Ga(CH_3)_3$, hydrogen (H) radicals, and NH_3 as reactants [139]. The deposited films at 100 °C were polycrystalline with hexagonal wurtzite crystal structure. No oxygen contamination was reported while very significant 10 −35 at% carbon contamination was found inside GaN, leading to nanocrystalline and amorphous films. The growth mechanism for such a low temperature GaN growth is believed to result from the electron stimulated desorption (ESD) of hydrogen which produces dangling bonds facilitating Ga−N bond formation [139].

Within the III-nitride semiconductor family, ALD of AlN has been most extensively studied [140–145]. PEALD of AlN has been studied using $AlCl_3$ and NH_3/H_2 plasma reactants which produced AlN wurtzite (100) microcrystallites in an amorphous matrix [146]. Thermal [147] and UV assisted ALD [148] of AlN has been reported in a temperature range of 320 °C–470 °C and 240 °C–370 °C, respectively. However, in these studies self-limiting behavior was not observed as surface reactions between $Al(CH_3)_3$ and NH_3 takes places with sufficient rates only at those temperatures where $Al(CH_3)_3$ decomposition takes place. Generally, PEALD of AlN has been investigated extensively due to superior reactivity of plasma reactants which decreases the growth temperature significantly. In thermal ALD of AlN, NH_3 has been the most common nitrogen source whereas in plasma-assisted ALD of AlN, either NH_3 or N_2/H_2 plasma have been employed as nitrogen source [144]. ALD of AlN with self-limiting growth behavior has been demonstrated using a combination of $Al(CH_3)_3$ and N_2/H_2 plasma reactants by several research groups [141–144, 149–151]. Grown films were polycrystalline with wurtzite structure. Optical analysis was carried out and an optical band edge of 5.8–6.04 eV has been reported [141–145, 149–152]. Refractive index values of the films were reported in the range of 1.94–2.05 [141–145, 149–152]. A comparison of thermal and plasma-enhanced ALD of AlN has been reported, where it has been shown that incubation period only occurred for thermal ALD, while growth initiated without any nucleation delay with PEALD, which is attributed to higher nuclei density due to plasma [144]. PEALD grown AlN films also showed higher refractive index below 30 nm which saturated as film thickness was increased above 30 nm [144]. A comparison of as-deposited and annealed AlN films was presented which revealed that hydrogen impurities in the as grown films desorb after annealing at ⩾400 °C and films started to oxidize after 600 °C [145]. In another report, it was argued that AlN films grown at low temperatures on sapphire have higher crystallinity when compared to the same films grown on silicon substrates [153]. Current transport mechanism was evaluated by fabricating and measuring metal-insulator-semiconductor (MIS) capacitor devices whereby ohmic conduction, trap assisted tunneling, and Frenkel–Poole (FP) emission were determined to be the main electrical transport mechanisms [150]. Trap levels in AlN films were attributed to nitrogen vacancies and DX centers formed with involvement of Si atoms in the film [150]. A comparison of different plasma chemistries for AlN ALD growth showed that N_2-only plasma is not suitable for AlN growth while films grown with NH_3 and N_2/H_2 were nitrogen rich and heavily hydrogenated [140]. Additionally, higher carbon content was found in films grown with N_2/H_2 plasma which might be originating from

an undesirable reaction occurring during the plasma step between nitrogen species and surface CH groups [140].

The most common precursors for ALD of InN are $In(CH_3)_3$ and N_2 plasma [154–157]. Atomic layer epitaxy of InN has been reported using $In(CH_3)_3$ and N_2 plasma as reactants and novel cubic or a hexagonal phase of InN were synthesized [158]. Two different atomic layer epitaxy growth temperature windows were found between 175 °C−185 °C and 220 °C−260 °C; cubic phase was grown in the low temperature window whereas common hexagonal phase of InN was found in the films grown within the higher temperature window [158]. In another investigation, it was reported that addition of H_2 plasma with N_2 plasma as nitrogen precursor produced InN films with poor crystalline quality, high level of C and O impurities, and significant void structures [154]. Films grown with N_2/H_2 plasma contained a combination of turbostratic and hexagonal phases, while films grown with N_2-plasma only were single-phase hexagonal InN [154]. A detailed PEALD optimization study of InN has been reported using $In(CH_3)_3$ and N_2 plasma as reactants and it was found that longer N_2 plasma exposure time helped in removing carbonaceous ligands more effectively, which at the same time reduced the GPC of InN [157]. In contrast to band gap of single crystal InN (0.7 eV), an effective optical band gap of ∼1.9 eV was extracted for ALD-grown InN [157].

Finally, boron nitride (BN) has been deposited using BCl_3/BBr_3 and NH_3 reactants by thermal ALD within 230 °C–750 °C [159, 160]. Films grown were either amorphous or turbostratic, in which BBr_3/NH_3 and BCl_3/NH_3 reactants were utilized. In another report, BN was deposited via laser-assisted ALD using BBr_3/NH_3 reactants which produced turbostratic BN with a relatively high deposition rate [161]. BN was also grown using $(C_2H_5)_3B$ and N_2/H_2 plasma reactants at 350 °C and 450 °C, yielding hexagonal polycrystalline film with relatively low impurities [162]. Thermal decomposition of $(C_2H_5)_3B$ was found to start around 350 °C and therefore the deposition regime of BN at higher temperatures was not self-limiting. BN has been grown by atomic layer epitaxy on Co (0001) template at 327 °C using BCl_3/NH_3 reactants, resulting in epitaxial p-type BN with an average domain size of at least 1900 Å [163]. More recently, atomic layer epitaxy of stoichiometric BN was accomplished at 600 K using BCl_3/NH_3 precursors with very low impurity levels [164].

2.3. Sulfides

One of the very first ALD process (known as atomic layer epitaxy at that time) was demonstrated in early 1975s by Suntola *et al* for the deposition of ZnS for thin-film electro-luminescent displays [165]. Despite ZnS being one of the first ALD coated semiconducting films, the literature on ALD of sulfides is narrower when compared to the vast literature on oxide ALD. Initial atomic layer epitaxy of ZnS process used elemental Zn and S as reactants at 500 °C [165]. Soon, molecular precursors such as ZnI_2 or $ZnCl_2$ replaced the elemental precursors which provide better ligand exchange mechanisms leading to ideal self-limiting surface reactions [166]. However, halide precursors required higher source temperatures for vaporization and therefore higher deposition temperatures which cause halide impurity contamination, posing challenges for critical device applications [166]. In order to overcome these issues, organometallic precursors have been used to develop ZnS ALD processes. In almost all the cases, H_2S was used as S source whereas $(C_2H_5)_2Zn$ was used as Zn precursor [167–173]. Use of metal-organic precursors enabled a wide growth temperature range and considerably higher GPCs owing to their higher reactivity and thermal stability [167–173]. When $(C_2H_5)_2Zn$ and H_2S reactants were employed, GPC of ZnS decreased monotonically with increasing growth temperature which was attributed to the decrease in surface functional group coverage with temperature [69, 171]. ZnS grown with metal organic/H_2S precursor at low temperatures was generally cubic while a change in phase appeared at higher growth temperatures (>300 °C) leading to formation of hexagonal ZnS [171, 172]. *In situ* monitoring of ZnS film growth was investigated during the initial cycles of ALD using scanning tunneling microscopy (STM) technique [168]. It was found that grain morphology is temperature-dependent and grain size increases with deposition temperature from 100 °C to 160 °C [168]. H_2S has been commonly used as S source because of its volatility and reactivity with metalorganic precursors [174]. Nevertheless, H_2S presents several challenges which includes its flammable, corrosive, and toxic character [174]. Therefore, ALD reactors need to be designed carefully for H_2S compatibility. In some reports, H_2S was generated *in situ* for ZnS ALD to eliminate the need to store high pressure H_2S gas [171, 175]. The H_2S precursor was generated by heating thioacetamide to 150 °C in an inert atmosphere, producing acetonitrile and H_2S [171].

There are only a few reports on ALD of CdS. Atomic layer epitaxy of CdS is reported where Cd and S precursors were used at substrate temperature of 340 °C [176]. Atomic layer epitaxy of CdS is also performed using $Cd(CH_3)_2$ and H_2S on a ZnSe (100) substrate at room temperature [177]. Annealing of CdS is performed at 250 °C which produced zincblende CdS, a crystal structure similar to the substrate [177]. Bakke *et al* reported ALD of CdS using $Cd(CH_3)_2$ and *in situ* generated H_2S on Si (100) or glass substrate in a temperature range of 100 °C–400 °C [178]. Films grown at low temperatures were a mixture of wurtzite and zincblende crystal structures while films grown at higher temperature (400 °C) were dominantly wurtzite [178].

Cu_xS exists in five solid phases at room temperature: chalcocite ($x = 2$), djurleite ($x = 1.96$), digenite ($x = 1.8$), anilite ($x = 1.75$), and covellite ($x = 1$). ALD of Cu_xS has been reported by using three different Cu precursors: $Cu(thd)_2$ (thd = 2,2,6,6-tetramethyl-3,5-heptanedione), bis(N,N-di-sec-butylacetamidinato)dicopper(I) $Cu_2(DBA)_2$, and copper(II) acetylacetonate [179–184]. In all these studies, H_2S was used as the sulfur precursor. Depending on different process parameters and precursors employed, different stoichiometry and compositions of Cu_xS were obtained. With the use of $Cu_2(DBA)_2$ precursor as Cu source material, mainly chalcocite phase (Cu_2S) of Cu_xS was obtained [181, 182]. On the other hand, with the use of $Cu(thd)_2$ precursor, either covellite (CuS) phase or digenite ($Cu_{1.8}S$) phase of Cu_xS was synthesized [183, 184]. When $Cu(acac)_2$ precursor

was employed, researchers obtained p-type Cu_xS film with either multiphase compounds (made of digenite $Cu_{1.8}S$, chalcocite Cu_2S, djurleite $Cu_{31}S_{16}$, and covellite CuS) or single-phase digenite $Cu_{1.8}S$ film depending on number of growth cycles [179].

ALD of PbS films has been studied by only one research group [185–187]. Bis(2,2,6,6-tetramethyl-3,5-heptanedionato)lead(II) ($Pb(tmhd)_2$) and H_2S were the precursors employed at a growth temperature of 160 °C [185–187]. The grown PbS film was polycrystalline with grain sizes ranging from 30 to 150 nm. Effect of size quantization on band gap of ALD grown PbS were demonstrated by fabricating PbS quantum wells with sub-10 nm thickness [185]. Bandgap of the films was varied from 0.4 to 2.75 eV by varying only the number of ALD cycles [185].

ALD of another sulfide semiconductor, SnS was initially reported by Kim *et al* using ($Sn(acac)_2$) and H_2S reactants [188]. GPC of SnS was relatively low (0.24 Å); the reason might be that Sn–O bonds (532 kJ mol^{-1}) are stronger than Sn–S bonds (464 kJ mol^{-1}) which results in an unfavorable thermodynamic enthalpy change [188]. SnS growth on Al_2O_3 substrate had nucleation issues and displayed very small GPCs which might be caused by Al(acac)* site blocking surface species [188]. Films contained 15–20 at% oxygen after air exposure and such oxidized SnS films exhibited a band gap of ∼1.87 eV, higher than the reported SnS bulk band gap value (∼1.3 eV) [188]. Higher GPCs (0.86–0.90 Å) were obtained with the use of Bis(N,N′-diisopropylacetamidinato)tin(II) [$Sn(MeC(N\text{-}iPr)_2)_2$], $Sn(amd)_2$ tin precursor at lower growth temperatures [189]. Impurities in the film deposited with $Sn(amd)_2$ precursors were negligible and films were p-type with a band gap value of 1.30–1.42 eV which is closer to bulk band gap value of SnS films [189]. ALD of SnS has also been reported with tetrakis(dimethylamino)tin (TDMASn, $[(CH_3)_2N]_4Sn$) precursor where it has been shown that crystal structure of SnS_x can be tuned by changing the growth temperature [190]. Below 120 °C, SnS_x films were amorphous while SnS_x films were SnS_2 hexagonal at 140 °C and 150 °C, and orthorhombic above 160 °C [190].

ALD of In_2S_3 has been reported by McCarthy *et al* using In(III) N,N′-diisopropylacetamidinate ($In(amd)_3$) and H_2S reactants in a temperature range of 140 °C–240 °C [191]. Deposited films were n-type with free electron concentrations up to 10^{18} cm^{-3} and carrier mobilities in the order of ∼1 cm^2 V^{-1} s^{-1} [192]. There is a single report for ALD of GaS_x in which films were synthesized using hexakis(dimethylamido)digallium and H_2S reactants at a growth temperature range of 125 °C–225 °C [193]. Growth was self-limiting in the temperature range of 125 °C–225 °C while the films were amorphous as promising lithium ion battery anode material. For further reading about ALD of sulfides, reader may consult to the review of Dasgupta *et al* which specifically focuses on ALD of metal sulfide materials [174].

2.4. Selenides and tellurides

ALD of selenides and tellurides have been only limited to selenides and tellurides of Zn and Cd, as those are rare cases where constituent elements can be used as precursors [194–197]. Selenides and tellurides are less explored because their hydride compounds are toxic and would require extensive safety precautions. Alkyl compounds of selenium and tellurium have been more commonly employed as CVD reactants but in ALD they are unable to provide efficient ligand exchange reactions with the common metal precursors [194]. In a breakthrough discovery, ALD of various selenides and tellurides has been reported using alkylsilyl compounds of Se and Te [194]. Compared to common alkyls and alkylamides of Se and Te, $(R_3Si)_2Se$ and $(R_3Si)_2Te$ offered straight forward elimination of ligands of the metal precursors. In $(R_3Si)_2Se$ and $(R_3Si)_2Te$, there is an unfavorable hard-soft Lewis acid-base pair, as in these compounds a hard Lewis acid is bonded to the heavy group 16 elements which are soft Lewis bases. When there is an exchange reaction of these compounds with metal chlorides, silicon becomes bonded to harder base thus allowing an easy ligand exchange reaction [194].

2.5. Arsenides

To date, there is only one recent report on ALD of arsenide compounds where synthesis of GaAs was demonstrated. Dechlorosilylation reaction between $GaCl_3$ and $(Et_3Si)_3As$ precursors was found to be successful in depositing GaAs films via ALD [198]. The films were uniform, amorphous, and stoichiometric, while film crystallization was achieved by post-deposition annealing process [198].

2.6. Elemental semiconductors

ALD of elemental semiconductors is less explored due to the challenge of synthesizing crystalline group-IV semiconductor films with low impurities [199, 200]. ALD of Si was initially explored using $Si(C_6H_{10})_2$ precursor [201]. Upon reacting with substrate, hydrocarbon rings of $Si(C_6H_{10})_2$ precursor transform into dimethylbutadiene (C_6H_{10}), which is very volatile and readily desorb. This chemistry provided Si with high level of carbon impurities. ALD of Si was demonstrated using Si_2H_6 and $SiCl_4$ precursors in temperature range of 355 °C–385 °C [202]. Films were smooth with arithmetic average roughness of 0.26 nm, however, no elemental characterization data was reported from the bulk of film.

Ge ALD was performed using alternating exposures of $GeCl_4$ and atomic hydrogen. After the first self-limiting exposure of $GeCl_4$, atomic hydrogen extracted surface terminating chlorine in the second exposure which resulted in Ge film growth [200]. Recently, Ge ALD was demonstrated using $GeCl_4$ and 1,4-bis(trimethylsilyl)-1,4-dihydropyrazine as reducing agent. Smooth continuous films were obtained only on platinum substrates. X-ray photoelectron spectroscopy (XPS) and x-ray diffraction (XRD) data revealed the formation of $PtGe_2$ alloy initially, followed by smooth Ge film growth [203].

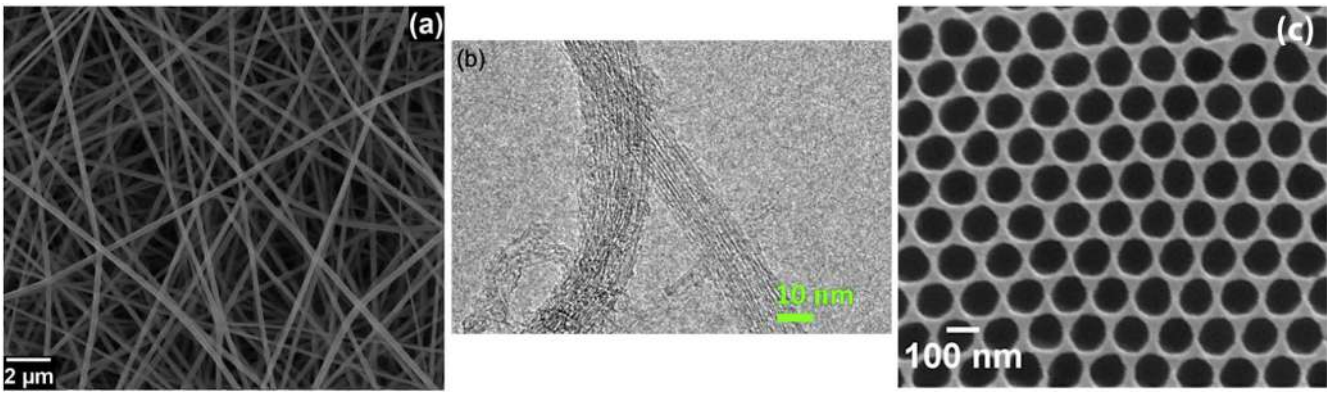

Figure 1. Various nanostructured templates used for template assisted ALD. (a) SEM image of nylon 6,6 polymeric nanofibers. (b) TEM image of single wall carbon nanotubes. (c) SEM image of porous AAO template. Reprinted with permission from [284, 335]. Copyright (2014, 2015) AIP publishing, Elsevier.

3. Nanostructured semiconductor growth via ALD

Mainly two approaches exist for nanostructured materials growth via ALD: (i) Bottom-up growth via catalyst-assisted or catalyst-free method (ii) Template-assisted growth. In template-assisted strategy, material growth is carried out on nanostructured templates (figure 1) such as carbon nanotubes, polymers, or anodic aluminum oxide (AAO) [283–285]. Subsequent to growth, template material might be removed via high-temperature treatment (calcination) or physical/chemical etching to obtain various kinds of freestanding functional nanostructures.

Bottom up growth method can be further classified into mainly two types: catalyst-assisted and catalyst-free methods. Catalyst-assisted growth typically occurs via vapor liquid solid growth where nanostructures are fabricated along a supersaturated catalytic liquid metal such as Ni or Au [283]. Catalyst free methods generally utilize selective area growth of preferential growing crystallographic planes over non-preferential planes by altering the processing conditions in order to favor growth of material in one dimension [286, 287]. In certain chemistries of ALD, growth of islands is observed rather than formation of continuous films during the initial stages of deposition [288–290]. Quantum dots and nanoparticles are synthesized by taking advantage of the so-called incubation period of ALD. This way of synthesizing 0D nanostructures can also be classified as catalyst-free bottom up growth approach. Below we summarize the reported major achievements in the field of 0D, 1D, 2D, and core–shell structured semiconductor materials.

3.1. 0D structures

Table 2 provides a summary of ALD-grown 0D semiconductor nanostructures. ALD of ZnO has been carried out on SiO_2 film having nanoscale voids between them which allow subsequent deposition within the voids of the films [291, 292]. ZnO nanodots were fabricated in this way within SiO_2 film and resulted in a significant blue shift in the photoluminescence properties of ZnO, mainly due to the quantum confinement effect. ZnO filling between voids of a SiO_2 film has affected the mechanical, photoluminescence, and photosensitivity properties of the film [291, 292]. Nanoparticular TiO_2 growth has been reported on CNTs during the incubation period of TiO_2 growth [293]. TiO_2 was grown in uniform thin film form on CNTs at 100 °C, but the growth at 300 °C resulted in nanoparticles during the initial cycles of the ALD process [293]. It was argued that island ALD growth mode at 300 °C occurred because of recombination between the byproducts and $TiCl_4$ molecules [293]. Fabrication of TiO_2 nanoparticle chains has been reported on CNTs by calcination of conformally TiO_2 coated multi-walled carbon nanotubes (MWCNTs) [294]. During annealing process, thin tubular layer of TiO_2 has been transformed into nanoparticle chains with an enhanced ultra-high surface area [294].

Quantum dots of semiconducting PbS (figure 2) and CdS have been synthesized by utilizing the incubation period observed during the initial stages of ALD where growth of islands is observed rather than formation of continuous films [288–290]. Note that this type of growth mode has only been observed in certain ALD chemistries [288, 289]. This very strategy of synthesizing quantum dots using ALD provides several unique advantages. Size of quantum dots can be varied by simply changing the number of growth cycles. Excellent infiltration of quantum dots can be obtained on high-surface area nanostructured templates by utilizing the high conformality of ALD processes. Moreover, as opposed to conventional quantum dot fabrication techniques, ALD eliminates the use of solutions and solution-based byproducts [288–290]. Islands with sub-10 nm diameters were observed during the initial ALD cycles (10–40 growth cycles) of PbS on Si nanowire array (figure 2) and PL measurements showed a blue shift when number of ALD cycles are decreased confirming successful quantum confinement in PbS quantum dots (figure 3) [290].

3.2. 1D structures

ALD grown 1D nanostructures are summarized in table 3. Majority of reports on ZnO nanostructures utilized nanoscale templates with the intention of disposing the template after deposition in order to obtain various kinds of ZnO

Table 2. Overview of the growth conditions employed to synthesize 0D nanostructures using ALD. The materials deposited, the morphology, precursors used, the temperature during ALD, and preparation method are mentioned.

Material	1st precursor	2nd precursor	Growth temperature	Morphology	Preparation method	References
ZnO	$Zn(C_2H_5)_2$	H_2O	180 °C	Quantum dots	ALD of ZnO on silica nanoparticles	[292]
	$Zn(C_2H_5)_2$	H_2O_2	200 °C, 300 °C	Nanodots	ALD of ZnO on Si and SiO_2 films	[208]
	$Zn(C_2H_5)_2$	H_2O	200 °C	Nanoparticles	ALD of ZnO on nylon nanofibers	[295]
TiO_2	Tetrakis(dimethylamido) titanium (TDMAT)	O_3	100 °C	Nanoparticle chains	TiO_2 growth on carbon nanotubes followed by annealing	[294]
	$TiCl_4$	H_2O	200 °C, 300 °C	Nanoparticles	Growth during initial growth cycles of TiO_2 on carbon nanotubes	[293]
CdS	Dimethyl cadmium	H_2S	150 °C	Quantum dots	Utilizing the incubation period of CdS growth by ALD on TiO_2	[288]
PbS	Bis(2,2,6,6-tetra-methyl-3,5-heptanedionato)lead(II) ($Pb(tmhd)_2$)	H_2S	160 °C	Quantum dots	Utilizing the nucleation stage of ALD PbS growth	[290]
	Bis(2,2,6,6-tetra-methyl-3,5-heptanedionato)lead(II) ($Pb(tmhd)_2$)	H_2S	160 °C	Quantum dots	Utilizing the nucleation stage of ALD PbS growth	[289]
SnSe	Et_4Sn	H_2O	200 °C–450 °C	Sphere shaped particles	Growth temperature dependent morphology of SnSe structures	[296]

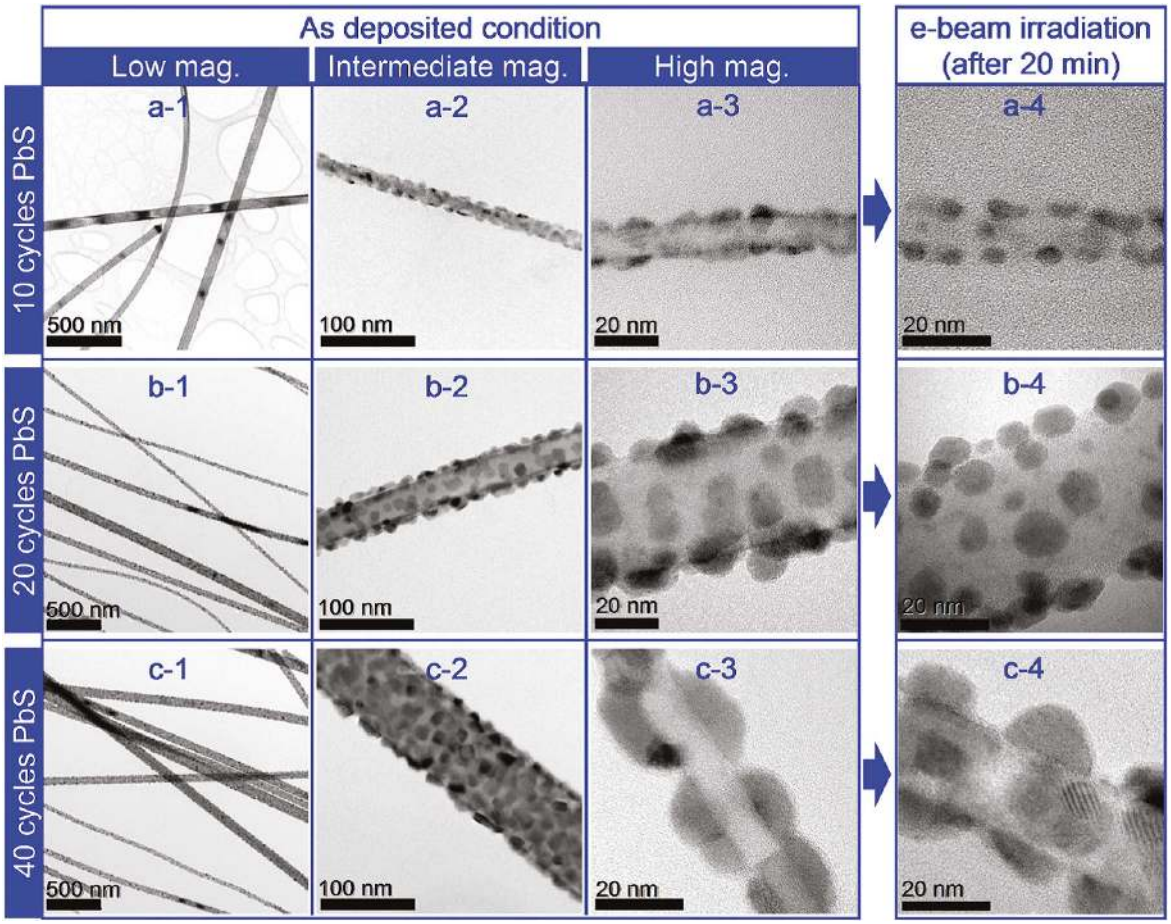

Figure 2. TEM images of Si nanowires coated by ALD PbS shown at different magnifications after (a) 10 cycles, (b) 20 cycles, and (c) 40 cycles. Also shown is the effect of 20 min e-beam irradiation on the dot-coated Si nanowires. (As a result of the e-beam irradiation process, the crystallite morphology changes to a dome shape to lower the surface to volume ratio providing better contrast in TEM imaging.) Reprinted with permission from [290]. Copyright (2011) American Chemical Society.

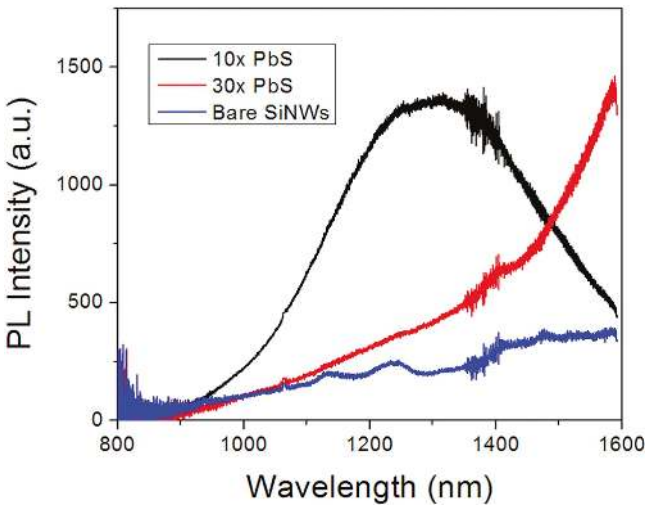

Figure 3. Photoluminescence spectra for bare Si nanowires (blue), 10 cycles of ALD PbS (black), and 30 cycles of ALD PbS (red). Reprinted with permission from [290]. Copyright (2011) American Chemical Society.

nanostructures [297–301]. Mainly three types of templates have been used: anodized alumina (AAO) templates, polymeric templates, and bio-nano-templates made out of biological materials [298, 301–304]. These templates have also been used to study the conformality of ZnO as well as to make multi-segmented ZnO nanotubes [305, 306]. ZnO growth inside the pores of AAO was limited by precursor diffusion into the high aspect ratio wells and therefore long exposure times were necessary to obtain conformal coatings (120 s exposure time for aspect ratio of ∼5000) [305, 306]. Moreover, with the utilized long exposure times, also extensive purging times were required to ensure the complete removal of the excess reactants and byproducts which will ensure the elimination of any unwanted gas-phase CVD reaction.

ZnO 1D structures such as nanorods or nanowires have been fabricated by utilizing lithography techniques or by performing growth directly on nanostructured templates [307–312]. In one study, combination of phase-shift lithography and plasma was utilized to synthesize a photoresist nanodot pattern on Si which was used to etch Si afterwards

Table 3. Overview of the growth conditions employed to synthesize 1D nanostructures using ALD. The materials deposited, the morphology, precursors used, the temperature during ALD, and preparation method are mentioned.

Material	1st precursor	2nd precursor	Growth temperature	Morphology	Preparation method	References
ZnO	$Zn(C_2H_5)_2$	H_2O	250 °C	Nanotube and nanorod arrays	Deposition of ZnO on AAO/Si templated followed by AAO etching	[308]
	$Zn(C_2H_5)_2$	H_2O	150 °C	Nanotubes	ALD of ZnO on aerogels fibrils followed by calcination	[316]
	$Zn(C_2H_5)_2$	H_2O	150 °C	Nanotubes	ALD of ZnO on Polyacrylonitrile fibers followed by annealing or O_2 plasma treatment	[299]
	$Zn(C_2H_5)_2$	H_2O	120 °C	Nanotubes	ALD of ZnO on SAMs-AAO	[306]
	$Zn(C_2H_5)_2$	H_2O	200 °C	Nanotubes	ALD of ZnO on Polyvinylacetate and AAO followed by annealing or etching	[337]
	$Zn(C_2H_5)_2$	H_2O	150 °C	Rod like morphology	ALD ZnO on MgO films	[338]
	$Zn(C_2H_5)_2$	H_2O	177 °C	Nanorods	Hydrothermal ZnO growth on ALD ZnO seed layer	[321]
	$Zn(C_2H_5)_2$	H_2O	100 °C	Nanorods	Hydrothermal ZnO growth on ALD ZnO seed layer	[300]
	$Zn(C_2H_5)_2$	H_2O	70 °C	Nanorods	Using polymer/Si porous structures to direct ALD of ZnO	[297]
	$Zn(C_2H_5)_2$	H_2O	100 °C	Nanorods	Wet chemical procedure on ALD grown ZnO	[320]
	$Zn(C_2H_5)_2$	H_2O	200 °C	Nanorods	ZnO deposition on high aspect ratio Si microwire arrays	[324]
	$Zn(C_2H_5)_2$	H_2O	200 °C	Nanorods	ALD of ZnO on AAO	[310]
	$Zn(C_2H_5)_2$	H_2O	200 °C	Nanorods	ALD of ZnO on AAO followed by chemical etching of AAO	[312]
	$Zn(C_2H_5)_2$	H_2O	70 °C–300 °C	Nanofibers	ALD of ZnO on inner shell membrane of hen's egg	[303]
	$Zn(C_2H_5)_2$	H_2O	150 °C	Nanofibers	ALD of ZnO on Polyvinylacetate nanofibers followed by annealing	[298]
	$Zn(C_2H_5)_2$	H_2O	200 °C	Nanofibers	ALD of ZnO on nylon nanofibers	[302]
	$Zn(C_2H_5)_2$	H_2O	150 °C	Nanofibers	ALD of ZnO on polyvinylpyrroli- done (PVP) fibers followed by annealing	[301]
	$Zn(C_2H_5)_2$	H_2O	200 °C	Nanofibers	ALD of ZnO on nylon nanofibers	[295]
	$Zn(C_2H_5)_2$	H_2O	50 °C–130 °C	Nanofibers	ALD of ZnO on polyacrylonitrile nanofibers	[339]
	$Zn(C_2H_5)_2$	H_2O	180 °C, 300 °C	Nanopillars	Preferential ALD of ZnO on ZnO seed layer	[304]
	$Zn(C_2H_5)_2$	H_2O	200 °C	Nanowires	Hydrothermal growth of ZnO on ALD grown ZnO seed layer	[323]
	$Zn(C_2H_5)_2$	H_2O	115 °C	Nanowires	Substitution of Si nanowires by ZnO NWs with a dry etching technique and atomic layer deposition	[307]

Table 3. (Continued.)

Material	1st precursor	2nd precursor	Growth temperature	Morphology	Preparation method	References
	$Zn(C_2H_5)_2$	H_2O	200 °C	Nanoneedles	Hydrothermal growth of ZnO on ALD ZnO/PAN nanofibers	[325]
	$Zn(C_2H_5)_2$	H_2O	200 °C	Nanofibers	ALD of ZnO on nylon nanofibers during incubation period	[295]
TiO_2	Titanium(IV) isopropoxide	H_2O	70 °C	Nanotubes	TiO_2 growth into AAO membranes	[326]
	$TiCl_4$	H_2O	100 °C	Nanotubes	TiO_2 growth into AAO membranes	[328]
	Titanium tetraisopropoxide	H_2O	150 °C, 250 °C	Nanotubes	TiO_2 growth into AAO membranes and carbon nanotubes	[327]
	$TiCl_4$	H_2O	250 °C	Nanotubes	TiO_2 growth on carbon nanotubes	[329]
	$TiCl_4$	H_2O	250 °C–300 °C	Nanotubes	TiO_2 growth into AAO membranes	[340]
	$TiCl_4$	H_2O	150 °C	Nanotubes	TiO_2 growth into AAO membranes	[330]
	$TiCl_4$	H_2O	600 °C	Nanorods	TiO_2 growth into AAO membranes	[341]
Ga_2O_3	Gallium (III) alkyl amidinate [mono-acetamidinatodiethylgallium(III), compound 1]	H_2O, O_2	450 °C	Nanowires	Self-seeding growth	[342]
SnO_2	$SnCl_4$	H_2O	150 °C–400 °C	Nanotubes	SnO_2 growth into AAO membranes followed by polishing and etching	[331]
	Tin(IV) alkoxides	Carboxylic acid	75 °C–250 °C	Nanotubes	SnO_2 growth on carbon nanotubes and boron nitride nanotubes	[332]
	$SnCl_4$	H_2O	200 °C–400 °C	Nanotubes	SnO_2 growth on carbon nanotubes	[343]
	Tin tert-butoxide	Acetic acid	200 °C	Nanotubes	SnO_2 growth on carbon nanotubes	[344]
GaN	$Ga(CH_3)_3$	N_2/H_2 plasma	200 °C	Flexible nanofibers	GaN growth on electrospun nanofibers	[285]
AlN	$Al_2(CH_3)_6$	NH_3 plasma	200 °C	Nanofibers	GaN growth on electrospun nanofibers followed by calcination	[333]
ZnS	$Zn(C_2H_5)_2$	H_2S	75 °C–180 °C	Nanotubes	ZnS growth on AAO template	[334]
Cu_2S	Bis(N,N'-disec-butylacetamidinato)dicopper(I) (CuAMD)	H_2S	135 °C	Nanotubes	ALD of Cu_2S on single walled carbon nanotubes	[335]
GaS_x	$Ga_2(NMe_2)_6$	H_2S	150 °C	Nanotubes	ALD of GaS_x on single walled carbon nanotubes	[336]

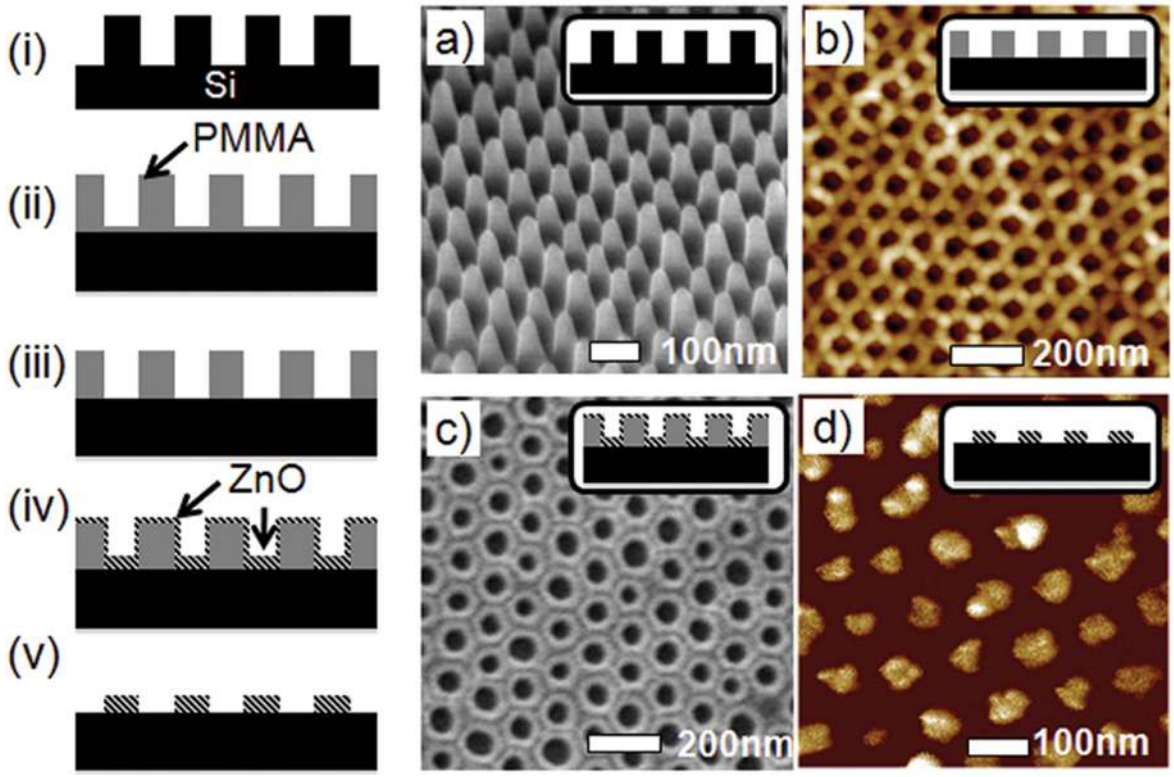

Figure 4. (i)–(v) Illustration of steps to fabricate ZnO nanoarrays using selective area ALD within templates defined by copolymer-derived NIL molds. (i) High-resolution silicon nanopillar molds (as shown in panel (a) as field effect scanning electron microscope (FESEM) image measured at 45° tilt). (ii) Nanoporous polymethylmethacrylate (PMMA) films obtained upon NIL (as shown in panel (b) by tapping mode atomic force microscope (AFM) image) and subsequently exposed to controlled O_2 plasma reactive ion etching (RIE) to obtain (iii) porous templates with through-holes. (iv) ALD of ZnO on the nanoporous templates (as shown by FESEM image in panel (c)), followed by removal of templates to obtain (v) ZnO nanoarrays (as shown by tapping mode AFM image in panel (d)). Reprinted with permission from [297]. Copyright (2012) American Chemical Society.

[307]. Another coating of photoresist and subsequent etching of Si nanowires resulted in a mask for ALD of ZnO nanowires. In another report, polymer templates synthesized through a combination of block copolymer lithography (BCL) and nanoimprint lithography (NIL) were used as a nanotemplate for subsequent ALD to obtain highly oriented and high-quality ZnO nanopatterns (illustration of fabrication steps are summarized in figure 4) [297]. The fabricated uniform array of ZnO nanostructures possessed sub-100 nm feature and spatial resolutions, exhibiting narrow distributions in size and separation, and superior mechanical stability. AAO template has been commonly used for ZnO nanorod fabrication; AAO features long-range ordered vertically aligned nanopores with varying aspect ratios whose dimensions can be easily controlled by adjusting the process conditions [308, 310, 312, 313]. It is a fairly simple technique to obtain ZnO nanorods by growing on these templates followed by the removal process of AAO, usually accomplished by chemical wet etching. The pulse/exposure time of the precursors needed to conformally coat inside the AAO pores is typically long as precursor molecules needs time to diffuse-in and react with the available adsorption sites within the high aspect ratio template walls.

Low temperature ALD of ZnO has enabled the use of bio-templates in ZnO nanostructuring. Cicada wings have been used as templates to fabricate ZnO nanopillars by taking advantage of the fact that nanopillars on the wing surface block ZnO growth [314, 315]. Other studies utilized fibrils of hen's egg shell and nanocellulose fibers as bio-nanotemplates for ZnO coating [303, 316]. Figure 5 shows the fabricated ZnO nanotubes through bio templating; in this strategy, first nanocellulose hydrogel is dried to aerogel, followed by coating with ZnO ALD to form composite organic/inorganic nanofibers, and finally calcinated to inorganic hollow nanotubes [316]. Peptide amphiphile nanofibrous templates were used as a soft template for ALD of ZnO and TiO_2 and resulting functional nanonetworks (figure 6) found applications in photocatalysis for organic dye degradation and as anodic material in dye sensitized solar cells [317, 318]. Overall, the use of bio-templates in ZnO nano-structuring is relatively less explored and this field might hold potential for future device applications.

There also are studies in which fabrication of ZnO nanorods or nanodots has been reported without using any templates. These studies take advantage of the incubation period of ZnO growth to form ZnO islands which can then be used as seeds for the growth of nanopillars [208, 304, 319]. In some reports, ALD-grown ZnO thin films have been utilized

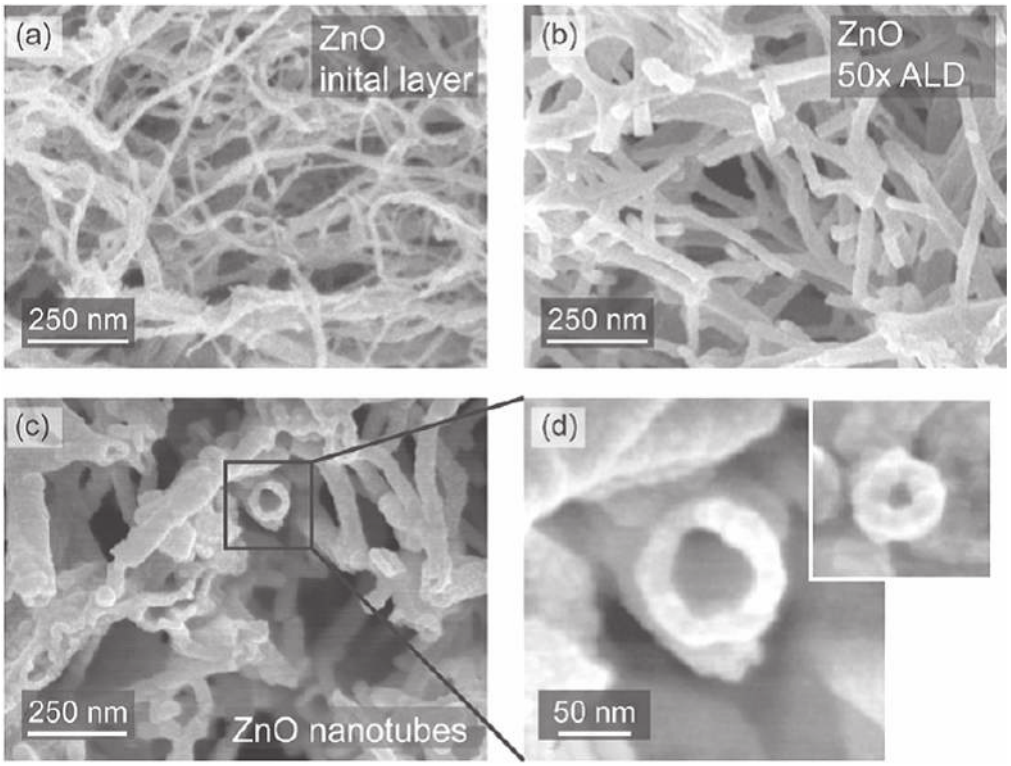

Figure 5. (a) A thin uniform ZnO layer formed on nanocellulose fibrils after initial exposure to the zinc precursor. (b) ZnO layer thickness is increased upon the ALD process (here 50 cycles). (c) Calcinated, hollow ZnO nanotubes are visibly rough. (d) Close-ups on ZnO nanotubes show that they are hollow. Reprinted with permission from [316]. Copyright (2011) American Chemical Society.

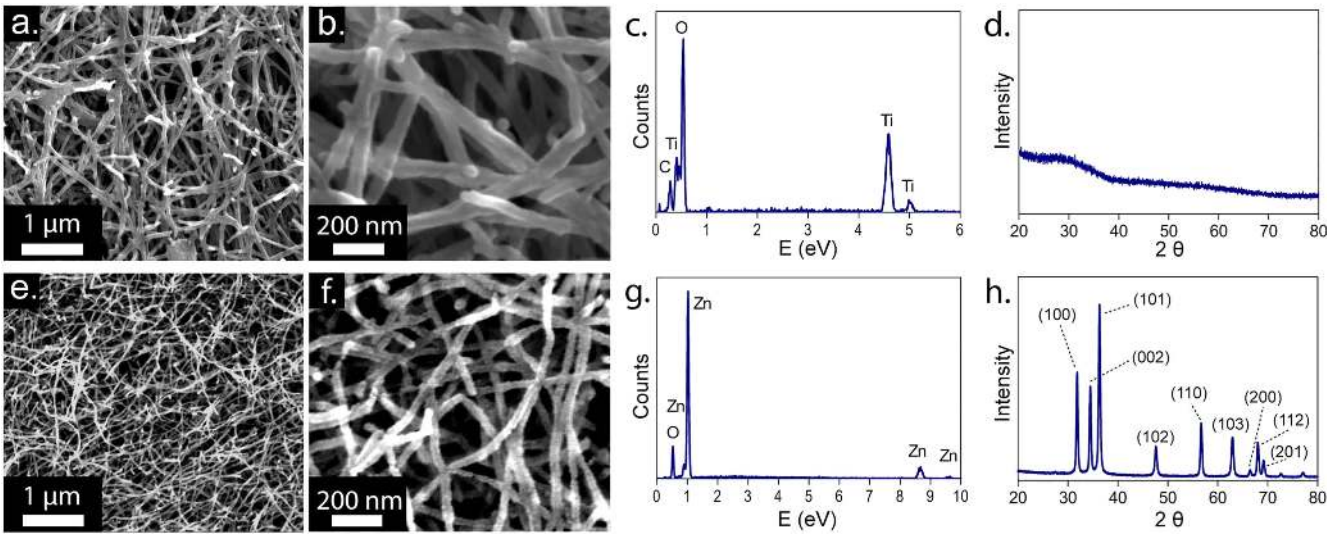

Figure 6. Characterization of as-synthesized TiO_2 and ZnO nanonetworks deposited with 350 and 100 ALD cycles, respectively. (a) and (b) Scanning electron microscope (SEM) images, (c) energy dispersive x-ray spectroscopy (EDX) spectrum, and (d) XRD pattern of TiO_2 nanonetworks. (e) and (f) SEM images, (g) EDX spectrum, and (h) XRD pattern of ZnO nanonetworks. Reprinted with permission from [318]. Copyright (2013) Nature publishing group.

as template for the subsequent growth of ZnO nanorods using hydrothermal process [320–324]. In these reports, ALD-grown ZnO provides a high-quality textured film to either act as a seed layer for nanorod growth or to protect the substrate from reagents of hydrothermal process. In another approach, ALD ZnO coated polyacrylonitrile (PAN) nanofibers were used as a template for over growth of ZnO nanoneedles via hydrothermal growth (figure 7) [325].

Nanostructured TiO_2 fabrication has been reported mostly in the form of nanotubes and the most common precursors utilized are $TiCl_4$ and H_2O [326–330]. Majority of reports utilized AAO as a template for TiO_2 growth which

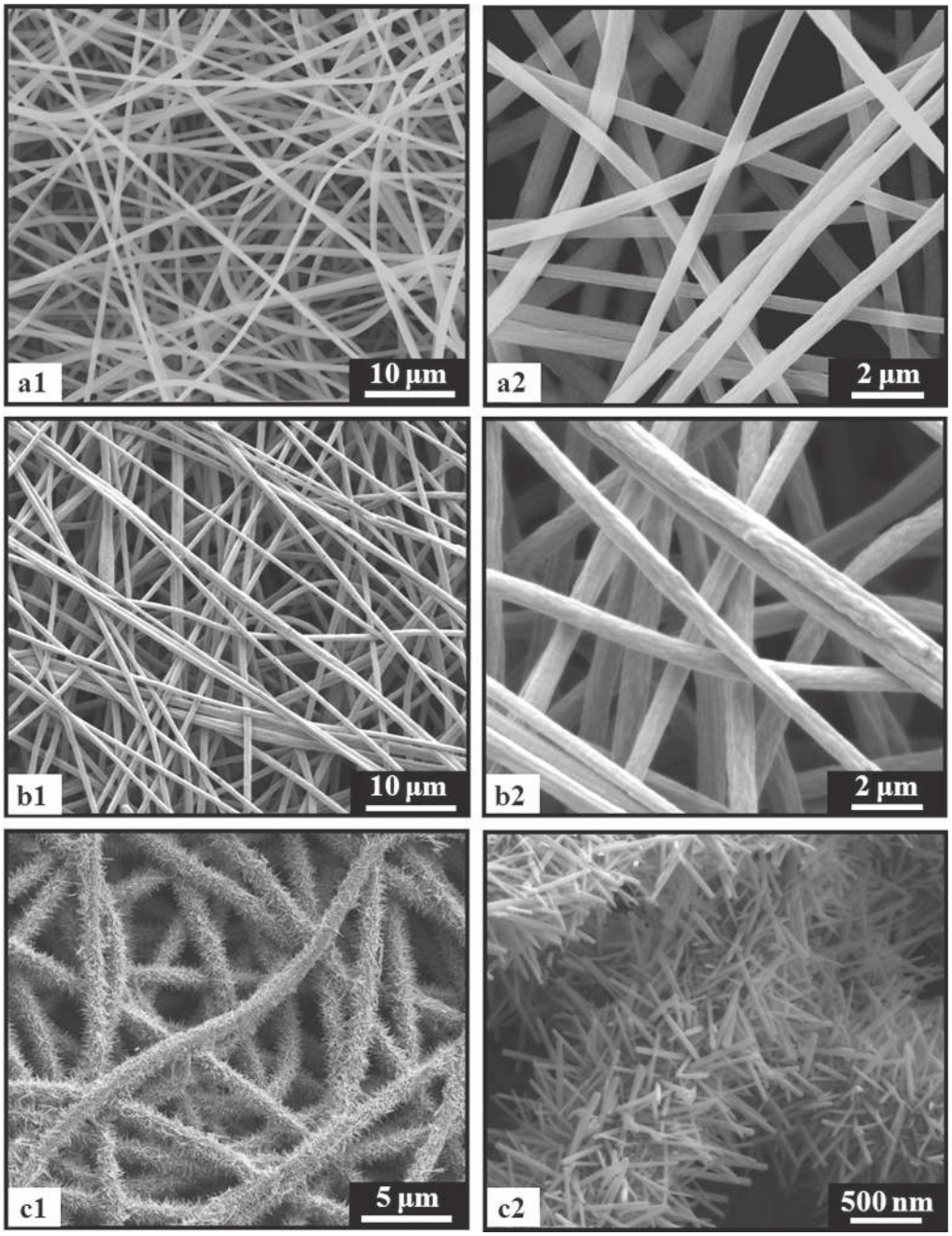

Figure 7. Representative SEM images of (a1 and 2) pristine PAN, (b1 and 2) PAN/ZnO seed, and (c1 and 2) PAN/ZnO needle nanofibers at different magnifications. Reprinted with permission from [325]. Copyright (2014) Elsevier.

was subsequently etched using NaOH solution to obtain TiO_2 nanotubes [326–328]. Crystal morphology of TiO_2 nanotubes has been tuned from amorphous to anatase phase when growth temperature was increased from 150 °C to 250 °C [327]. Figure 8 shows TiO_2 nanotubes fabricated via titania deposition into AAO membranes followed by AAO removal through etching [328].

$SnCl_4$ and H_2O precursors were employed to grow SnO_2 nanotubes using AAO as a template followed by etching of AAO [331]. Interestingly, three temperature-dependent growth modes were observed (figure 9): (i) layer-by-layer growth at temperature $T < 200$ °C; (ii) layer-by-particle growth at temperature 200 °C $\leqslant T <$ 400 °C; (iii) evolutionary particles at temperatures $T \geqslant 400$ °C [331]. It was believed that layer-by-layer growth occurred at low temperatures because of ligand exchange reactions and negligible change in reactive sites. Layer-by-particle growth occurred because of competing effects between ligand exchange and chlorination, i.e., lower growth temperatures prompt ligand exchange while higher temperatures can cause chlorination. Lastly, the evolutionary particle growth occurred at high growth temperatures mainly because of chlorination effects which caused certain nucleation sites on the substrate [331]. The layers were amorphous whereas particles were identified as crystalline. Hence in this way, morphology and phase of SnO_2 nanotubes were controlled via ALD growth temperature [331]. In another report it

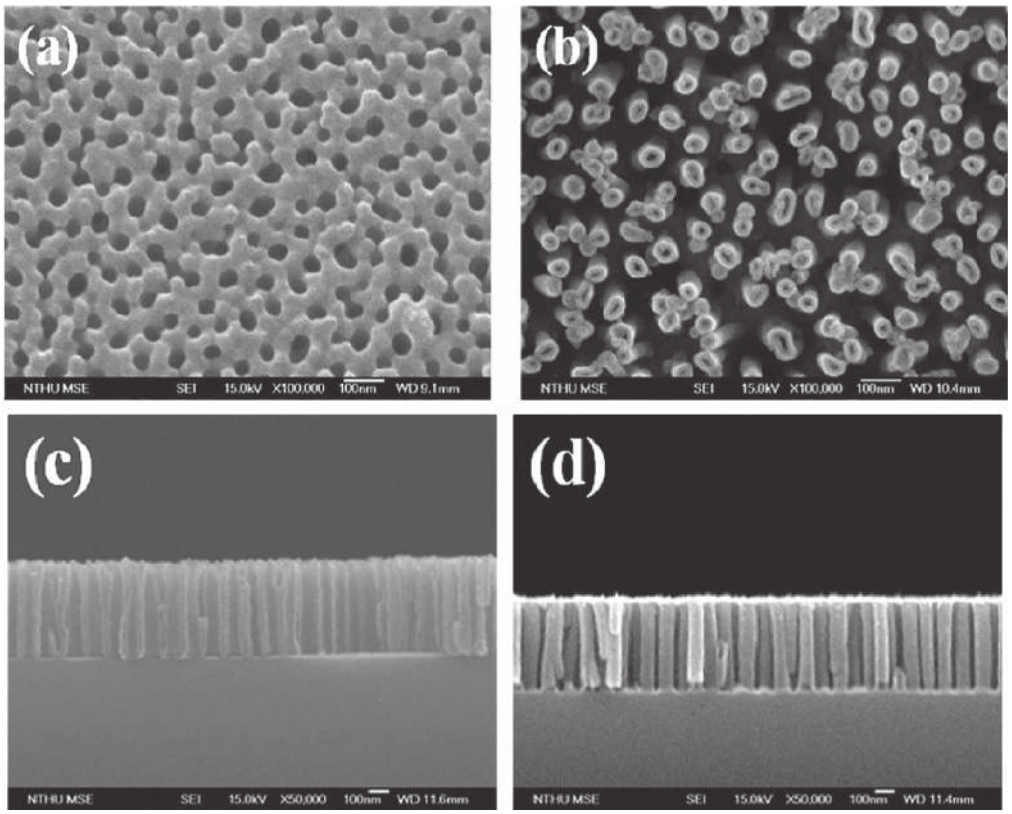

Figure 8. SEM images of (a), (c) TiO_2 in the AAO template, and (b), (d) pure TiO_2 nanotubes after removal of the AAO template. Reprinted with permission from [328]. Copyright (2011) American Chemical Society.

was demonstrated that the use of a tin(IV) alkoxide and carboxylic acid precursors are highly suitable for the fabrication of SnO_2 nanotubular structures at temperatures as low as 75 °C using templates such as carbon nanotubes (CNTs) and boron nitride nanotubes [332].

Flexible polymer–GaN organic–inorganic core–shell nanofibers (figure 10) were synthesized by performing remote PEALD growth of GaN on electrospun nylon 6,6 nanofibers at 200 °C [285]. The fabrication process resulted in ∼28 nm thick conformal polycrystalline wurtzite GaN shell layer on polymeric-core nanofibers with an average fiber diameter of ∼70 nm. The low process temperatures enabled the preservation of the flexibility of the resulting core–shell polymer/GaN nanofiber templates [285]. Polycrystalline hexagonal AlN hollow nanofibers (figure 11) were fabricated via PEALD using similar sacrificial electrospun polymeric nanofiber templates [333]. Deposition of AlN was carried out again at 200 °C on electrospun nylon 6,6 nanofibers followed by a high-temperature *in situ* calcination at 500 °C for 2 h to remove the sacrificial polymeric nanofiber template [333]. Recently, vertically aligned GaN, AlN, and InN hollow nano-cylindrical arrays (HNCs) on Si substrates were fabricated using anodized aluminum oxide (AAO) membrane based template-assisted plasma-assisted atomic layer deposition (PEALD). Fabrication scheme consisted of the following steps: (i) Electrochemical anodization of aluminum foil to obtain free-standing AAO membrane, followed by transfer and sticking of AAO membrane to Si substrate, (ii) Si patterning with Ar and CHF_3 based reactive ion etching (RIE) using AAO membrane as hard mask material to achieve nanoporous network on Si substrate, (iii) Conformal growth of GaN, AlN, and InN on nanoporous Si via low-temperature PEALD, (iv) Ar based RIE of PEALD coated III-nitride material from top surface of Si and SF_6 based isotropic RIE of surrounding Si to attain highly ordered vertical GaN, AlN, and InN hollow nano-cylinder arrays. Materials characterization revealead that ordered vertical arrays of III-nitride hollow nanocylinders were successfully integrated inside Si(100); a representative image of GaN HNCs fabricated using this strategy is given in figure 12.

High aspect ratio (⩾300) ZnS nanotubes were fabricated by performing growth into highly ordered pores of AAO templates at deposition temperatures as low as 75 °C [334]. The tubes exhibited smooth wall surface and their dimensions can be precisely tailored by varying the electrochemical and ALD processing parameters [334]. Cu_2S was grown on networks of single walled carbon nanotubes (SWCNTs) to obtain SWCNT-n-Cu_2S composite nanotube structure [335]. The resulting structures demonstrated an intimate contact between SWCNTs and Cu_2S, yet preserving the porosity for efficient transport of charges [335]. Similar strategy has been utilized to obtain Ga_xS-SWCNTs composite nanotubular structure [336]. Figure 13 shows TEM images of ALD-coated Ga_xS on SWNCTs yielding highly conformal Ga_xS-SWCNT core–shell 1D templates with the outer shell thickness depending on the number of Ga_xS growth cycles. The EELS maps in figures 13(g)–(i) correspond to the boxed region in Figure 13(f), and reveal that the coating is uniform and comprised of Ga and S.

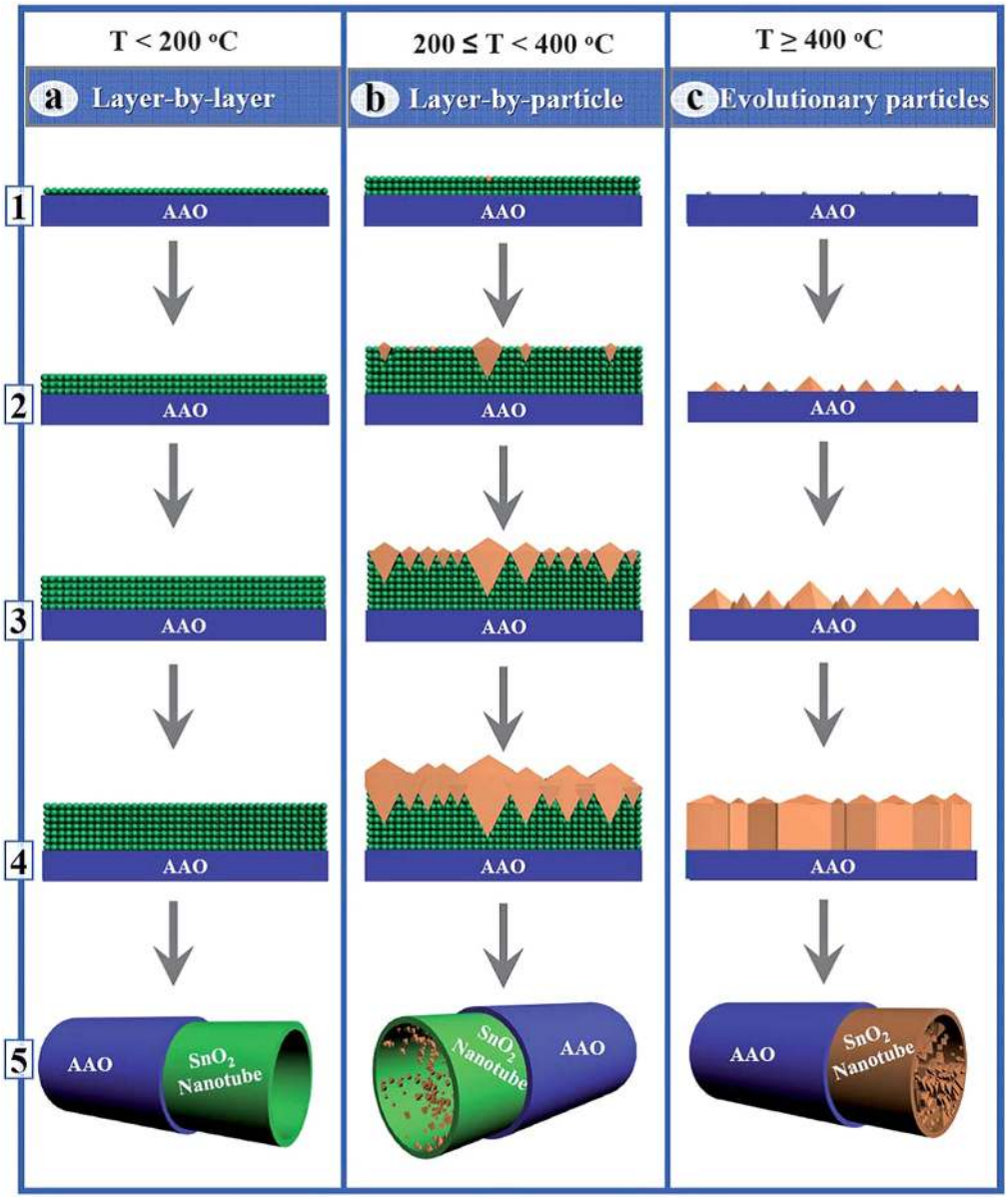

Figure 9. Three growth models for ALD-SnO_2 nanotube arrays. At a temperature lower than 200 °C, the ALD-SnO_2 was built up in AAO pores in a mode of (a) layer-by-layer growth, as schematically shown in (a1-4) with uniform films of increasing thickness; in the range 200 °C–400 °C, the ALD-SnO_2 experienced a mode of (b) layer-by-particle growth: (b1) amorphous layers prevailed at the initial stage but random nucleation happened with increased films, (b2) crystals grew laterally and radially while new nuclei appeared with increased films, (b3) crystals saturated on the surface and amorphous layers stopped growing, (b4) crystals stopped their lateral growth and competed with each other for their radial growth; at a temperature no less than 400 °C, the ALD-SnO_2 transferred to a mode of (c) evolutionary particle: (c1) nuclei formed immediately on the substrate surface at the starting of the ALD process, (c2) crystals grew quickly with increased ALD-cycles, (c3) crystals saturated on the substrate surface, (c4) crystals grew predominantly in their radial direction. In (a5), (b5), and (c5), the produced nanotubes were schematically illustrated. Reprinted with permission from [331]. Copyright (2011) The Royal Society of Chemistry.

3.3. 2D structures

Although ALD is known to be self-limiting, initial nucleation generally occurs through the formation of multi-layer islands which makes it difficult to achieve the layer controllability needed to deposit 2D semiconductors such as transition metal dichalcogenides (TMDs) [345–348]. It is therefore essential to maximize the self-limiting behavior of ALD process in order to achieve the layer controllability needed for 2D structures which requires careful selection of precursors and optimization of process conditions. Initial reports of WS_2 ALD growth employed WF_6 and H_2S reactants where zinc catalyzed the adsorption and reaction of WF_6 [349, 350]. In later reports, single crystal WS_2 nanosheets on SiO_2 substrates were synthesized by the sulfurization of a WO_3 film prepared by ALD. Utilization of ALD for preparation of WO_3 meant that WS_2 layers retained inherent characteristics of ALD processes such as thickness controllability, reproducibility, high conformality, and uniformity [351, 352]. MoS_2 thin films were deposited by ALD using $Mo(CO)_6$ and H_2S plasma as precursors which resulted in hexagonal nanocrystalline films [346]. In another report, $MoCl_5$ and H_2S were employed to grow MoS_2 where

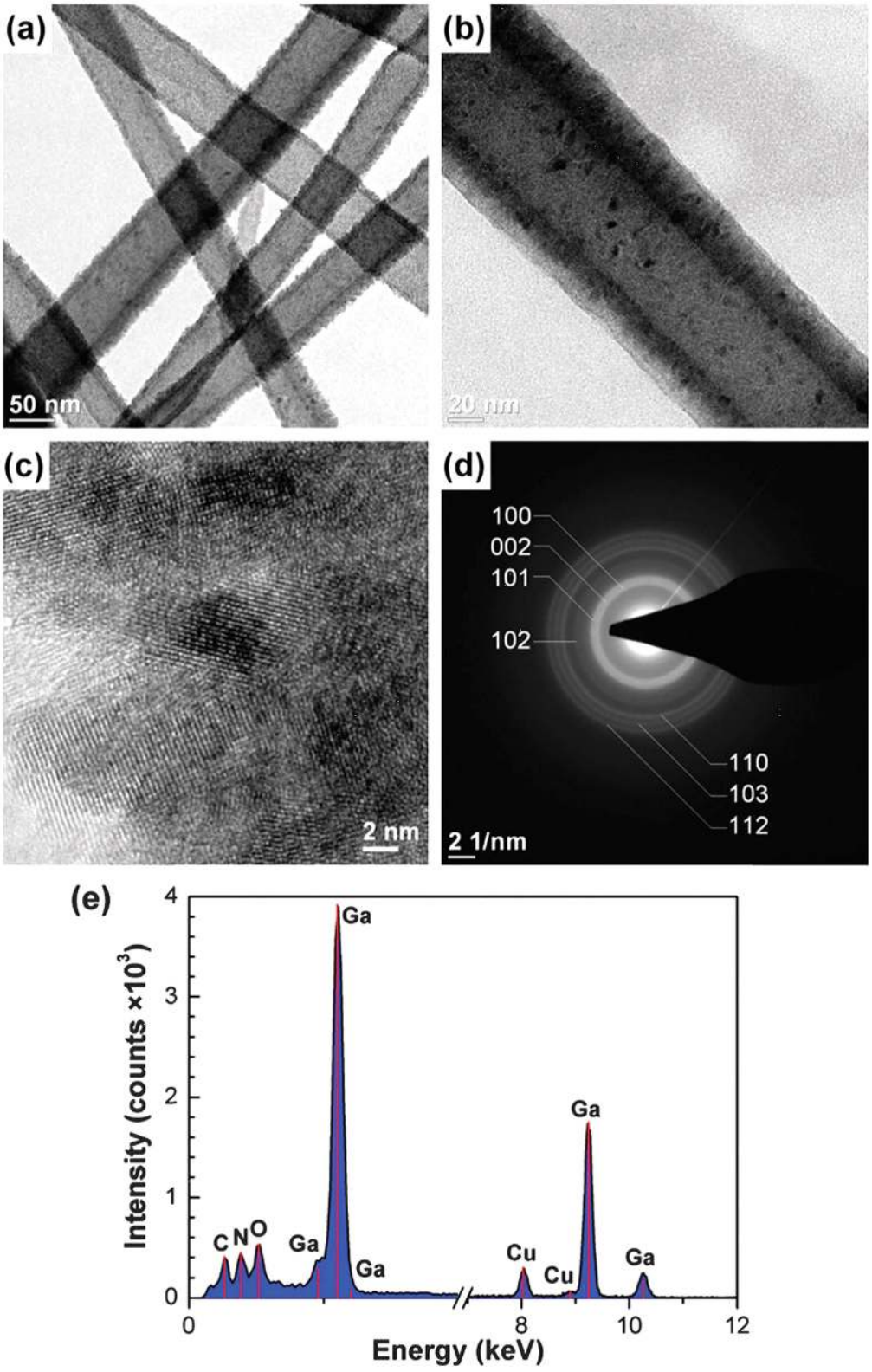

Figure 10. Representative (a) and (b) TEM, (c) high-resolution TEM images, (d) selected area electron diffraction (SAED) pattern, and (e) EDX spectrum of nylon–GaN core–shell nanofiber(s). Reproduced with permission from from [285]. Copy right (2015) The Royal Society of Chemistry.

number of layers formed were controlled by varying the growth temperature [348]. It is believed that lack of dangling bonds on MoS_2 surface caused the growth to self-terminate after few layers of MoS_2 have been grown at a certain temperature [348].

Recently, low temperature (400 °C) growth of graphene has also been demonstrated using PEALD [353]. Hexagonal carbon rings and carbon atoms were observed (figure 14) using aberration-corrected transmission electron microscopy which indicated highly crystalline structure of graphene.

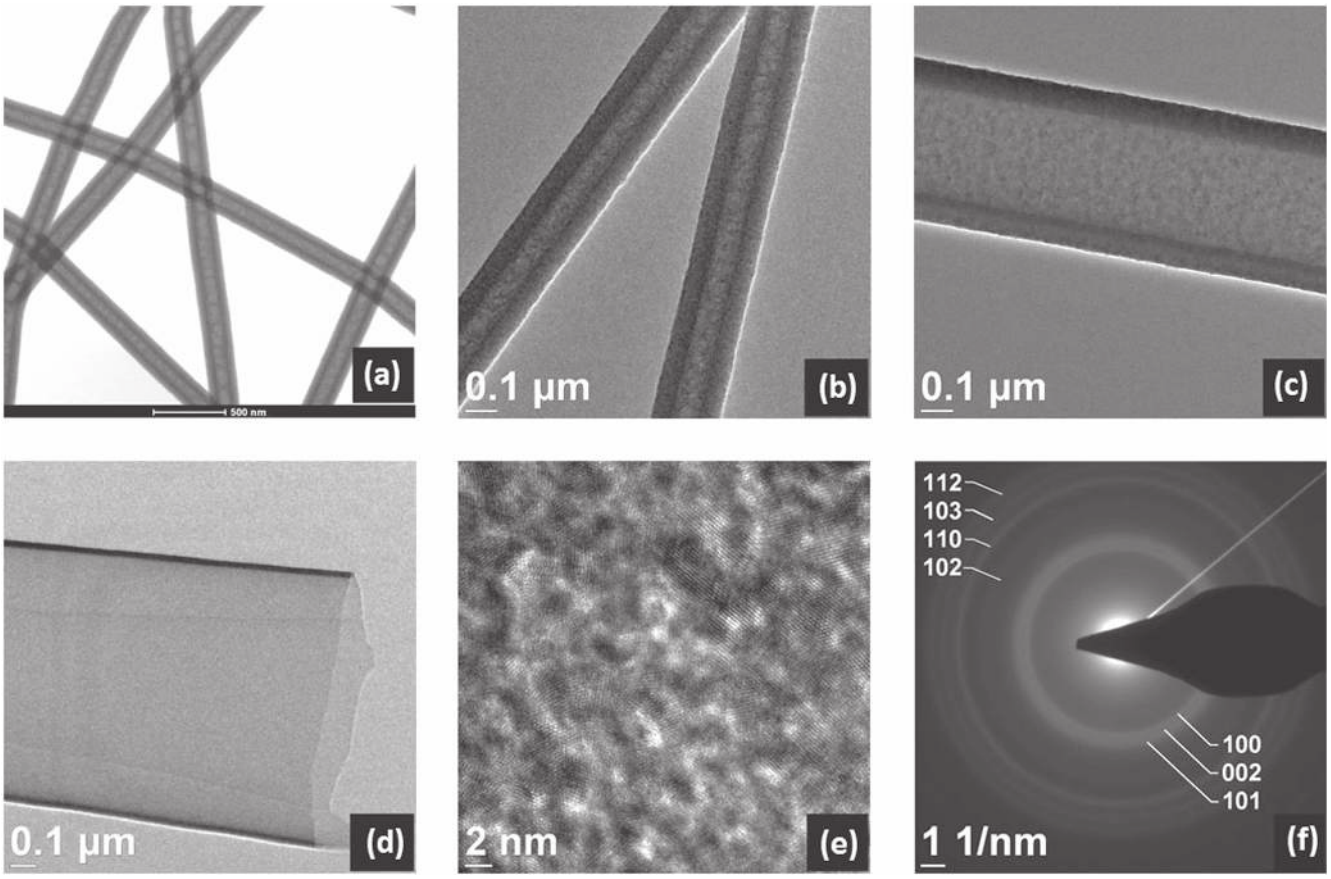

Figure 11. AlN hollow nanofibers synthesized by the deposition of 800 cycles AlN, followed by *in situ* calcination. (a) Bright field TEM image of hollow nanofibers synthesized using nylon 6,6 template having an average fiber diameter of ∼70 nm. (b)–(d) TEM images of hollow nanofibers synthesized using templates with average fiber diameters of ∼70, ∼330, and ∼740 nm, respectively. (e) High-resolution TEM image, and (f) SAED pattern of AlN hollow nanofibers synthesized using a template having ∼330 nm average fiber diameter. Reprinted with permission from [333]. Copyright (2013) John Wiley and Sons.

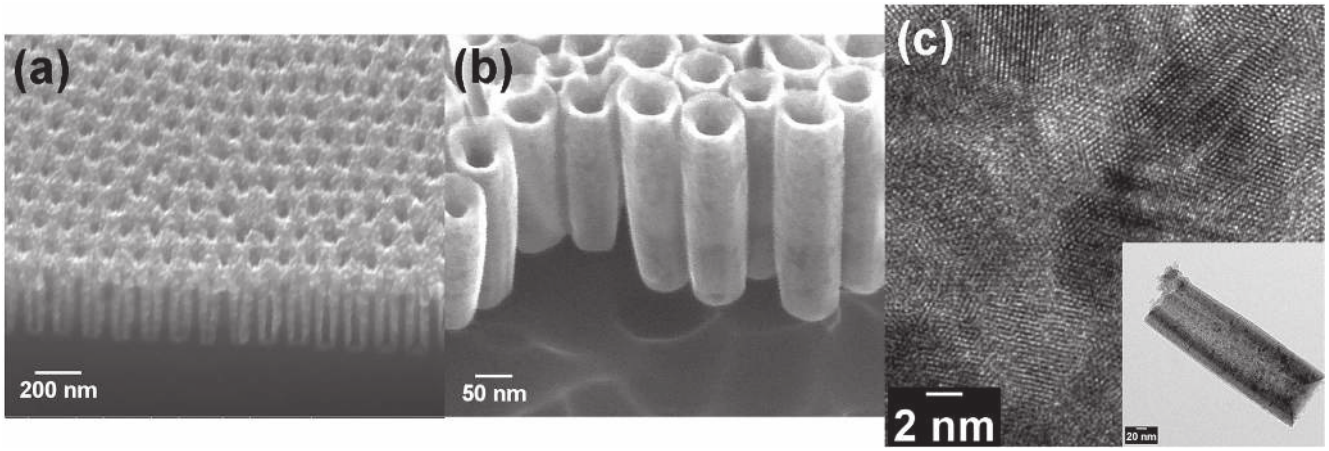

Figure 12. (a) SEM image of conformally coated GaN on porous Si structure using PEALD. (b) SEM image of GaN hollow nano-cylinders obtained after RIE etching of top GaN layer and surrounding Si substrate material. (c) High-resolution TEM image of GaN nano-cylinder, (Inset) TEM image of a single GaN hollow nano-cylinder.

Benzene is chosen as the carbon source and authors demonstrated that benzene molecules can be dehydrogenated and connected to each other to form the graphene structure [353]. An overview of semiconductor 2D nanostructures synthesized using ALD is presented in table 4.

3.4. Core–shell structures

Core–shell structures are formed when a 0D or 1D nanostructure, such as a nanoparticle or nanorod is coated with a thin layer of another material. Such core–shell nanostructures

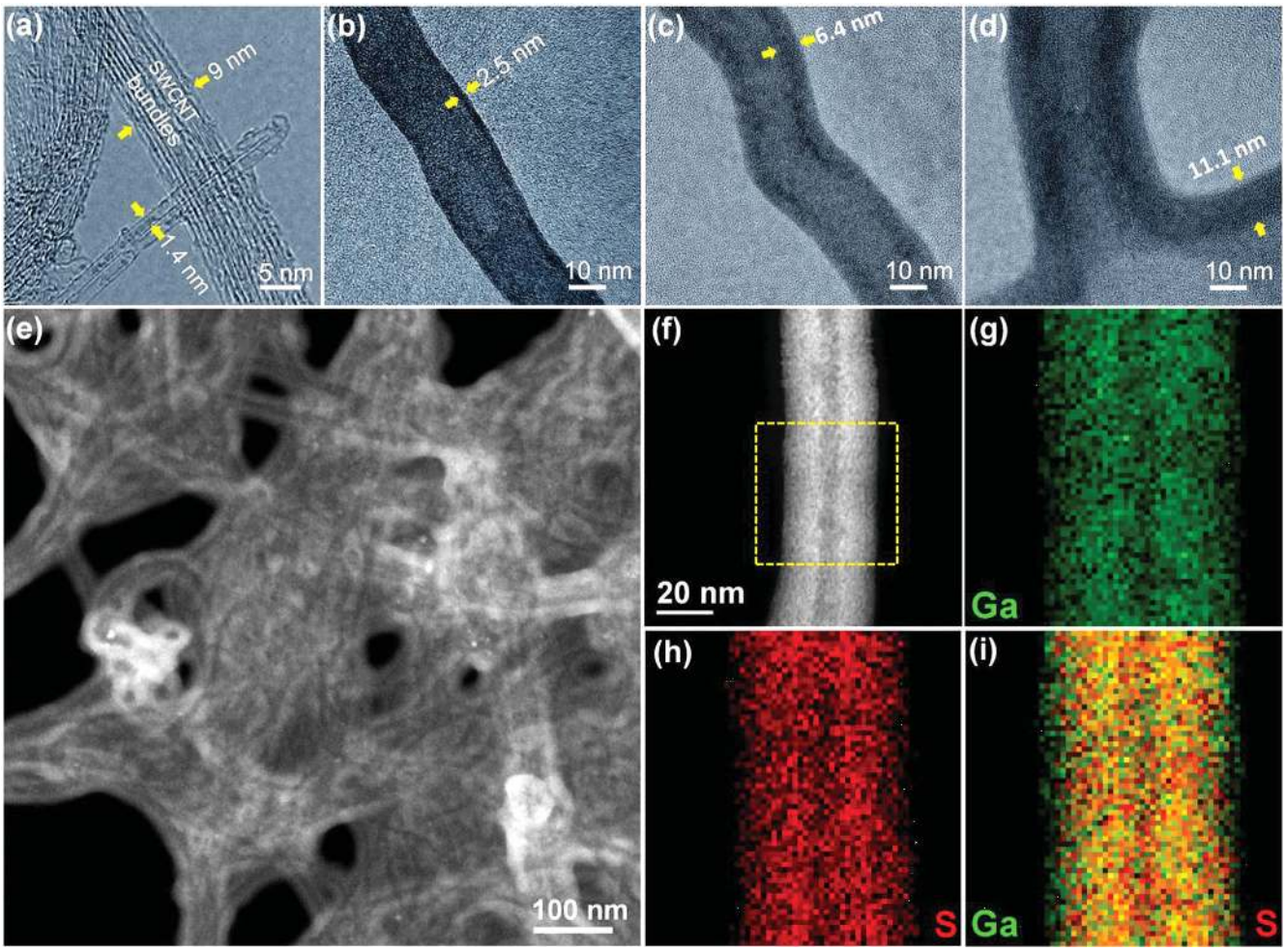

Figure 13. TEM (a)–(d) and STEM (e)–(i) images of: (a) SWCNTs and their bundles; SWCNTs coated by (b) 50-cycle, (c) 100-cycle, and (d) 150-cycle ALD GaS_x; (e), (f) ADF-STEM images; and STEM-EELS mapping of (g) gallium, (h) sulfur, and (i) both gallium and sulfur. Reprinted with permission from [336]. Copyright (2014) John Wiley and Sons.

might show enhanced material properties when compared to the core-only nanostructure, which provide significant potential for numerous applications

ALD of ZnO has been implemented to coat particles of Si [358], SiO_2 [359–362], TiO_2 [363], and Al_2O_3 [364] for applications in photocatalysis. A viscous flow or fluidized bed reactor configuration is suitable for coating nanoparticles using ALD. More commonly, ALD of ZnO has been performed on 1D structures such as nanorods, nanotubes, nanofibers, and nanowires made of Si or SiO_2 [365–372], SnO_2 [373–376], TiO_2 (figure 15) [377], and Al_2O_3 [378, 379]. Alternatively, ALD of TiO_2 has been performed on ZnO nanofibers (figure 15) to produce TiO_2–ZnO core–shell nanofibers [377]. Generally, the fabrication of these structures are more application centered and concentrated on photoluminescence and chemo-resistive properties of the fabricated nanostructures [358, 361, 368, 369, 378, 379]. Typically, 1D core part of these structures is prepared using alternative techniques such as hydrothermal or vapor liquid solid (VLS) growth due to the relative difficulty of fabricating 1D structures directly with ALD [362, 363, 365, 367, 370, 373, 376, 380–383]. Taking advantage of high conformality and uniformity of ALD coatings, shell portions of these structures are commonly grown using ALD [368, 375, 382, 384–386]. AlN/BN core shell hollow nanofibers (HNFs) (figure 16) have been synthesized by successive ALD of AlN and low temperature sequential CVD of BN on electrospun nylon polymer nanofibrous templates [284]. Material characterization showed that crystalline BN/AlN nanofibers were fabricated with relatively low impurity content. The nanoneedle-like 3D morphology of BN ALD-coating is particularly noteworthy in this study [284]. Overview of core–shell nanostructures prepared inpart or totally by ALD is provided in table 5.

4. Applications of ALD-grown nanostructured semiconductors

Material/crystalline properties of low-temperature ALD-grown thin-film semiconductors are considerably weaker than high-temperature epitaxial counterpart films grown via MOCVD, CVD, MBE, etc. Therefore, its quite hard for ALD-grown semiconductor films to compete with epitaxial films in terms of device performance. Despite this drawback,

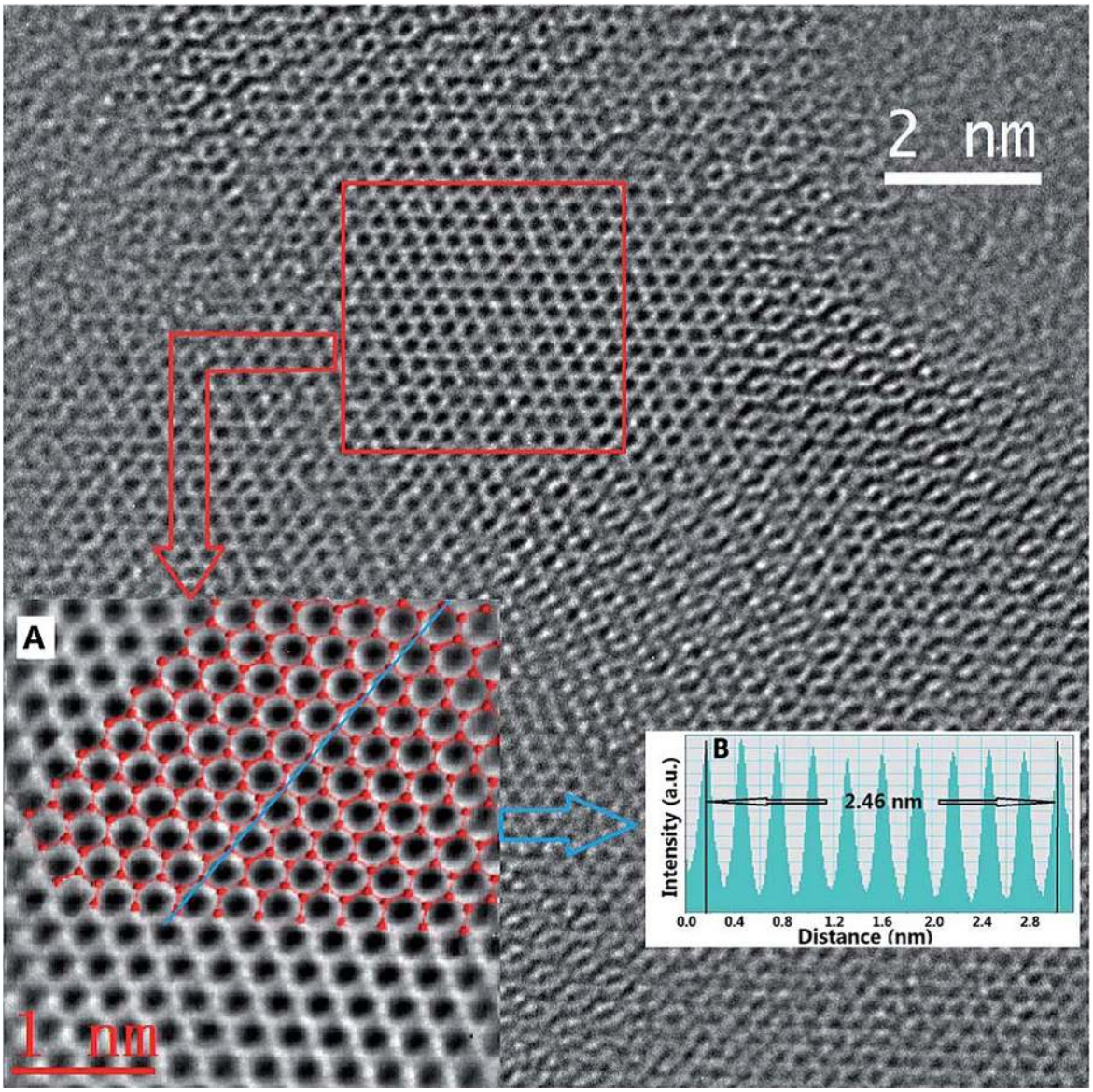

Figure 14. High-resolution images of the graphene deposited by 10 ALD cycles. The atomic-resolution image was obtained using an FEI Titan G2 60–300 at an acceleration voltage of 300 kV (the scale bar is 2 nm). Inset (A): filtered image of the area within the red rectangular frame. Inset (B): pixel intensity profile of the graphene along the blue line in inset (A), which was used to calculate the distance between the second-nearest neighboring carbon atoms in the hexagonal carbon rings using the Digital Micrograph software. Reprinted with permission from [353]. Copy right (2014) The Royal Society of Chemistry.

ALD-grown thin-film semiconductors might find use particularly in applications where low-temperature deposition is critical. Flexible electronics is such a field which can be utilized in wearable and implantable devices including chemical and optical sensors, active matrix displays with integrated thin-film transistors (TFT), etc. ZnO and GaN have been the main materials of choice for the development of ALD-grown active device layers for TFT, photodetector, and sensors [397–401].

On the other hand, as overviewed in section 3, ALD is an attractive method for the fabrication of complex and high-surface area 0D, 1D, 2D, and core–shell nanostructures which can be hardly accomplished via conventional high-temperature epitaxial growth techniques. For this reason, in this part, we would like to overview the device applications where only nanostructured semiconductors grown/fabricated by ALD are utilized. Among various device applications demonstrated in literature based on nanostructured semiconductors, energy storage, catalysis, photocatalysis, solar cells, opto-electronics, and chemical sensing constitute the vast majority of reports.

4.1. Energy storage

Many of the deficiencies of Li-ion batteries such as limited power density, storage capacity, and slow charging/discharging can be alleviated to certain extent by nanostructuring the electrode which can implicate shorter Li^+ and electron diffusion paths. By having a large contact area with the electrolyte (low thickness) and/or the current collector may allow the use of materials with low conductivity which will result in high power capability. Besides, certain nano-scale

Table 4. Overview of the growth conditions employed to synthesize 2D nanostructures using ALD. The materials deposited, the morphology, precursors used, the temperature during ALD, and preparation method are mentioned.

Material	1st precursor	2nd precursor	Growth temperature	Morphology	Preparation method	References
MoS_2	Molybdenum hexacarbonyl ($Mo(CO)_6$)	H_2S	120 °C–200 °C	Nanosheets	ALD of MoS_2 on Si	[354]
	$Mo(CO)_6$	H_2S	175 °C–225 °C	Nanosheets	ALD of MoS_2 on SiO_2	[346]
	$MoCl_5$	H_2S	475 °C	Nanosheets	ALD of MoS_2 on SiO_2/Si and quartz	[355]
	$MoCl_5$	H_2S	350 °C–450 °C	Nanosheets	ALD of MoS_2 on SiO_2/Si	[347]
	$MoCl_5$	H_2S	500 °C–900 °C	Nanosheets	ALD of MoS_2 on SiO_2/Si	[348]
	$Mo(CO)_6$	Dimethyl disulfide	100 °C	Nanosheets	ALD of MoS_2 on Carbon fiber papers and Si	[356]
	$Mo(NMe_2)_4$	$(HS(CH_2)_2SH)$	50 °C followed by annealing	Nanosheets	ALD of MoS_2 on SiO_2/Si and silica nanoparticles	[345]
WS_2	WF_6	H_2S	300 °C–350 °C	Nanosheets	ALD of WS_2 on Si, SiO_2, stainless steel, and polycrystalline Si	[350]
	WF_6	H_2S	250 °C–300 °C	Nanosheets	ALD of WS_2 on Rolling element bearing	[349]
	$WH_2(iPrCp)_2$	O_2	300 °C followed by sulfurization of WO_3	Nanosheets	ALD of WS_2 on SiO_2/Si substrates	[351]
	$WH_2(iPrCp)_2$	O_2	300 °C followed by sulfurization of WO_3	Nanosheets	ALD of WS_2 on SiO_2/Si substrates	[352]
	Bis(tert-butylimido)-bis(dimethylamido) tungsten $(((tBuN)_2(Me_2N)_2W))$	O_2	150 °C followed by CS_2 vulcanization	Nanosheets	ALD of WS_2 on Quartz	[357]
Graphene	Benzene	H_2	400 °C	Layer of graphene	ALD of graphene on Cu foil	[353]

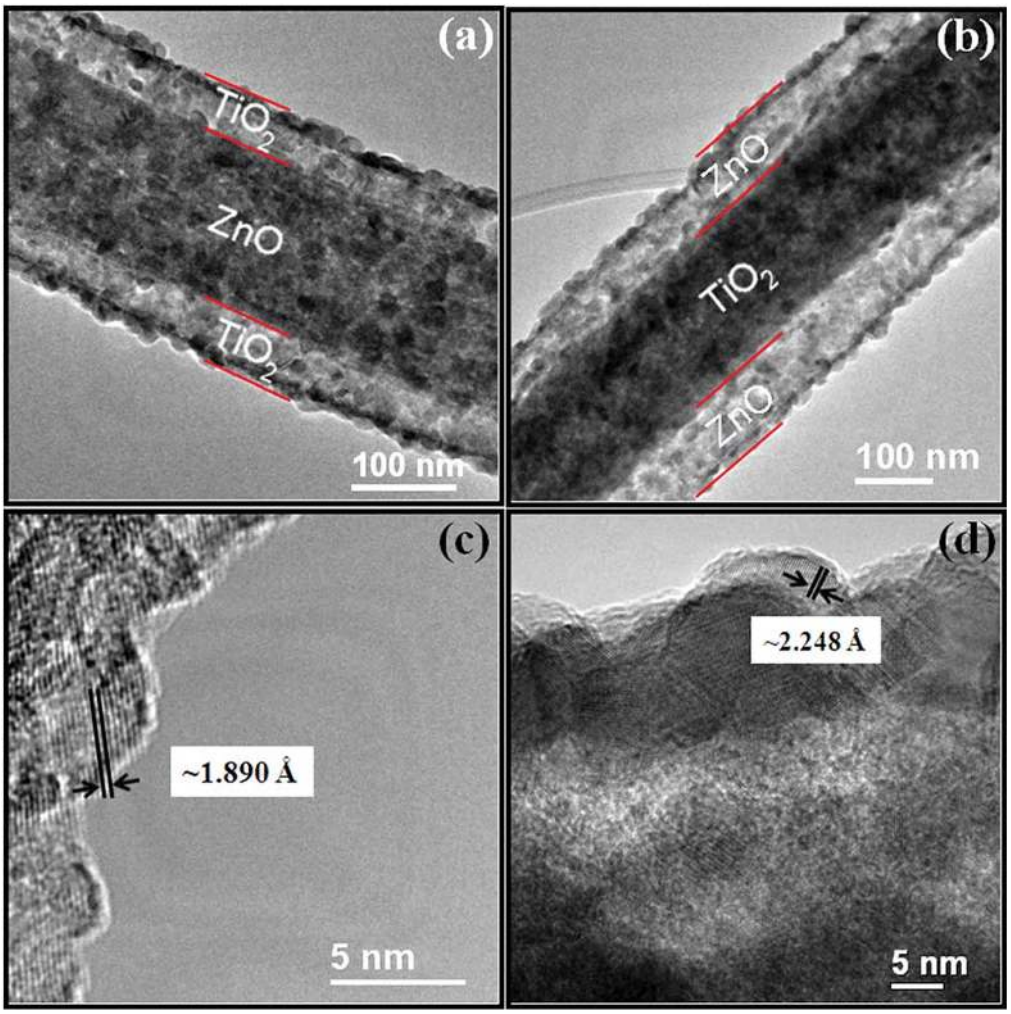

Figure 15. Representative TEM images of the core–shell heterojunction nanofibers (a) ZnO–TiO_2, (b) TiO_2–ZnO; (c) and (d) HRTEM images of the 'shell' regions of (a) and (b), respectively. Reprinted with permission from [377]. Copy right (2014) The Royal Society of Chemistry.

quantum-size effects can increase the electrode storage capacity as well. Moreover, nanostructured electrodes can withstand stresses due to volume expansion and contraction which enables enhanced reversible cycling of the electrode material [404–408].

As described in previous sections, ALD with its conformal growth mechanism, can be effectively used to produce nanostructures via template-assisted strategy. Such nanostructures can then be used as electrode materials to enhance the energy storage capacity of Li-ion and other alternative (Li–O_2, Li-polymer, Li-air, etc) batteries. Conformal and ultra-thin ALD-grown coatings can also be used as electrode protection/passivation layers to reduce electrolyte decomposition on the surface of the electrode and dissolution of electrode material into the electrolyte [415–418]. Some examples from the literature are presented in this section.

Battery application of ALD nanocoatings was first demonstrated in energy storage devices using particle based electrodes where TiN was coated on $Li_4Ti_5O_{12}$ aimed for improving inter-particle electrical conductivity [402]. The film in this study was quite thin (~6 nm) and therefore, did not cause any performance problems with Li^+ ion diffusion process [402]. ALD has also assisted in making composite nanoparticle electrodes for Li-ion batteries. In one such report, SnO_2/graphene nanosheets composite electrode was fabricated by performing SnO_2 ALD on graphene nanosheet powder [403]. ALD-grown TiO_2 has also been employed in Li-ion batteries [404, 405]. TiO_2 has been used as an anode material and features the advantage of relatively high redox potential [392, 406–414]. TiO_2 was coated on peptide nanofibers followed by calcination at high temperature which removed peptide material as well as crystallized the TiO_2 to anatase phase [405]. The resulting TiO_2 hollow nanonetwork demonstrated higher storage capacity and charge rate performance (figure 17) when compared with TiO_2 nanopowder electrodes, which was attributed to prominent nanosize effects in TiO_2 nanonetwork [405]. In another study, TiO_2 coated on Au nanoparticles was utilized as Li ion battery anode material (figure 18) [413]. Power performance of the electrode improved with the decrease in TiO_2 thickness by reducing the

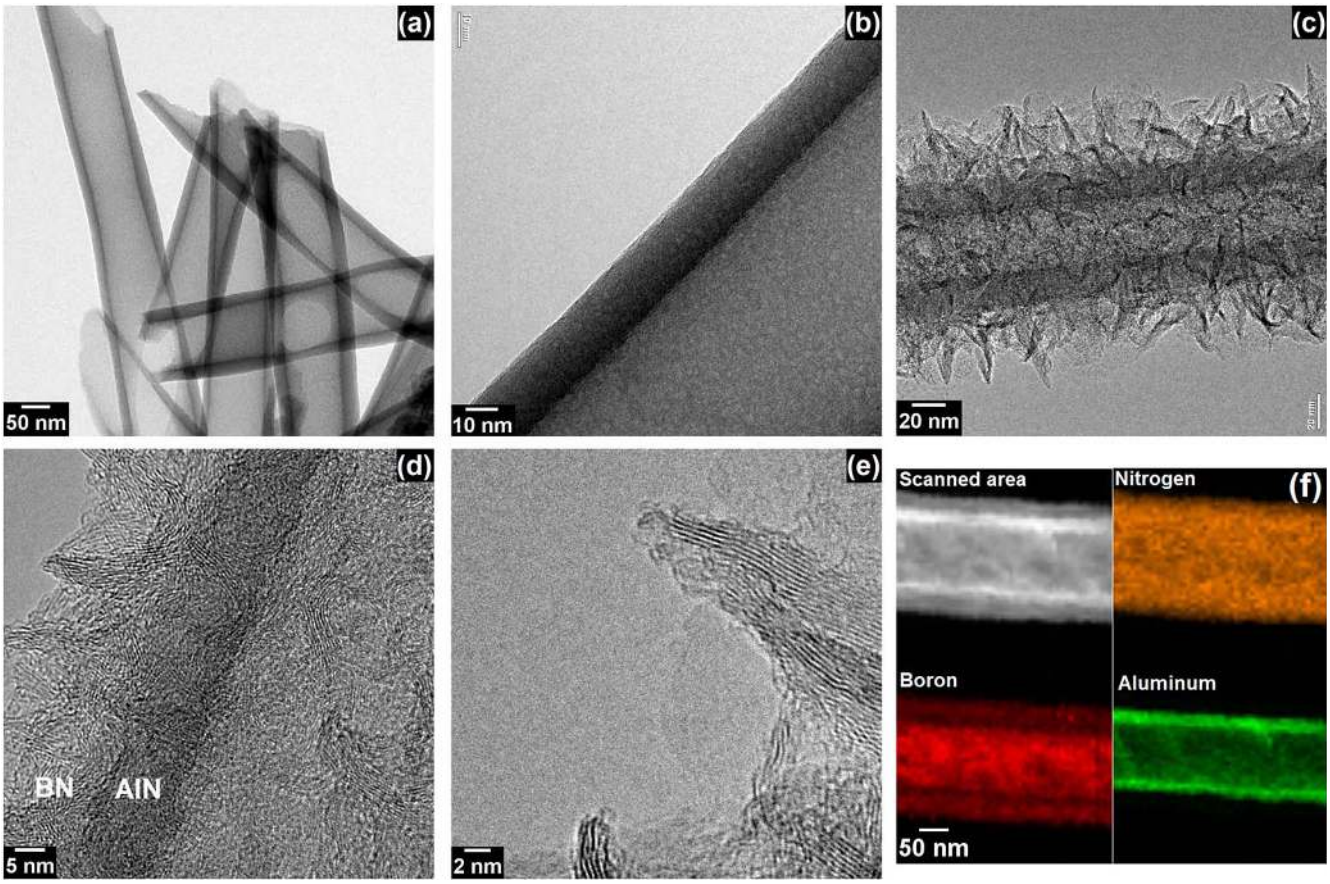

Figure 16. (a) and (b) Representative bright field TEM images of AlN HNFs. (c) and (d) Representative bright field TEM images of AlN/BN bishell HNF having an average inner fiber diameter of ~100 nm with an average wall thickness of ~20 nm and ~35 nm of AlN and BN, respectively. (e) Representative HR-TEM image of AlN/BN bishell HNF. (f) EDX elemental map of aluminum, boron, and nitrogen from an individual AlN/BN HNF. Reprinted with permission from [284]. Copyright (2014) AIP publishing.

Li^+ diffusion pathway, enhancing the Li^+ solid solubility, and minimizing the voltage drop across the electrode/electrolyte interface (figure 19) [413].

For Li–S batteries, ALD has been used to develop a 3D structured thin TiO_2 shell which acts as a cathode material and provides high electronic and ionic conductivity [415]. An inverse opal structure has been formed which aids against polysulfide dissolution due to O_2 vacancies which facilitate S–Ti–O interactions. These oxygen vacancies were created from reduction of TiO_2 with hydrogen [415]. Polysulfide dissolution or shuttle effect is a common problem with Li–S batteries where polysulfides react with Li metal at electrode to form lower order polysulfides. This phenomena leads to the formation of a high-impedance solid–electrolyte interface (SEI) layer that consumes the electrolyte and active material and causes anode decay eventually leading to battery cell failure.

TiN and TaN grown using remote plasma ALD have been applied in 3D all-solid-state micro-batteries as Li diffusion barrier layers [416, 417]. The Li diffusion barrier properties of ALD TiN was significantly better than sputtered TiN barriers. ALD grown TiN in Si pores was shown to behave as excellent barrier layer and current collector [418]. In that study, low pressure chemical vapor deposition (LPCVD) grown Si was used as an anode material and was coated with ALD TiN to serve as Li barrier and current collector [418]. ALD grown V_2O_5 was demonstrated to be a good alternative cathode material [419]. Especially, the V_2O_5 annealed at 400 °C offered excellent electrochemical stability and cyclability for Li^+ ions [419]. ALD grown Co_3O_4 was shown to be a decent anode material as well where good cycling performance and high storage capacity were obtained in electrochemical tests [420].

4.2. Photocatalysis

Hydrogen produced from water splitting is a potentially clean fuel with its high energy density and environmental friendliness. Production of hydrogen from water splitting needs an external energy source and solar energy is an attractive choice, forming a complete renewable energy cycle. Photoelectrochemical splitting of water on semiconductor electrode materials (n-type TiO_2) is an efficient and inexpensive way of producing clean hydrogen fuel [421–430]. The major challenges in this research field range from reactor design to the discovery of novel high-surface area nanostructured materials that can achieve decent activity levels [421–430]. ALD has played a significant role in fabricating a large variety of nanostructured semiconductor materials for applications in photocatalysis.

Table 5. Overview of the growth conditions employed to synthesize core–shell nanostructures using ALD. The materials deposited, the morphology, precursors used, the temperature during ALD, and preparation method are mentioned.

Core–shell Materials	Precursors for 1st material	Precursors for 2nd material	Growth temperature	Morphology	Preparation method	References
ZnSe–CdSe	Elemental Zn and Se	Elemental Cd and Se	400 °C–420 °C	Nanowires	Growth initiation using gold nanoparticles and the vapor–liquid–solid mechanism	[387]
ZnO–ZrO_2	$Zn(CH_2CH_3)_2$ and H_2O	—	177 °C	Nanoparticles	ZnO growth on ZrO_2 nanoparticles	[388]
ZnO–$BaTiO_3$	$Zn(CH_2CH_3)_2$ and H_2O	—	177 °C	Nanoparticles	ZnO growth on $BaTiO_3$ nanoparticles	[388]
SiO_x–ZnO	$(C_2H_5)_2Zn$ and H_2O	SiO_x growth through CVD	170 °C	Nanowires	ZnO shell layer growth on SiO_x nanowires	[365]
ZnO–SiO_2	$(C_2H_5)_2Zn$ and H_2O	Commercially purchased SiO_2 particles	177 °C	Nanoparticles	ZnO growth on SiO_2 nanoparticles	[362]
ZnO–TiO_2	$(C_2H_5)_2Zn$ and H_2O	Commercially purchased TiO_2 particles	177 °C	Nanoparticles	ZnO growth on TiO_2 nanoparticles	[362]
ZnO–TiO_2	$(C_2H_5)_2Zn$ and H_2O_2	Commercially purchased TiO_2 nanopowder	50 °C, 100 °C, and 177 °C	Nanoparticles	ZnO growth on TiO_2 particles	[363]
ZnO–polystyrene (PS)	$Zn(CH_2CH_3)_2$ and H_2O	—	80 °C and 90 °C	Nanocrystals	ZnO growth on monodisperse PS colloidal nanospheres	[380]
ZnO–SnO_2	$(C_2H_5)_2Zn$ and H_2O	SnO_2 nanofibers prepared by electrospinning	150 °C	Nanofibers	ZnO growth on SnO_2 nanofibers	[373]
TiO_2–ZnO	$(C_2H_5)_2Zn$ and H_2O	TiO_2 nanofibers prepared by electrospinning	150 °C	Nanofibers	ZnO growth on TiO_2 nanofibers	[381]
Bi_2O_3–ZnO	$(C_2H_5)_2Zn$ and H_2O	Thermal evaporation of Bi_2O_3 nanowires		Nanowires	ZnO growth on Bi_2O_3 nanowires	[383]
ZnO–Si	$(C_2H_5)_2Zn$ and H_2O	Si nanowires growth using CVD	25 °C	Nanowires	ZnO growth on Si nanowires	[367]
$CoFe_2O_4$–TiO_2	Titanium Isopropoxide and acetic acid	Directed assembly of colloidal $CoFe_2O_4$ in a Langmuir–Blodgett monolayer	200 °C	Nanoparticles/film composites	TiO_2 growth on $CoFe_2O_4$ nanoparticles/film composites	[384]
$CoFe_2O_4$–ZnO	$(C_2H_5)_2Zn$ and H_2O	Directed assembly of colloidal $CoFe_2O_4$ in a Langmuir–Blodgett monolayer	70 °C	Nanoparticles/film composites	ZnO growth on $CoFe_2O_4$ nanoparticles/film composites	[384]
ZnTe–ZnO	$(C_2H_5)_2Zn$ and H_2O	ZnTe nanowires growth using gold catalyzed vapor–liquid–solid mechanism	60 °C, 100 °C, 150 °C and 200 °C	Nanowires	ZnO growth on ZnTe nanowires	[382]
ZnO–Si	$(C_2H_5)_2Zn$ and H_2O	Si nanopillars fabricated by self-masking dry etching in hydrogen-containing plasma	200 °C	Nanopillars	ZnO growth on Si nanopillars	[370]

Table 5. (Continued.)

Core–shell Materials	Precursors for 1st material	Precursors for 2nd material	Growth temperature	Morphology	Preparation method	References
ZnMnTe/ZnO	$(C_2H_5)_2Zn$ and H_2O	ZnMnTe nanowires fabricated through MBE technique using gold-catalyzed vapor– liquid–solid mechanism.	200 °C, 250 °C, and 300 °C	Nanowires	ZnO growth on ZnMnTe nanowires	[389]
ZnO–SnO_2	$SnCl_4$ and H_2O	ZnO nanorods prepared by thermal evaporation	350 °C	Nanorods	SnO_2 growth on ZnO nanorods	[376]
ZnO–Al_2O_3	$Al_2(CH_3)_6$ and H_2O	ZnO nanorods synthesized by aqueous chemical route	180 °C	Nanorods	Al_2O_3 growth on ZnO nanorods	[385]
ZnO–ZnO	$(C_2H_5)_2Zn$ and H_2O	ZnO nanorods synthesized by aqueous chemical route	180 °C	Nanorods	ALD ZnO growth on ZnO nanorods	[385]
ZnO–Si	$(C_2H_5)_2Zn$ and H_2O	Si nanopillars obtained by dry etching using silver nanodots as mask	200 °C	Nanopillars	ZnO growth on Si nanopillars	[371]
ZnO–SiO_2	$(C_2H_5)_2Zn$ and H_2O	Silica nanosprings grown using vapor liquid solid mechanism	175 °C	Nanosprings	ZnO growth on silica nanosprings	[368]
ZnO–SnO_2	$(C_2H_5)_2Zn$ and H_2O	SnO_2 nanowires growth via vapor liquid solid mechanism	150 °C	Nanorods	ZnO growth on SnO_2 nanorods	[375]
ZnO–SnO_2	$(C_2H_5)_2Zn$ and H_2O	SnO_2 nanowires growth via vapor liquid solid mechanism		Nanowires	ZnO layer growth on SnO_2 Nanowires	[386]
ZnO–Si	$(C_2H_5)_2Zn$ and H_2O	Si nanotips fabrication using high-density electron cyclotron resonance (ECR) plasma etching	90 °C	Nanotips	ZnO layer growth on Si Nanotips	[372]
SnO_2–TiO_2	$TiCl_4$ and H_2O	Rod-like SnO_2 Particles prepared through a basic synthetic route.	300 °C	Nanoparticles	TiO_2 grown on SnO_2 particles	[390]
ZnO–Si	$(C_2H_5)_2Zn$ and H_2O	Si nanowires fabrication through electroless metal deposition	50 °C	Nanowires	ZnO growth on Si nanowires	[369]
ZnO–$ZnSnO_4$	$(C_2H_5)_2Zn$ and H_2O	Synthesis of Zn_2SnO_4 nanorods through thermal evaporation of a mixture of ZnO, SnO_2, and graphite powders	150 °C	Nanorods	ZnO growth on $ZnSnO_4$ nanorods	[374]
ZnO–Al doped ZnO	$(C_2H_5)_2Zn$, $Al_2(CH_3)_6$, and H_2O	Fabrication of ZnO nanowires using thermal evaporation	150 °C	Nanowires	Al-doped ZnO growth on ZnO nanowires	[378]
ZnO–Cu	$(C_2H_5)_2Zn$ and H_2O	Cu e-beam evaporation	120 °C	Nanoclusters	ZnO growth on Cu nanoclusters	[391]
ZnO–TiO_2	$(C_2H_5)_2Zn$ and H_2O	Tetrakis(dimethylamido)titanium and H_2O	200 °C	Nanofibers	ALD of TiO_2 and ZnO on electrospun polymer fibers	[377]

Table 5. (Continued.)

Core–shell Materials	Precursors for 1st material	Precursors for 2nd material	Growth temperature	Morphology	Preparation method	References
ZnS–CuS	Bis (2,2,6,6-tetramethyl-3,5-heptanedionato)zinc and H_2S	Bis(2,2,6,6-tetramethyl-3,5 heptanedionato)copper and H_2S	200 °C	Multilayer films	ZnS and CuS deposited on top of each other	[180]
TiO_2–SnO_2	Tetrakis(dimethylamino)tin (IV) and H_2O	Titanium(IV) isopropoxide and H_2O	175 °C and 160 °C for SnO_2 and TiO_2 growth, respectively.	Nanotube arrays	TiO_2-SnO_2 nanotubes fabricated using porous alumina membrane template	[392]
ZnO–HfO_2	Hafnium tetrakis(ethylmethylamino) and H_2O	ZnO nanowires prepared through hydrothermal method	200 °C	Nanowires	HfO_2 growth on ZnO nanowires	[393]
ZnO–Al_2O_3	$Al_2(CH_3)_6$ and H_2O	ZnO nanorods prepared through hydrothermal method	100 °C	Nanorods	Al_2O_3 growth on ZnO nanorods	[394]
ZnO–Fe_2O_3	$(C_2H_5)_2Zn$ and H_2O	Thermal oxidation of Fe foils to obtain Fe_2O_3 nanorods	150 °C	Nanorods	ZnO growth on Fe_2O_3 nanorods	[395]
ZnO–TiO_2	$TiCl_4$ and H_2O	$(C_2H_5)_2Zn$ and H_2O	120 °C, 160 °C, 200 °C, or 240 °C	Multilayers	ZnO and TiO_2 deposited on top of each other	[396]
ZnO–TiO_2, TiO_2–ZnO	Tetrakis(dimethylamino)tin (IV) and H_2O	$(C_2H_5)_2Zn$ and H_2O	200 °C	Nanofibers	ZnO ALD on TiO_2 nanofibers or vice versa	[377]
BN-AlN	TMA and N_2/H_2	$(C_2H_5)_3B$ and N_2/H_2	AlN at 100 °C and BN at 450 °C	Nanofibers	AlN growth on polymeric nanofibers followed by BN growth	[284]

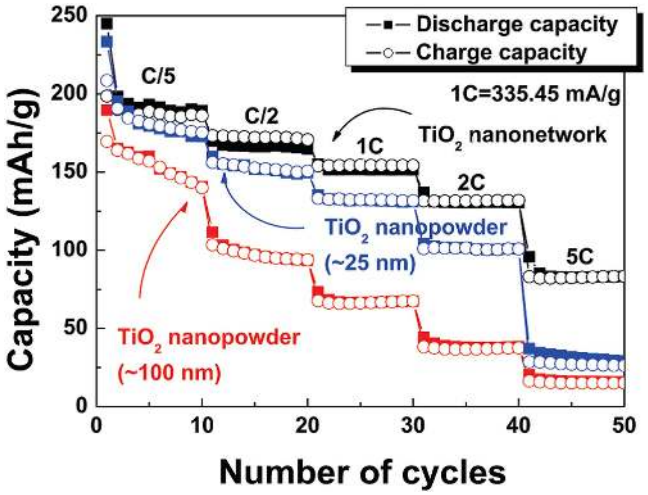

Figure 17. Rate capability of the TiO_2 nanonetwork, the 25 nm- and 100 nm-TiO_2 nanopowders from C/5 to 5 C for 10 cycles. Reprinted with permission from [405]. Copyright (2009) American Chemical Society.

ALD-grown nanostructured TiO_2 and ZnO semiconductors are active materials for applications in photocatalysis for organic dye degradation, photoelectrochemical water splitting, and metal-insulator-semiconductor (MIS) photocatalysts for hydrogen generation [421–430]. A good example features $TiO_2/TiSi_2$ core/shell nanostructures which were fabricated by combining CVD and ALD [431]. High surface area material network was particularly useful in improving photon absorption which in combination with high electrical conductance, provides superior charge transport properties. Photoelectrochemical water splitting was shown with this nanonetwork with a peak efficiency of 16.7% [431]. In another study, CdS/TiO_2 nanotube-array coaxial heterogeneous structures were fabricated and characterized for photocatalytic reactions such as water splitting and degradation of organic pollutants [432]. CdS was deposited conformally on TiO_2 nanotubes using electrochemical ALD; an analog of ALD based on surface limited reactions using under-potential deposition method [432]. The coaxial CdS/TiO_2 hetereostructure significantly enhanced active contact area with electrolyte which reduced the distance that electrons and holes must travel resulting in enhanced photon absorption and photocurrent generation [432]. ALD of hematite was reported on $TiSi_2$ nanonets [433]. The nanonets performed a dual role of structural support and charge collector, allowing for an enhanced photon to charge conversion and resulting in enhanced photocurrents [433].

Paracchino *et al* reported a highly active photocathode for solar H_2 production which consisted of electrodeposited cuprious oxide protected against photocathodic decomposition in water by a thin ALD coating of Al-doped ZnO and TiO_2 [434]. Finally, electrodeposited Pt nanoparticles activated the nanostructures for hydrogen evolution. The electrodes showed photocurrents up to $-7.6\,mA\,cm^{-2}$ at a potential of 0 V versus the reversible hydrogen electrode at mild pH [434].

Pan *et al* fabricated TiO_2 porous structures by depositing TiO_2 on a reticular sponge template followed by a subsequent heat treatment [429]. Annealing of free standing TiO_2 porous structure resulted in phase transition and production of oxygen vacancies [429]. The porous TiO_2 structure demonstrated excellent photocatalytic ability owing to co-action of high surface area, oxygen vacancies, and the optimal crystal structure [429]. Singh *et al* reported design and fabrication of high-surface-area photocatalysts by depositing TiO_2 on fibrous nanosilica (KCC-1) using ALD [427]. Size quantization effects were observed from TiO_2 nanoparticles which were obtained after heat treatment of these ALD-coated samples of KCC-1 [427]. Enhanced photocatalytic activity was observed which was attributed to unique textural properties and morphology of KCC-1 and TiO_2 nanoparticle formation and their size quantization. Zhang *et al* fabricated novel model of MIS photocatalysts for hydrogen generation in the ultraviolet to near-infrared region [421]. The MIS photocatalysts consisted of metal co-catalyst (Pt), electron tunneling layer (ALD grown TiO_2), and photoactive non-stoichiometric core (Ti^{3+} dopedTiO_2 nanocrystal). The MIS photocatalysts exhibited efficient hydrogen generation ($52\,\mu mol\,h^{-1}\,g^{-1}$), good reusability (16 h), and long-term stability (>7 d) [421]. ALD of ZnO was conducted on electrospun nylon 6,6 nanofibers (figure 20) and the core–shell nylon 6,6-ZnO nanofiber mats were utilized as a filtering/membrane material for treatment of organic pollutants for water purification (figure 21) owing to their efficient photocatalytic properties, structural flexibility, and stability [302]. ALD growth cycles numbers were changed to grow either ZnO nanoparticles or a continuous film on electrospun polymeric nanofibers (figure 22) for the fabrication of flexible photocatalytic nanofibrous membranes [295].

4.3. Photovoltaics and optoelectronics

Solar cell device technology have been under continuous development over the past five decades. Their wide spread usage is hindered by two main factors; limited conversion efficiency and high cost. ALD as a conformal thin film coating technique has been extensively utilized for surface passivation and humidity barrier of Si-based solar cells to improve cell efficiency [435]. Here, we will focus on the use of ALD to fabricate semiconductor nanostructures for applications in photovoltaics and optoelectronics.

ALD has been used to fabricate high surface area ZnO nanotube photoanodes using AAO templates for application in dye sensitized solar cells (DSSCs) [436]. ALD was used to coat AAO pores which provides a path for charge collection over tens of micrometer thickness. ZnO nanotube cells showed superior photovoltage and fill factor (FF) as compared to similar ZnO based devices [436]. In another study, ALD was used to deposit ITO in a porous template as a high-surface area photoelectrode, which was sequentially coated with amorphous TiO_2 [437]. Due to radial collection of electrons, this new photoelectrode architecture revealed higher current densities as compared to their counterpart control devices which lack efficient current collection [437]. Hamann *et al* fabricated photoanodes

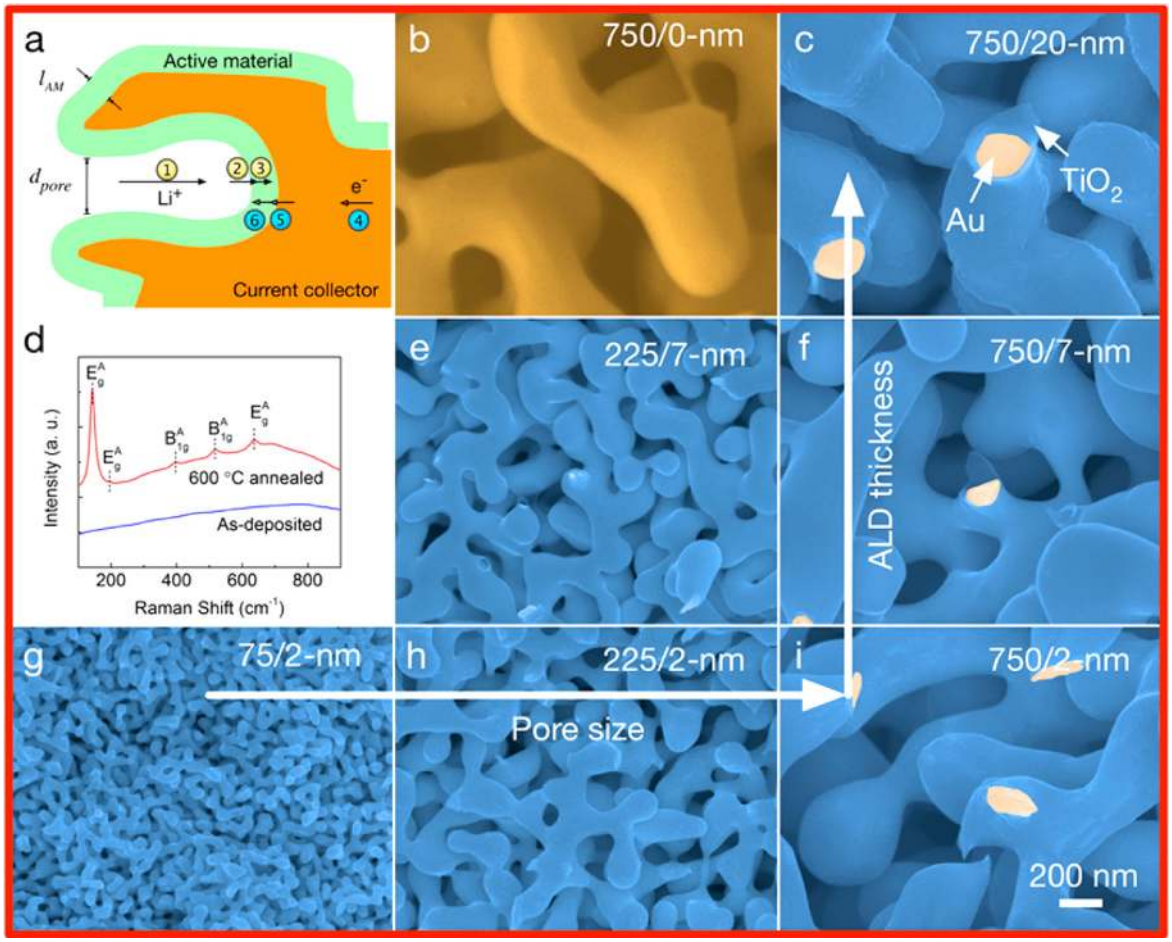

Figure 18. Relevant transport processes and microstructure of 3D np-Au/TiO_2 electrodes for lithium ion batteries. (a) An illustration of relevant transport processes in 3D porous LIB electrodes: (1) Li^+ transport through the electrolyte; (2) charge transfer at the electrolyte/electrode interface; (3) Li^+ transport in the active material; (4) electron transport in the current collector; (5) electron transfer from the current collector to the active material; (6) Li^+/electron recombination. (b) Scanning electron micrograph (SEM) of np-Au with a pore size of 750 nm. (c), (e)–(i) SEM images of TiO_2 ALD coated np-Au samples after annealing at 600 °C for various pore size (75, 225, and 750 nm) and TiO_2 film thickness (2, 7, and 20 nm). All SEM images were taken at the same magnification. (d) Raman spectra from a TiO_2-coated np-Au sample measured before and after annealing at 600 °C revealing the phase transition from as-deposited amorphous TiO_2 to anatase. Reprinted with permission from [413]. Copyright (2015) American Chemical Society.

using high surface area mesoporous aerogel thin films as templates [438]. ZnO with a controlled variable thickness was conformally deposited on aerogels using ALD [438]. The electrodes used in DSSCs showed enhanced light harvesting and power conversion efficiency compared to other ZnO based DSSCs. Owing to its ease of fabrication, flexibility of design, and excellent initial performance, ALD-coated aerogel-based photoanodes are promising alternatives to nanoparticle based electrodes in DSSCs [438]. In another report, Park *et al* fabricated ZnO nanocrystallites coated with ultrathin TiO_2 ALD layer to increase the power conversion efficiency of DSSCs [438]. TiO_2 layer increased both FF and open circuit voltage as a result of decreased surface charge recombination without compromising on photocurrent density [438]. Foong *et al* employed a liquid-phase atomic layer deposition (LALD) process to coat TiO_2 in porous anodic alumina templates followed by alumina dissolution for application in hybrid solar cells [439]. The LALD overcomes the vacuum conditions needed in conventional gas phase ALD and provides yet an ALD-like GPC and high conformality [439]. The viability of TiO_2 nanotube arrays grown on indium tin oxide (ITO)–glass electrodes was also examined for use in model hybrid poly(3-hexylthiophene) (P_3HT):TiO_2 solar cell devices [439].

Chandiran *et al* fabricated mesoscopic photoanodes for solid-state perovskite absorber solar cells by employing ALD grown TiO_2 overlayer on the mesoporous nanoparticle TiO_2 films [440]. The nanoparticle-TiO_2-ALD TiO_2 film is infiltrated with perovskite absorber. Authors showed that their structured photoanodes block electron recombination effectively and it overrides the commonly used multi-step passivation prevailing in the DSC community [440]. Observations revealed that even a 2 nm thick TiO_2 can impede the electron back reaction effectively from FTO and TiO_2 surface

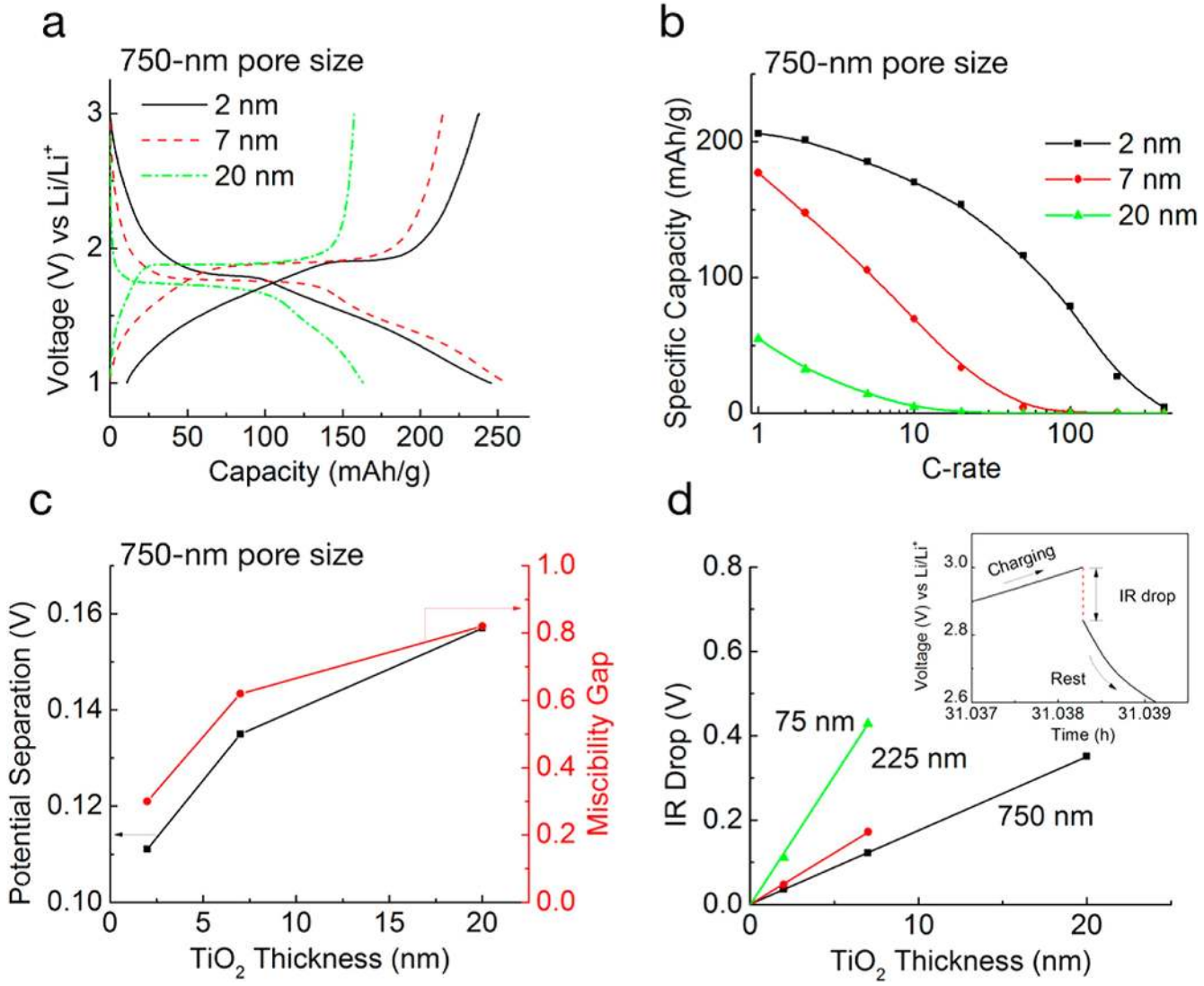

Figure 19. Effect of the TiO_2 layer thickness on (a) charge/discharge voltage profiles (measured at 0.1 C) and (b) the rate performance of nanoparticle-Au/TiO_2 electrodes with 750 nm pores. (c) Potential separation and miscibility gap measured at 0.1 C as a function of the TiO_2 layer thickness. (d) IR drop/TiO_2 layer thickness dependency for various pore sizes measured by the current interrupt method. The inset shows a typical charge-rest-discharge voltage profile collected from a 750/7 nm sample (charge/discharge at 10 C, interrupted at 3 V). Note the linear correlation between IR drop and TiO_2 layer thickness. Reprinted with permission from [413]. Copyright (2015) American Chemical Society.

resulting in a photovoltaic power conversion efficiency of 11.5% [440]. In another similar work, authors examined the passivation effect of ALD TiO_2 on hydrothermally grown one-dimensional (1D) TiO_2 nanorod (NR) arrays (figure 23) for solid-state perovskite-sensitized solar cells [441]. Their findings revealed that 4 nm thick ALD-grown TiO_2 passivated NR sample controls the back flow reactions and shows a power conversion efficiency as high as $\eta = 12.53\%$ for the $CH_3NH_3PbI_3$ perovskite absorbing layer [441].

Nanostructured ALD ZnO and TiO_2 are the leading materials used for UV photodetection owing to their suitable band gap [339, 442–446]. High-quality ZnO–TiO_2 core shell nanowires revealed enhanced UV sensing properties owing to superior anti-reflection properties and electron–hole separation mechanism. The preparation comprised of two steps: ZnO nanowires fabrication by hydrothermal synthesis followed by ALD of TiO_2. The photoresponsivity was 495 A/W at 373 nm under −10 V which is ∼8 times higher than photodetector fabricated from bare ZnO NWs (figure 24) [445]. Three-dimensional polyacrylonitrile/ZnO material were prepared by combination of electrospinning and atomic layer deposition. The UV photoresponse current for this configuration was enhanced by a factor of 250 compared to a flat electrode [339]. TiO_2/Ag nanorods (figure 25) were fabricated by successive glancing angle deposition of Ag on Ag film/Si template and ALD of TiO_2. Nanostructured devices showed a photo response enhancement factor of 1.49×10^2 under 3 V reverse bias (figure 26) [442].

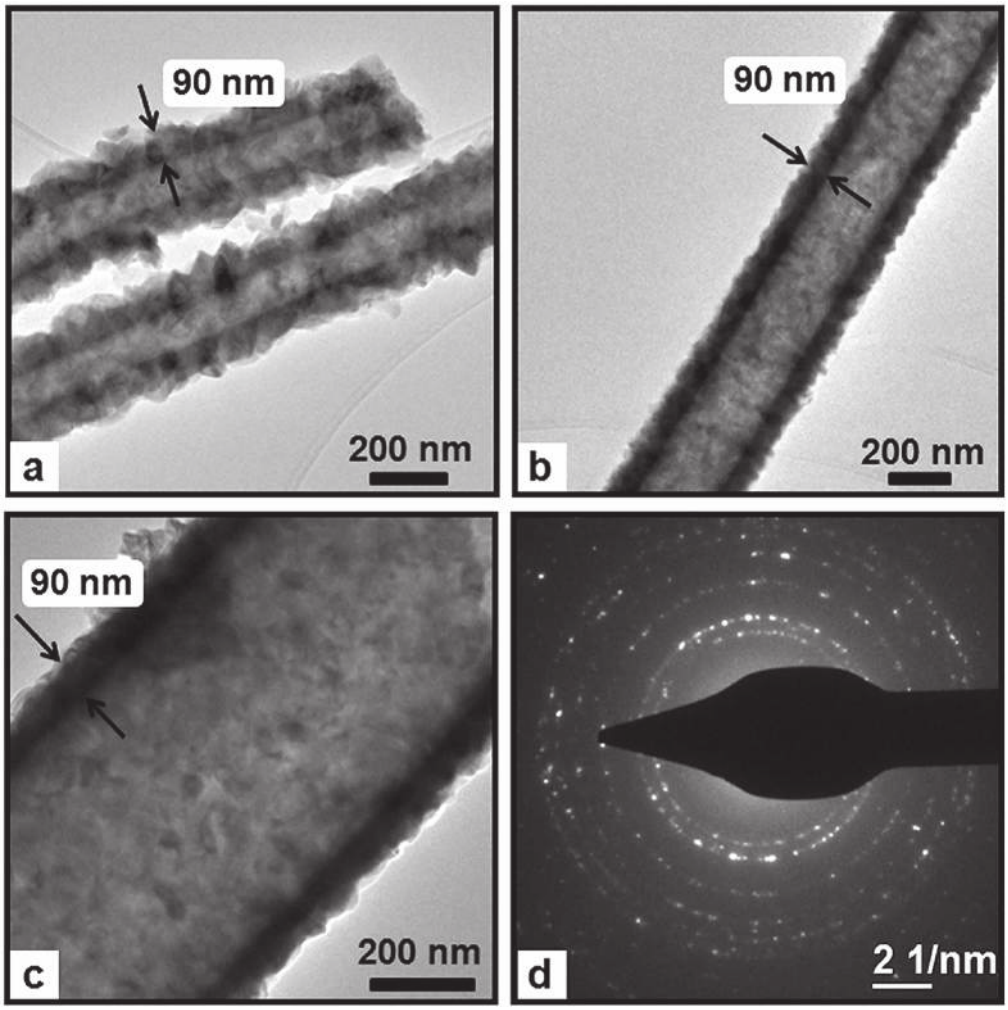

Figure 20. Representative TEM images of (a) 8%-nylon 6,6/FA-ZnO, (b) 5%-nylon 6,6/HFIP-ZnO, (c) 8%-nylon 6,6/HFIP-ZnO core−shell nanofibers; (d) representative SAED pattern of the core−shell nylon 6,6-ZnO nanofibers (8%-nylon 6,6/HFIP-ZnO NF). Reprinted with permission from [302]. Copyright (2012) American Chemical Society.

4.4. Chemical sensing

Gas sensors work on the basis of the modulation of the materials' physical properties (e.g., electrical, optical) in presence of the target species/molecules. Thin-film and nanostructured metal-oxide semiconductors are most widely used as active layers in chemo-resistive gas sensors, where SnO_2 is one of the most intensely studied semiconductor material [312, 395, 447–454]. Owing to the strong correlation between grain size and sensor response, use of ALD-grown nanostructured and heterostructured materials show promise in the enhancement of gas sensing capacity.

Chemical sensors find important applications in everyday life which modify their properties (e.g., electrical, optical) in presence of target species. In general, ALD-grown semiconductor metal oxides have been utilized as active layers in chemo-resistive sensors and the most prominent one is SnO_2 [312, 395, 447–454]. One of the recent notable work in this area was from Kim *et al* who reported superior toluene sensing properties of SnO_2–ZnO core–shell nanowires functionalized with Pt nanoparticles (figure 27) [453]. SnO_2 nanowires were fabricated via vapor–liquid–solid growth on patterned electrode and ZnO shell layers were grown subsequently via ALD process. Pt nanoparticles were attached to core–shell nanowires via γ-ray radiolysis [453]. An exceptional sensitivity of 279 was obtained for 100 ppb of toluene, where the response was measured R_a/R_g, where R_a and R_g represent the device resistance values in the absence and presence of an analyte gas, respectively. The dual effect of the expanded electron-depleted region in the ZnO layer and the catalytic effect of the functionalized Pt NPs are the reason behind exceptional toluene sensitivity and selectivity [453].

Park *et al* examined the ethanol gas sensing properties of In_2O_3/ZnO core–shell nanowires [450]. The core–shell nanowires were grown by evaporation of indium powder in an oxidizing atmosphere and subsequent atomic layer deposition of ZnO [450]. The In_2O_3/ZnO core–shell nanowires exhibited more than 6-fold higher response to 1000 ppm ethanol at 300 °C than pristine In_2O_3 nanowires (figure 28) [450].

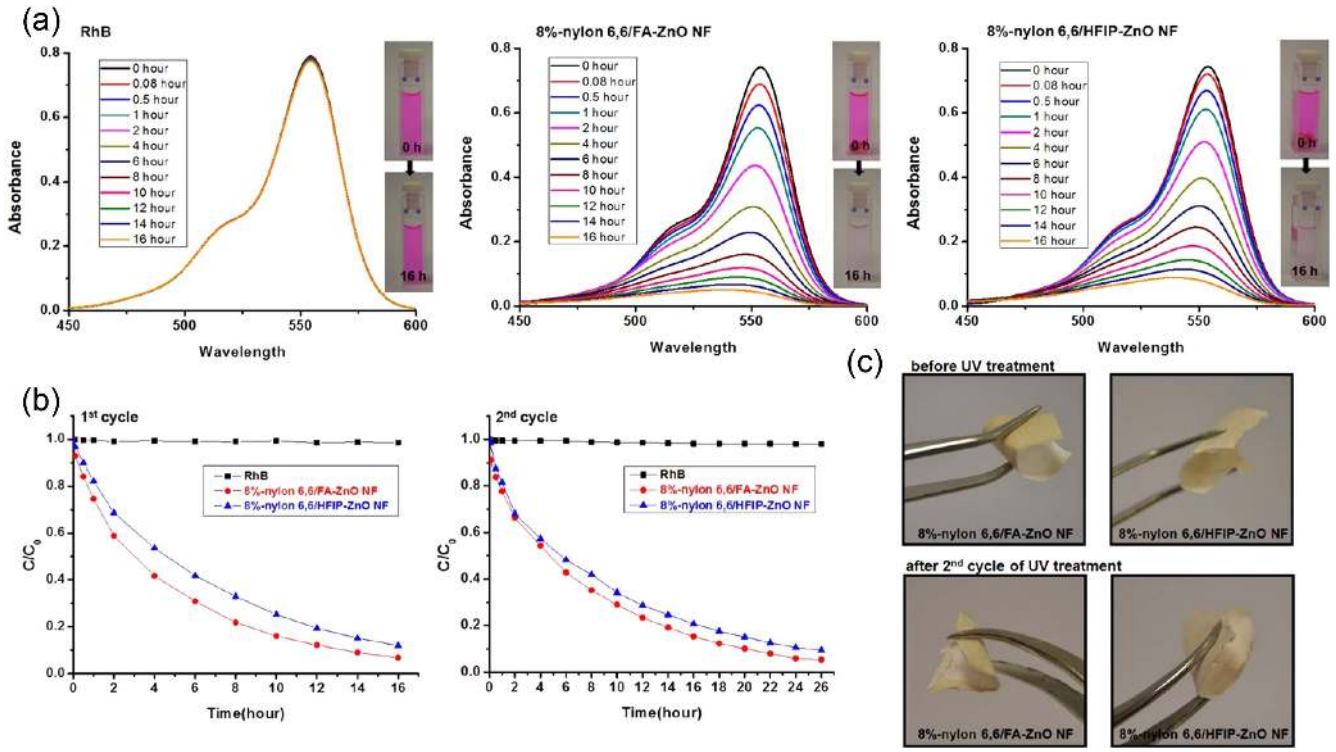

Figure 21. (a) UV–vis spectra of the Rh–B solution with and without core–shell nylon 6,6-ZnO nanofibers as a function of the UV irradiation time for 1st cycle experiment, (b) the rate (C/C_0) of Rh–B degradation of the Rh–B solution with and without core–shell nylon 6,6-ZnO nanofibers by exposing UV light with 365 nm wavelength for 1st and 2nd cycle experiments; (c) representative photographs of the flexible nylon 6,6-ZnO core–shell nanofibers before UV treatment and after 2nd cycle of UV treatment. Reprinted with permission from [302]. Copyright (2012) American Chemical Society.

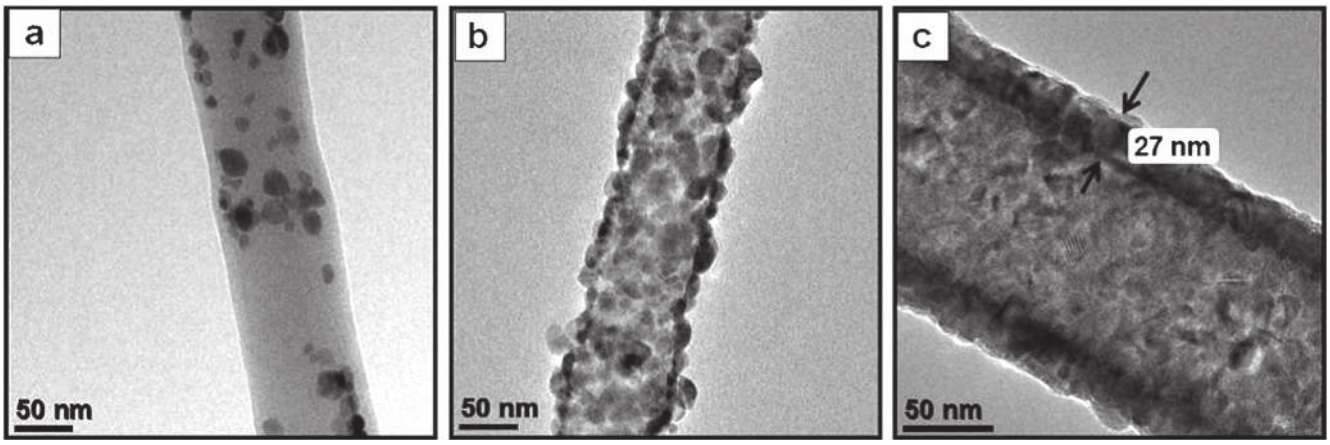

Figure 22. Representative TEM images of nanofibers: (a) nylon–ZnO nanoparticles, (b) nylon–ZnO nanoparticles (highly dense), and (c) nylon–ZnO nanocoating. Reprinted with permission from [295]. Copyright (2013) Royal Society of Chemistry.

Katoch *et al* reported fabrication of TiO_2/ZnO double-layer hollow fibers (DLHFs) as superior sensing materials for reducing gases [447]. The DLHFs were synthesized by sequentially growing TiO_2 and ZnO on sacrificial polymer templates followed by a final thermal treatment [447]. The outer ZnO layer becomes more resistive after donating electrons to inner TiO_2 layer. After the exposure of reducing gases such as CO, the outer resistive ZnO layer partially regains its original resistivity [447].

5. Conclusions and outlook

ALD-grown nanoscale compound semiconductor materials have already demonstrated significant potential for energy conversion and storage, opto-electronics, flexible/wearable electronics, photocatalysis, and sensing applications. ALD shows its superiority particularly in high-surface area nano-templated semiconductors, where lack of precise thickness control and 3D conformality are detrimental. However, the

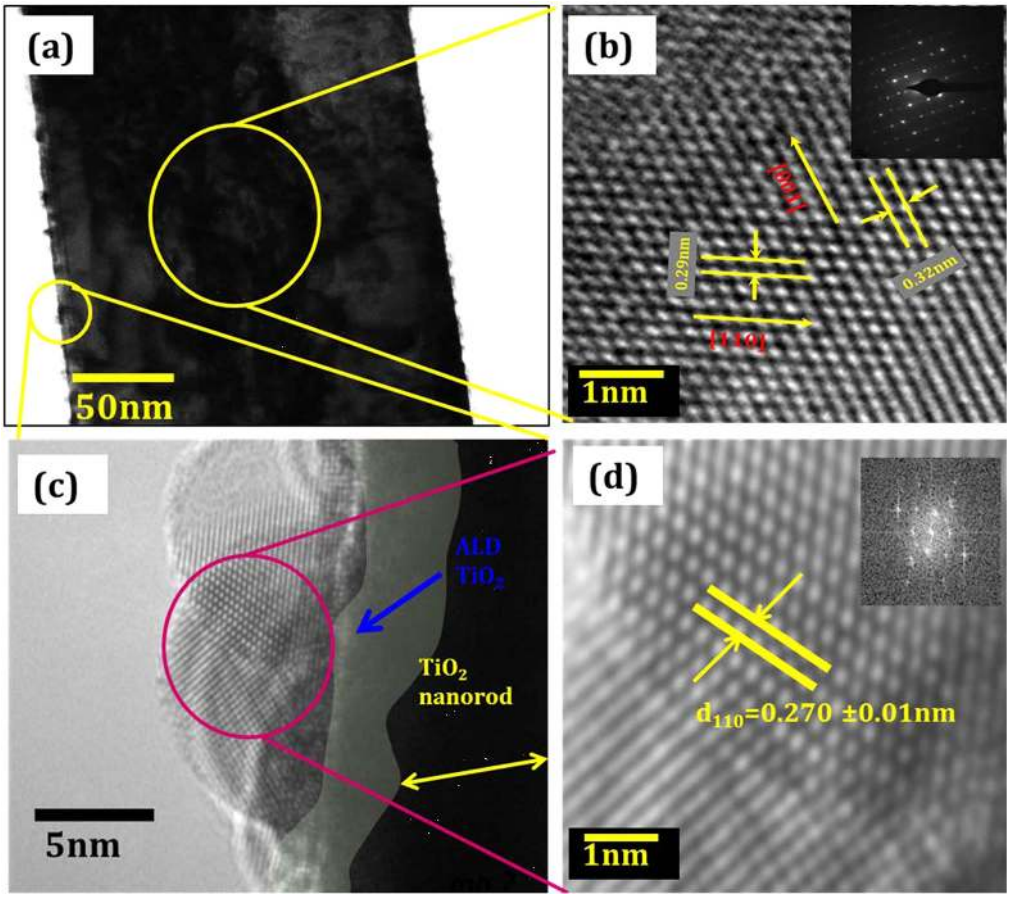

Figure 23. TEM and HRTEM images of TiO_2 nanorods coated with $CH_3NH_3PbI_3$. (a) TEM image of a $CH_3NH_3PbI_3$-covered TiO_2 nanorod. (b) HRTEM image of a TiO_2 nanorod. The inset shows the SAED pattern. (c) Highly magnified HRTEM image of the $CH_3NH_3PbI_3$ and TiO_2. The ALD layers and TiO_2 nanorods are indicated by the respective colors. (d) HRTEM image and (inset) live FFT pattern of the selected area of $CH_3NH_3PbI_3$ nanoparticles in (c). Reprinted with permission from [441]. Copyright (2015) American Chemical Society.

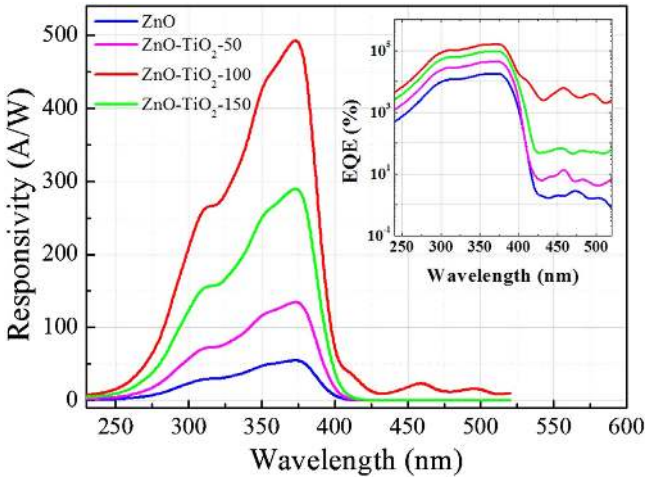

Figure 24. Photoresponsivity spectra of the photodetectors fabricated from the bare ZnO NWs and from the ZnO–TiO_2 core–shell NWs. Reprinted with permission from [445]. Copyright (2014) Elsevier.

full potential of these materials is hampered by the insufficient crystalline quality due to relatively high impurity incorporation within the films as a result of low substrate temperatures and incomplete ligand-exchange surface reactions. Nevertheless, there is an increasing effort in developing novel ALD recipes for semiconductor materials using alternative precursor chemistries, innovative reactor designs, and finely tuned deposition parameters. As materials and device engineering rapidly approaches the atomic-scale era, there is an increasing need for precisely engineered atomic-scale materials covering an even wider spectrum of alternative set of materials. Device sizes and individual layer dimensions are shrinking towards single-digit nm and even sub-nm scale, where poly-crystalline material might even meet local epitaxial quality by featuring sufficiently large crystal sizes. Moreover, the needed device layer thicknesses are reducing below the critical thickness values which might eliminate the lattice mismatch problem for semiconductor heterostructures. As a result, ALD will most probably be an even stronger contender to deliver new materials solutions at the atomic-scale, including compound and elemental semiconductors for future complex device architectures.

Finally, we would like to share our opinions regarding future perspectives, challenges, and opportunities for ALD-grown nanoscale semiconductors:

- The crystalline quality of low-temperature ALD-grown layers should be further improved via systematic studies featuring various alternative activation mechanism including plasma, radical/electron, UV/photo/e-beam-assisted

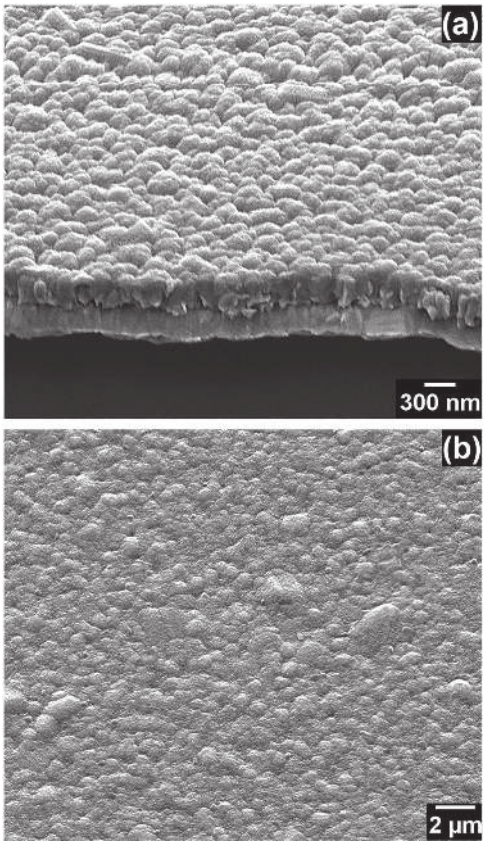

Figure 25. (a) Tilted and (b) top view SEM images of TiO_2 deposited on Ag nanorods/Ag thin film/Si by ALD, respectively. Reprinted with permission from [442]. Copyright (2015) AIP publishing.

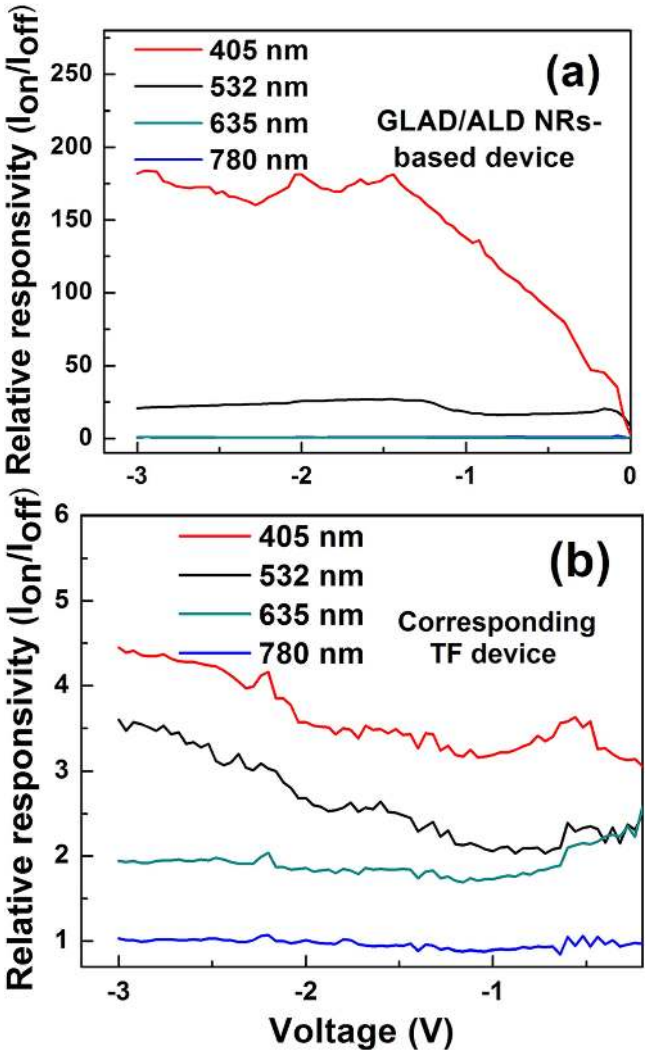

Figure 26. Relative responsivity values measured versus applied reverse bias of the fabricated (a) Al/TiO_2/Ag(NRs)/Ag(TF)/Si and (b) Al/TiO_2/Ag(TF)/Si photodiodes under illumination of different laser diodes. Reprinted with permission from [442]. Copyright (2015) AIP publishing.

approaches, substrate bias, optimized reactor designs, and novel precursor chemistries

- In the post-Moore era, CMOS technology needs more than ever novel materials solutions with atomic-scale precision engineering. ALD is already an integral part of CMOS processing and will play an even more critical role in feature sub-10 nm or single-digit nm technology nodes (7, 5, 3, 2 nm), where low-temperature grown atomic-scale semiconductors might find use within the 3D device architectures.
- Atomic-scale materials processing era will unleash quantum-size effects in low-dimensional semiconductors, thereby introducing challenges as well as opportunities for novel device designs. ALD-grown semiconductors might play a significant role at such reduced dimensions. Moreover, even non-semiconducting materials such as certain semi-metals might exhibit semiconductor-like properties due to quantum confinement effect at few atomic-layer dimensions [455]. The exploitation of materials at the atomic level will enable an unprecedented power of materials and device engineering.
- ALD-grown semiconductors might enable a wide range of emerging device applications for future internet of things (IoT) platform and cyber-physical systems, which necessitates compact, autonomous sensors with integrated energy harvesting and storage systems, and wireless communication transmitter/receiver modules on cost-effective substrates such as flexible and low-temperature compatible polymers
- ALD know-how in semiconductor materials will trigger other atomic layer processing techniques including atomic layer etching and atomic layer doping to form a complete semiconductor processing toolbox with atomic-scale precision and control
- In order to develop atomic-scale device structures without the need for highly complex and expensive advanced lithography techniques, an ultimate advancement in materials processing would be to develop self-aligned processes, which necessitates selective material deposition and etching recipes. Towards this lithography-free device fabrication goal, selective atomic layer processing of dielectrics, metals, and semiconductors should be developed. Such a bottom-up processing tool-box will lead to atomic-level precision manufacturing capability.

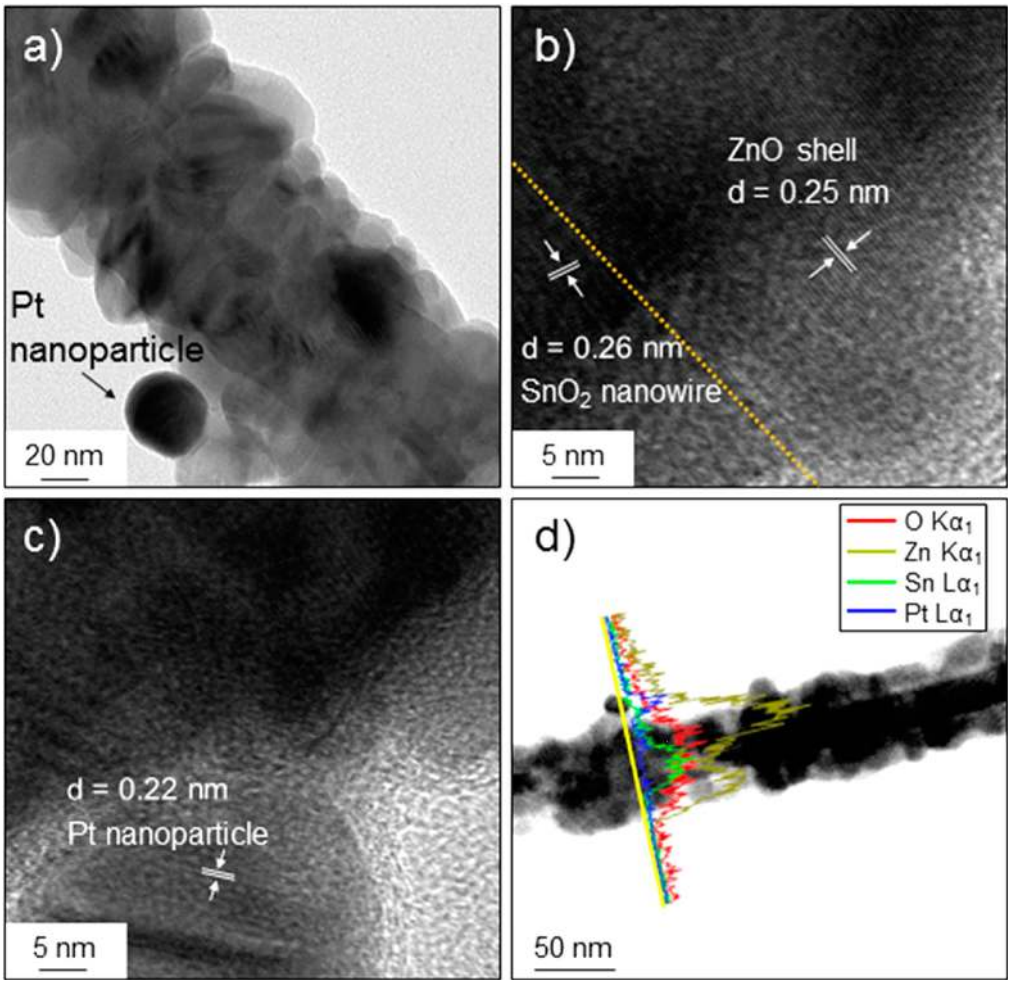

Figure 27. TEM images of the Pt NP-functionalized SnO_2–ZnO core–shell NWs with a ZnO shell thickness of 50 nm. (a) A low-magnification TEM image. (b), (c) High-resolution lattice images. (d) EDS line profiles for O, Sn, Zn, and Pt. Reprinted with permission from [453]. Copyright (2015) American Chemical Society.

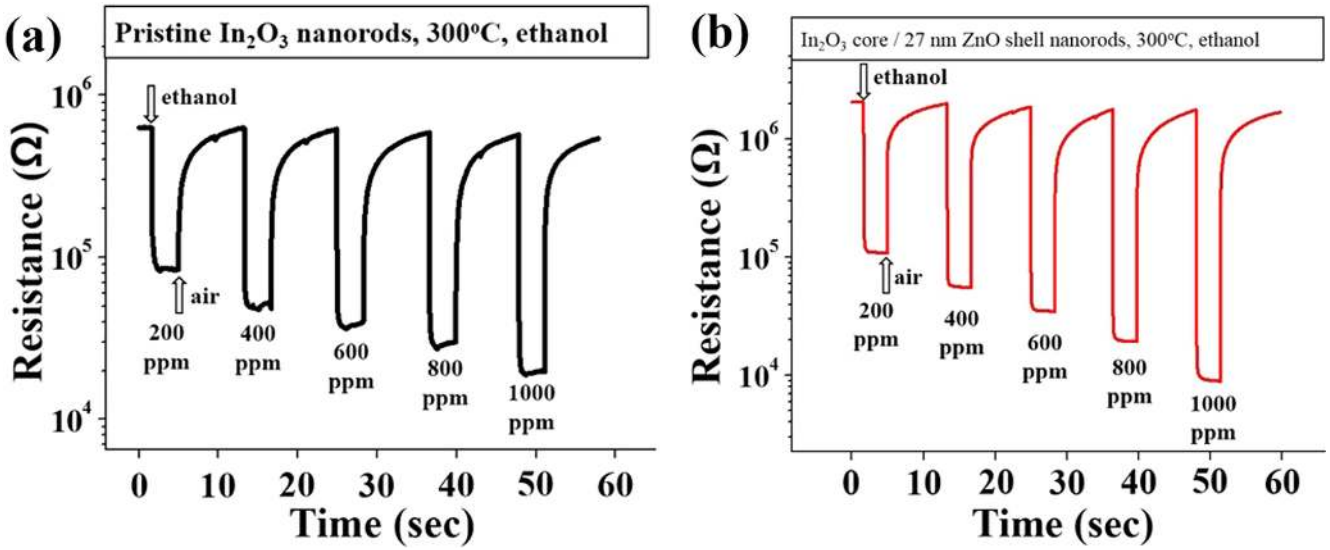

Figure 28. Electrical responses of the gas sensors fabricated from (a) pristine In_2O_3. (b) In_2O_3-core/ZnO-shell nanowires. Reprinted with permission from [450]. Copyright (2014) American Chemical Society.

Acknowledgements

Authors would like to acknowledge support from National Nanotechnology Research Center (UNAM) and Scientific and Technological Research Council of Turkey (TUBITAK) (Project # 112M482, 112M004, 112M578, 214M015). A. H. acknowledges Higher Education Commission of Pakistan (HEC) for Human resource development (HRD) fellowship for MS leading to PhD.

References

[1] Ahvenniemi E *et al* 2017 Review article: recommended reading list of early publications on atomic layer deposition—outcome of the 'virtual project on the history of ALD' *J. Vac. Sci. Technol.* A **35** 010801
[2] Puurunen R L 2014 A short history of atomic layer deposition: tuomo suntola's atomic layer epitaxy *Chem. Vapor Depos.* **20** 332–44
[3] Johnson R W, Hultqvist A and Bent S F 2014 A brief review of atomic layer deposition: from fundamentals to applications *Mater. Today* **17** 236–46
[4] Ritala M and Leskelä M 1999 Atomic layer epitaxy—a valuable tool for nanotechnology? *Nanotechnology* **10** 19–24
[5] Puurunen R L 2005 Surface chemistry of atomic layer deposition: a case study for the trimethylaluminum/water process *J. Appl. Phys.* **97** 121301
[6] Miikkulainen V, Leskela M, Ritala M and Puurunen R L 2013 Crystallinity of inorganic films grown by atomic layer deposition: overview and general trends *J. Appl. Phys.* **113** 021301
[7] George S M 2010 Atomic layer deposition: an overview *Chem. Rev.* **110** 111–31
[8] Van Bui H, Grillo F and van Ommen R 2016 Atomic and molecular layer deposition: off the beaten track *Chem. Commun.* **53** 45–71
[9] Kim H and Oh I 2014 Review of plasma-enhanced atomic layer deposition: technical enabler of nanoscale device fabrication *Japan. J. Appl. Phys.* **53** 03DA01
[10] Profijt H B, Potts S E, van de Sanden M C M and Kessels W M M 2011 Plasma-assisted atomic layer deposition: basics, opportunities, and challenges *J. Vac. Sci. Technol.* A **29** 050801
[11] Poodt P, Cameron D C, Dickey E, George S M, Kuznetsov V, Parsons G N, Roozeboom F, Sundaram G and Vermeer A 2012 Spatial atomic layer deposition: a route towards further industrialization of atomic layer deposition *J. Vac. Sci. Technol.* A **30** 010802
[12] Tynell T and Karppinen M 2014 Atomic layer deposition of ZnO: a review *Semicond. Sci. Technol.* **29** 043001
[13] Meng X, Byun Y-C, Kim H S, Lee J S, Lucero A T, Cheng L and Kim J 2016 Atomic layer deposition of silicon nitride thin films: a review of recent progress, challenges, and outlooks *Materials* **9** 1007
[14] Bae C, Shin H and Nielsch K 2011 Surface modification and fabrication of 3D nanostructures by atomic layer deposition *MRS Bull.* **36** 887–97
[15] Ponraj J S, Attolini G and Bosi M 2013 Review on atomic layer deposition and applications of oxide thin films *Crit. Rev. Solid State Mater. Sci.* **38** 203–33
[16] Meng X, Wang X, Geng D, Ozgit-Akgun C, Schneider N and Elam J W 2017 Atomic layer deposition for nanomaterials synthesis and functionalization in energy technology *Mater. Horiz.* **4** 133–54
[17] Van Delft J A, Garcia-Alonso D and Kessels W M M 2012 Atomic layer deposition for photovoltaics: applications and prospects for solar cell manufacturing *Semicond. Sci. Technol.* **27** 074002
[18] Wang T, Luo Z, Li C and Gong J 2014 Controllable fabrication of nanostructured materials for photoelectrochemical water splitting via atomic layer deposition *Chem. Soc. Rev.* **43** 7469–84
[19] Mackus A J M, Bol A A and Kessels W M M 2014 The use of atomic layer deposition in advanced nanopatterning *Nanoscale* **6** 10941–60
[20] Biyikli N *et al* 2015 Template-assisted synthesis of III-nitride and metal-oxide nano-heterostructures using low-temperature atomic layer deposition for energy, sensing, and catalysis applications (presentation recording) *Proc. SPIE* **9553** 95530C
[21] Yousfi E B, Fouache J and Lincot D 2000 Study of atomic layer epitaxy of zinc oxide by *in-situ* quartz crystal microgravimetry *Appl. Surf. Sci.* **153** 223–34
[22] Lin Y-T, Chung P-H, Lai H-W, Su H-L, Lyu D-Y, Yen K-Y, Lin T-Y, Kung C-Y and Gong J-R 2009 Self-limiting growth of ZnO films on (0001) sapphire substrates by atomic layer deposition at low temperatures using diethyl-zinc and nitrous oxide *Appl. Surf. Sci.* **256** 819–22
[23] Yamada A, Sang B and Konagai M 1997 Atomic layer deposition of ZnO transparent conducting oxides *Appl. Surf. Sci.* **112** 216–22
[24] Wójcik A, Godlewski M, Guziewicz E, Minikayev R and Paszkowicz W 2008 Controlling of preferential growth mode of ZnO thin films grown by atomic layer deposition *J. Cryst. Growth* **310** 284–9
[25] Yuan H, Luo B, Yu D, Cheng A, Campbell S A and Gladfelter W L 2015 Atomic layer deposition of Al-doped ZnO films using ozone as the oxygen source: a comparison of two methods to deliver aluminum *J. Vac. Sci. Technol.* A **30** 01A138
[26] Wang T, Wu H, Chen C and Liu C 2012 Growth, optical, and electrical properties of nonpolar *m*-plane ZnO on p-Si substrates with Al_2O_3 buffer layers *Appl. Phys. Lett.* **100** 011901
[27] Tammenma M, Koskinen T, Hiltunen L and Niinisto L 1985 Zinc chalcogenide thin films grown by the atomic layer epitaxy technique using zinc acetate as source material *Thin Solid Films* **124** 125–8
[28] Min Y-S, An C J, Kim S K, Song J and Hwang C S 2010 Growth and characterization of conducting ZnO thin films by atomic layer deposition *Bull. Korean Chem. Soc.* **31** 2503–8
[29] Lin M-C, Wu M-K, Yuan K-Y, Chen M-J, Yang J-R and Shiojiri M 2011 Structural and photoluminescence properties of ZnO films grown on 6H-SiC substrates by low-temperature atomic layer deposition *J. Electrochem. Soc.* **158** H1213–7
[30] Jeon S, Bang S, Lee S, Kwon S, Jeong W, Jeon H, Chang H J and Park H-H 2008 Structural and electrical properties of ZnO thin films deposited by atomic layer deposition at low temperatures *J. Electrochem. Soc.* **155** H738–43
[31] Guziewicz E *et al* 2010 Zinc oxide grown by atomic layer deposition—a material for novel 3D electronics *Phys. Status Solidi* **247** 1611–5
[32] Baji Z, Lábadi Z, Horváth Z E, Molnár G, Volk J, Bársony I and Barna P 2012 Nucleation and growth modes of ALD ZnO *Cryst. Growth Des.* **12** 5615–20
[33] Sang B and Konagai M 1996 Growth of transparent conductive oxide zno films by atomic layer deposition *Japan. J. Appl. Phys.* **35** L602–5
[34] Ko Park S-H and Lee Y E 2004 Controlling preferred orientation of ZnO thin films by atomic layer deposition *J. Mater. Sci.* **39** 2195–7

[35] Gong S C, Bang S, Jeon H, Park H-H, Chang Y C and Chang H J 2010 Effects of atomic layer deposition temperatures on structural and electrical properties of ZnO films and its thin film transistors *Met. Mater. Int.* **16** 953–8

[36] Illiberi A, Roozeboom F and Poodt P 2012 Spatial atomic layer deposition of zinc oxide thin films *ACS Appl. Mater. Interfaces* **4** 268–72

[37] Saito K, Watanabe Y, Takahashi K, Matsuzawa T, Sang B and Konagai M 1997 Photo atomic layer deposition of transparent conductive ZnO films *Sol. Energy Mater. Sol. Cells* **49** 187–93

[38] Chiang T-Y, Dai C-L and Lian D-M 2011 Influence of growth temperature on the optical and structural properties of ultrathin ZnO films *J. Alloys Compd.* **509** 5623–6

[39] Lee S, Im Y H, Kim S H and Hahn Y B 2006 Structural and optical properties of high quality ZnO films on Si grown by atomic layer deposition at low temperatures *Superlattices Microstruct.* **39** 24–32

[40] Chai Z, Lu X and He D 2012 Atomic layer deposition of zinc oxide films: effects of nanocrystalline characteristics on tribological performance *Surf. Coat. Technol.* **207** 361–6

[41] Ott A W and Chang R P H 1999 Atomic layer-controlled growth of transparent conducting ZnO on plastic substrates *Mater. Chem. Phys.* **58** 132–8

[42] Janocha E and Pettenkofer C 2011 ALD of ZnO using diethylzinc as metal-precursor and oxygen as oxidizing agent *Appl. Surf. Sci.* **257** 10031–5

[43] Kim D, Kang H, Kim J M and Kim H 2011 The properties of plasma-enhanced atomic layer deposition (ALD) ZnO thin films and comparison with thermal ALD *Appl. Surf. Sci.* **257** 3776–9

[44] Sultan S M, Clark O D, Masaud T B, Fang Q, Gunn R, Hakim M M A, Sun K, Ashburn P and Chong H M H 2012 Remote plasma enhanced atomic layer deposition of ZnO for thin film electronic applications *Microelectron. Eng.* **97** 162–5

[45] Cheng Y-C, Kuo Y-S, Li Y-H, Shyue J-J and Chen M-J 2011 Stable p-type ZnO films grown by atomic layer deposition on GaAs substrates and treated by post-deposition rapid thermal annealing *Thin Solid Films* **519** 5558–61

[46] Malm J, Sahramo E, Perälä J, Sajavaara T and Karppinen M 2011 Low-temperature atomic layer deposition of ZnO thin films: control of crystallinity and orientation *Thin Solid Films* **519** 5319–22

[47] Lim J and Lee C 2007 Effects of substrate temperature on the microstructure and photoluminescence properties of ZnO thin films prepared by atomic layer deposition *Thin Solid Films* **515** 3335–8

[48] Elam J W, Sechrist Z A and George S M 2002 ZnO/Al_2O_3 nanolaminates fabricated by atomic layer deposition: growth and surface roughness measurements *Thin Solid Films* **414** 43–55

[49] Kim C R *et al* 2008 Effects of annealing temperature of buffer layer on structural and optical properties of ZnO thin film grown by atomic layer deposition *Solid State Commun.* **148** 395–8

[50] Krajewski T, Guziewicz E, Godlewski M, Wachnicki L, Kowalik I A, Wojcik-Glodowska A, Lukasiewicz M, Kopalko K, Osinniy V and Guziewicz M 2009 The influence of growth temperature and precursors' doses on electrical parameters of ZnO thin films grown by atomic layer deposition technique *Microelectronics J.* **40** 293–5

[51] Yuan N Y, Wang S Y, Tan C B, Wang X Q, Chen G G and Ding J N 2013 The influence of deposition temperature on growth mode, optical and mechanical properties of ZnO films prepared by the ALD method *J. Cryst. Growth* **366** 43–6

[52] Lin P-Y, Gong J-R, Li P-C, Lin T-Y, Lyu D-Y, Lin D-Y, Lin H-J, Li T-C, Chang K-J and Lin W-J 2008 Optical and structural characteristics of ZnO films grown on (0001) sapphire substrates by ALD using DEZn and N_2O *J. Cryst. Growth* **310** 3024–8

[53] Kawamura Y, Hattori N, Miyatake N and Uraoka Y 2013 Comparison between ZnO films grown by plasma-assisted atomic layer deposition using H_2O plasma and O_2 plasma as oxidant *J. Vac. Sci. Technol.* A **31** 01A142

[54] Huang H-W, Chang W-C, Lin S-J and Chueh Y-L 2012 Growth of controllable ZnO film by atomic layer deposition technique via inductively coupled plasma treatment *J. Appl. Phys.* **112** 124102

[55] Mousa M B M, Oldham C J, Jur J S and Parsons G N 2012 Effect of temperature and gas velocity on growth per cycle during Al_2O_3 and ZnO atomic layer deposition at atmospheric pressure *J. Vac. Sci. Technol.* A **30** 01A155

[56] Guziewicz E *et al* 2009 ZnO grown by atomic layer deposition: a material for transparent electronics and organic heterojunctions *J. Appl. Phys.* **105** 122413

[57] Guziewicz E, Kowalik I A, Godlewski M, Kopalko K, Osinniy V, Wójcik A, Yatsunenko S, Łusakowska E, Paszkowicz W and Guziewicz M 2008 Extremely low temperature growth of ZnO by atomic layer deposition *J. Appl. Phys.* **103** 033515

[58] Tapily K, Gu D, Baumgart H, Namkoong G, Stegall D and Elmustafa A A 2011 Mechanical and structural characterization of atomic layer deposition-based ZnO films *Semicond. Sci. Technol.* **26** 115005–7

[59] Rowlette P C, Allen C G, Bromley O B, Dubetz A E and Wolden C A 2009 Plasma-enhanced atomic layer deposition of semiconductor grade ZnO using dimethyl zinc *Chem. Vapor Depos.* **15** 15–20

[60] Kim J-E, Bae S-M, Yang H-S and Hwang J-H 2010 Electrical and optical properties of zinc oxide thin films deposited using atomic layer deposition *J. Korean Ceram. Soc.* **47** 353–6

[61] Pung S-Y, Choy K-L, Hou X and Shan C 2008 Preferential growth of ZnO thin films by the atomic layer deposition technique *Nanotechnology* **19** 435609

[62] Makino H, Kishimoto S, Yamada T, Miyake A, Yamamoto N and Yamamoto T 2008 Effects of surface pretreatment on growth of ZnO on glass substrate *Phys. Status Solidi Appl. Mater. Sci.* **205** 1971–4

[63] Luka G, Krajewski T, Wachnicki L, Witkowski B, Lusakowska E, Paszkowicz W, Guziewicz E and Godlewski M 2010 Transparent and conductive undoped zinc oxide thin films grown by atomic layer deposition *Phys. Status Solidi* **207** 1568–71

[64] Kudrawiec R, Misiewicz J, Wachnicki Ł, Guziewicz E and Godlewski M 2011 Contactless electroreflectance of ZnO layers grown by atomic layer deposition at low temperature *Semicond. Sci. Technol.* **26** 075012

[65] Kawamura Y, Hattori N, Miyatake N, Horita M and Uraoka Y 2011 ZnO thin films fabricated by plasma-assisted atomic layer deposition *Japan. J. Appl. Phys.* **50** 04DF05

[66] Thomas M A and Cui J B 2012 Highly tunable electrical properties in undoped ZnO grown by plasma enhanced thermal-atomic layer deposition *ACS Appl. Mater. Interfaces* **4** 3122–8

[67] Kim S K, Hwang C S, Park S-H K and Yun S J 2005 Comparison between ZnO films grown by atomic layer deposition using H_2O or O_3 as oxidant *Thin Solid Films* **478** 103–8

[68] Makino H, Miyake A, Yamada T, Yamamoto N and Yamamoto T 2009 Influence of substrate temperature and Zn-precursors on atomic layer deposition of polycrystalline ZnO films on glass *Thin Solid Films* **517** 3138–42

[69] Tanskanen J T, Bakke J R, Pakkanen T A and Bent S F 2011 Influence of organozinc ligand design on growth and material properties of ZnS and ZnO deposited by atomic layer deposition *J. Vac. Sci. Technol.* A **29** 031507

[70] Kopalko K, Wójcik A, Godlewski M, Łusakowska E, Paszkowicz W, Domagała J Z, Godlewski M M, Szezerbakow A, ŚwiąTek K and Dybko K 2005 Growth by atomic layer epitaxy and characterization of thin films of ZnO *Phys. Status Solidi* C **2** 1125–30

[71] Chen H C, Chen M J, Liu T C, Yang J R and Shiojiri M 2010 Structure and stimulated emission of a high-quality zinc oxide epilayer grown by atomic layer deposition on the sapphire substrate *Thin Solid Films* **519** 536–40

[72] Wachnicki Ł, Krajewski T, Łuka G, Witkowski B, Kowalski B, Kopalko K, Domagala J Z, Guziewicz M, Godlewski M and Guziewicz E 2010 Monocrystalline zinc oxide films grown by atomic layer deposition *Thin Solid Films* **518** 4556–9

[73] Ku C S, Huang J M, Lin C M and Lee H Y 2009 Fabrication of epitaxial ZnO films by atomic-layer deposition with interrupted flow *Thin Solid Films* **518** 1373–6

[74] Lim J, Shin K, Kim H and Lee C 2005 Enhancement of ZnO nucleation in ZnO epitaxy by atomic layer epitaxy *Thin Solid Films* **475** 256–61

[75] Lim J, Shin K, Kim H W and Lee C 2004 Photoluminescence studies of ZnO thin films grown by atomic layer epitaxy *J. Lumin.* **109** 181–5

[76] Liu C H, Yan M, Liu X, Seelig E and Chang R P H 2002 Effect of electric field upon the ZnO growth on sapphire (0001) by atomic layer epitaxy method *Chem. Phys. Lett.* **355** 43–7

[77] Shin K and Lee C 2004 Comparison of ECR plasma pretreatment techniques for ZnO atomic layer epitaxy on the sapphire substrate *Phys. Status Solidi* C **1** 2545–9

[78] Saito K, Nagayama K, Hosokai Y, Ishida K and Takahashi K 2004 Effects of GaN template on atomic-layer-epitaxy growth of ZnO *Phys. Status Solidi* C **972** 969–72

[79] Kumagai H, Tanaka Y, Murata M, Masuda Y and Shinagawa T 2010 Novel TiO_2/ZnO multilayer mirrors at 'water-window' wavelengths fabricated by atomic layer epitaxy *J. Phys.: Condens. Matter* **22** 474008

[80] Kopalko K, Godlewski M, Lusakowska E, Paszkowicz W, Domagala J Z, Szczerbakow A, Ivanov V Y, Godlewski M M and Phillips M R 2004 Monocrystalline ZnO films grown by atomic layer epitaxy—growth and characterization *Phys. Status Solidi* C **1** 892–5

[81] Kopalko K, Godlewski M, Domagala J Z, Lusakowska E, Minikayev R, Paszkowicz W and Szczerbakow A 2004 Monocrystalline ZnO films on GaN/Al_2O_3 by atomic layer epitaxy in gas flow *Chem. Mater.* **16** 1447–50

[82] Ku C S, Lee H Y, Huang J M and Lin C M 2010 Epitaxial growth of *m*-plane ZnO thin films on $(10\bar{1}0)$ sapphire substrate by atomic layer deposition with interrupted flow *Cryst. Growth Des.* **10** 1460–3

[83] Yang S, Lin B H, Liu W-R, Lin J-H, Chang C-S, Hsu C-H and Hsieh W F 2009 Structural characteristics and annealing effect of ZnO epitaxial films grown by atomic layer deposition *Cryst. Growth Des.* **9** 5184–9

[84] Kaiya K, Yoshii N, Takahashi N and Nakamura T 2000 Atmospheric pressure atomic layer epitaxy of ZnO on a sapphire (0001) substrate by alternate reaction of $ZnCl_2$ and O_2 *J. Mater. Sci. Lett.* **19** 2089–90

[85] Murata M, Tanaka Y, Sanjo Y, Kumagai H, Shinagawa T and Chigane M 2011 Atomic layer epitaxy of TiO_2/ZnO multilayer optics using ZnO buffer layer for water-window x-ray *Proc. SPIE* **7927** 79270Q

[86] Wu C C, Wuu D S, Chen T N, Yu T E, Lin P R, Horng R H and Sun S 2008 Characteristics of ZnO nanowall structures grown on GaN template using organometallic chemical vapor deposition *J. Nanosci. Nanotechnol.* **8** 3851–6

[87] Ramos K B, Clavel G, Marichy C, Cabrera W, Pinna N and Chabal Y J 2013 *In situ* infrared spectroscopic study of atomic layer-deposited TiO_2 thin films by nonaqueous routes *Chem. Mater.* **25** 1706–12

[88] Aarik J, Aidla A, Uustare T, Ritala M and Leskelä M 2000 Titanium isopropoxide as a precursor for atomic layer deposition: characterization of titanium dioxide growth process *Appl. Surf. Sci.* **161** 385–95

[89] Aarik J, Aidla A, Mändar H and Uustare T 2001 Atomic layer deposition of titanium dioxide from $TiCl_4$ and H_2O: investigation of growth mechanism *Appl. Surf. Sci.* **172** 148–58

[90] Aarik J, Aidla A, Uustare T, Kukli K, Sammelselg V, Ritala M and Leskelä M 2002 Atomic layer deposition of TiO_2 thin films from TiI_4 and H_2O *Appl. Surf. Sci.* **193** 277–86

[91] Pore V, Rahtu A, Leskelä M, Ritala M, Sajavaara T and Keinonen J 2004 Atomic layer deposition of photocatalytic TiO_2 thin films from titanium tetramethoxide and water *Chem. Vapor Depos.* **10** 143–8

[92] Rose M, Niinisto J, Michalowski P, Gerlich L, Wilde L, Endler I and Bartha J W 2009 Atomic layer deposition of titanium dioxide thin films from $Cp^*Ti(OMe)_3$ and ozone *J. Am. Chem. Soc.* **113** 21825–30

[93] Alekhin A P, Lapushkin G I, Markeev A M, Sigarev A A and Toknova V F 2010 Atomic layer deposition of titanium dioxide thin films from tetraethoxytitanium and water *Russ. J. Gen. Chem.* **80** 1091–6

[94] Kubala N G and Wolden C A 2010 Self-limiting growth of anatase TiO_2: a comparison of two deposition techniques *Thin Solid Films* **518** 6733–7

[95] Methaapanon R and Bent S F 2010 Comparative study of titanium dioxide atomic layer deposition on silicon dioxide and hydrogen-terminated silicon *J. Phys. Chem.* C **114** 10498–504

[96] Kääriäinen M-L and Cameron D C 2012 Nitrogen doping in atomic layer deposition grown titanium dioxide films by using ammonium hydroxide *Thin Solid Films* **526** 212–7

[97] Triani G, Campbell J A, Evans P J, Davis J, Latella B A and Burford R P 2010 Low temperature atomic layer deposition of titania thin films *Thin Solid Films* **518** 3182–9

[98] McDaniel M D, Posadas A, Wang T, Demkov A A and Ekerdt J G 2012 Growth and characterization of epitaxial anatase $TiO_2(001)$ on $SrTiO_3$-buffered Si(001) using atomic layer deposition *Thin Solid Films* **520** 6525–30

[99] Aarik J, Aidla A, Sammelselg V, Uustare T, Ritala M and Leskelä M 2000 Characterization of titanium dioxide atomic layer growth from titanium ethoxide and water *Thin Solid Films* **370** 163–72

[100] Xie Q, Jiang Y-L, Detavernier C, Deduytsche D, Van Meirhaeghe R L, Ru G-P, Li B-Z and Qu X-P 2007 Atomic layer deposition of TiO_2 from tetrakis-dimethyl-amido titanium or Ti isopropoxide precursors and H_2O *J. Appl. Phys.* **102** 083521

[101] Niskanen A, Arstila K, Leskela M and Ritala M 2007 Radical enhanced atomic layer deposition of titanium dioxide *Chem. Vapor Depos.* **13** 152–7

[102] Aarik J, Aidla A, Uustare T and Sammelselg V 1995 Morphology and structure of TiO_2 thin films grown by atomic layer deposition *J. Cryst. Growth* **148** 268–75

[103] Kääriäinen M L, Kääriäinen T O and Cameron D C 2009 Titanium dioxide thin films, their structure and its effect on their photoactivity and photocatalytic properties *Thin Solid Films* **517** 6666–70

[104] Iancu A T, Logar M, Park J and Prinz F B 2015 Atomic layer deposition of undoped TiO_2 exhibiting p-type conductivity *ACS Appl. Mater. Interfaces* **7** 5134–40

[105] Nieminen M, Niinisto L and Rauhala E 1996 Growth of gallium oxide thin films from gallium acetylacetonate by atomic layer epitaxy *J. Mater. Chem.* **6** 27–31

[106] Dezelah C L, Niinistö J, Arstila K, Niinistö L and Winter C H 2005 Atomic layer deposition of Ga_2O_3 films from a dialkylamido-based precursor *Chem. Mater.* **18** 471–5

[107] Choi D W, Chung K B and Park J S 2013 Low temperature Ga_2O_3 atomic layer deposition using gallium tri-isopropoxide and water *Thin Solid Films* **546** 31–4

[108] Donmez I, Ozgit-Akgun C and Biyikli N 2013 Low temperature deposition of Ga_2O_3 thin films using trimethylgallium and oxygen plasma *J. Vac. Sci. Technol.* A **31** 01A110

[109] Allen T G and Cuevas A 2015 Plasma enhanced atomic layer deposition of gallium oxide on crystalline silicon: demonstration of surface passivation and negative interfacial charge *Phys. Status Solidi* **9** 220–4

[110] Asikainen T, Ritala M and Leskeei M 1994 Growth of In203 thin films by atomic layer epitaxy *J. Electrochemical Soc.* **141** 3210–3

[111] Elam J W, Martinson A B F, Pellin M J and Hupp J T 2006 Atomic layer deposition of In_2O_3 using cyclopentadienyl indium: a new synthetic route to transparent conducting oxide films *Chem. Mater.* **18** 3571–8

[112] Nilsen O, Balasundaraprabhu R, Monakhov E V, Muthukumarasamy N, Fjellvåg H and Svensson B G 2009 Thin films of In_2O_3 by atomic layer deposition using In(acac)3 *Thin Solid Films* **517** 6320–2

[113] Lee D-J, Kwon J-Y, Lee J II and Kim K-B 2011 Self-limiting film growth of transparent conducting In_2O_3 by atomic layer deposition using trimethylindium and water vapor *J. Phys. Chem.* C **115** 15384–9

[114] Libera J A, Hryn J N and Elam J W 2011 Indium oxide atomic layer deposition facilitated by the synergy between oxygen and water *Chem. Mater.* **23** 2150–8

[115] Maeng W J, Choi D-W, Chung K-B, Koh W, Kim G-Y, Choi S-Y and Park J-S 2014 Highly conducting, transparent, and flexible indium oxide thin film prepared by atomic layer deposition using a new liquid precursor $Et_2InN(SiMe_3)_2$ *ACS Appl. Mater. Interfaces* **6** 17481–8

[116] Sheng J, Park J, Choi D-W, Lim J and Park J-S 2016 A study on the electrical properties of atomic layer deposition grown InO_x on flexible substrates with respect to N_2O plasma treatment and the associated thin-film transistor behavior under repetitive mechanical stress *ACS Appl. Mater. Interfaces* **8** 31136–43

[117] Rosental A, Tarre A, Gerst A, Sundqvist J, Hårsta A, Aidla A, Aarik J, Sammelselg V and Uustare T 2003 Gas sensing properties of epitaxial SnO_2 thin films prepared by atomic layer deposition *Sensors Actuators* B **93** 552–5

[118] Sundqvist J, Tarre A, Rosental A and Hårsra A 2003 Atomic layer deposition of epitaxial and polycrystalline SnO_2 films from the SnI_4/O_2 precursor combination *Chem. Vapor Depos.* **9** 21–5

[119] Takeuchi T, Doteshita I and Asami S 2004 Epitaxial growth of sub-nanometre thick tin dioxide films on sapphire substrates by pulsed atomic layer chemical vapour deposition *Surf. Interface Anal.* **36** 1133–5

[120] Du X, Du Y and George S M 2008 CO gas sensing by ultrathin tin oxide films grown by atomic layer deposition using transmission FTIR spectroscopy *J. Phys. Chem.* A **112** 9211–9

[121] Niskanen A J, Varpula A, Utriainen M, Natarajan G, Cameron D C, Novikov S, Airaksinen V M, Sinkkonen J and Franssila S 2010 Atomic layer deposition of tin dioxide sensing film in microhotplate gas sensors *Sensors Actuators* B **148** 227–32

[122] Nazarov D V, Bobrysheva N P, Osmolovskaya O M, Osmolovsky M G and Smirnov V M 2015 Atomic layer deposition of tin dioxide nanofilms: a review *Rev. Adv. Mater. Sci.* **40** 262–75 www.ipme.ru/e-journals/RAMS/no_34015/07_34015_nazarov.pdf

[123] Marichy C, Ercolano G, Caputo G, Willinger M G, Jones D, Rozière J, Pinna N and Cavaliere S 2015 ALD SnO_2 protective decoration enhances the durability of a Pt based electrocatalyst *J. Mater. Chem.* A **4** 969–75

[124] Weimer M S, Hu B, Kraft S J, Gordon R G, Segre C U and Hock A S 2016 Synthetic and spectroscopic study of the mechanism of atomic layer deposition of tin dioxide *Organometallics* **35** 1202–8

[125] Kim S, Kim D H and Hong S H 2012 Epitaxial growth of orthorhombic SnO_2 films on various YSZ substrates by plasma enhanced atomic layer deposition *J. Cryst. Growth* **348** 15–9

[126] Choi G, Satyanarayana L and Park J 2006 Effect of process parameters on surface morphology and characterization of PE-ALD SnO_2 thin films for gas sensing *Appl. Surf. Sci.* **252** 7878–83

[127] Karam N H, Parodos T, Colter P, McNulty D, Rowland W, Schetzina J, El-Masry N and Bedair S M 1995 Growth of device quality GaN at 550 °C by atomic layer epitaxy *Appl. Phys. Lett.* **67** 94–6

[128] Huang S-C, Wang H-Y, Hsu C-J, Gong J-R, Chiang C-I, Tu S-L and Chang H 1998 Growth of wurtzite GaN on (0 0 1) GaAs substrates at low temperature by atomic layer epitaxy *J. Mater. Sci. Lett.* **17** 1281–5

[129] Kim O H, Kim D and Anderson T 2009 Atomic layer deposition of GaN using $GaCl_3$ and NH_3 *J. Vac. Sci. Technol.* A **27** 923–8

[130] Ozgit C, Donmez I, Alevli M and Biyikli N 2012 Atomic layer deposition of GaN at low temperatures *J. Vac. Sci. Technol.* A **30** 01A124

[131] Ozgit-Akgun C, Goldenberg E, Okyay A K and Biyikli N 2014 Hollow cathode plasma-assisted atomic layer deposition of crystalline AlN, GaN and $Al_xGa_{1-x}N$ thin films at low temperatures *J. Mater. Chem.* C **2** 2123–36

[132] Alevli M, Haider A, Kizir S, Leghari S A and Biyikli N 2016 Comparison of trimethylgallium and triethylgallium as 'Ga' source materials for the growth of ultrathin GaN films on Si (100) substrates via hollow-cathode plasma-assisted atomic layer deposition *J. Vac. Sci. Technol.* A **34** 01A137

[133] Alevli M, Gungor N, Haider A, Kizir S, Leghari S A and Biyikli N 2016 Substrate temperature influence on the properties of GaN thin films grown by hollow-cathode plasma-assisted atomic layer deposition *J. Vac. Sci. Technol.* A **34** 01A125

[134] Biyikli N, Ozgit-Akgun C, Goldenberg E, Haider A, Kizir S, Uyar T, Bolat S, Tekcan B and Okyay A K 2015 Hollow-cathode plasma-assisted atomic layer deposition: a novel route for low-temperature synthesis of crystalline III-nitride thin films and nanostructures *2015 IEEE 35th Int. Conf. Electron. Nanotechnology, ELNANO 2015* pp 218–21

[135] Haider A, Kizir S, Alevli M, Gungor N, Deminskyi P, Tsymbalenko O, Leghari S A and Biyikli N 2016 Effect of substrate temperature and ga source precursor on growth and material properties of GaN grown by hollow cathode plasma assisted atomic layer deposition *2016 IEEE 36th Int. Conf. Electron. Nanotechnology, ELNANO 2016* pp 132–4

[136] Deminskyi P, Haider A, Biyikli N, Ovsianitsky A, Tsymbalenko A, Kotov D, Matkivskyi V, Liakhova N and Osinsky V 2016 Investigation of native oxide removing from HCPA ALD grown GaN thin films surface utilizing HF solutions *2016 IEEE 36th Int. Conf. Electron. Nanotechnology, ELNANO 2016* pp 128–31

[137] Motamedi P, Dalili N and Cadien K C 2015 A route to low temperature growth of single crystal GaN on sapphire *J. Mater. Chem.* C **3** 7428–36

[138] Kizir S, Haider A and Biyikli N 2016 Substrate impact on the low-temperature growth of GaN thin films by plasma-assisted atomic layer deposition *J. Vac. Sci. Technol.* A **34** 041511

[139] Sprenger J K, Cavanagh A S, Sun H, Wahl K J, Roshko A and George S M 2016 Electron enhanced growth of crystalline gallium nitride thin films at room temperature and 100 °C using sequential surface reactions *Chem. Mater.* **28** 5282–94

[140] Perros A P, Hakola H, Sajavaara T, Huhtio T and Lipsanen H 2013 Influence of plasma chemistry on impurity incorporation in AlN prepared by plasma enhanced atomic layer deposition *J. Phys. D: Appl. Phys.* **46** 505502

[141] Ozgit C, Donmez I, Alevli M and Biyikli N 2012 Self-limiting low-temperature growth of crystalline AlN thin films by plasma-enhanced atomic layer deposition *Thin Solid Films* **520** 2750–5

[142] Motamedi P and Cadien K 2014 XPS analysis of AlN thin films deposited by plasma enhanced atomic layer deposition *Appl. Surf. Sci.* **315** 104–9

[143] Tarala V A, Altakhov A S, Shevchenko M Y, Valyukhov D P, Lisitsyn S V and Martens V Y 2015 Growth of aluminum nitride films by plasma-enhanced atomic layer deposition *Inorg. Mater.* **51** 728–35

[144] Van Bui H, Wiggers F B, Gupta A, Nguyen M D, Aarnink A A I, de Jong M P and Kovalgin A Y 2015 Initial growth, refractive index, and crystallinity of thermal and plasma-enhanced atomic layer deposition AlN films *J. Vac. Sci. Technol.* A **33** 01A111

[145] Broas M, Sippola P, Sajavaara T, Vuorinen V, Perros A P and Lipsanen H 2016 Structural and chemical analysis of annealed plasma-enhanced atomic layer deposition aluminum nitride films *J. Vac. Sci. Technol.* A **34** 041506

[146] Lee Y J 2004 Formation of aluminum nitride thin films as gate dielectrics on Si (100) *J. Cryst. Growth* **266** 568–72

[147] Riihela D, Ritala M, Matero R, Leskela M, Jokinen J and Haussalo P 1996 Low temperature deposition of AIN films by an alternate supply of trimethyl aluminum and ammonia *Chem. Vapor Depos.* **2** 277–83

[148] Eom D, No S Y, Hwang C S and Kim H J 2006 Properties of aluminum nitride thin films deposited by an alternate injection of trimethylaluminum and ammonia under ultraviolet radiation *J. Electrochem. Soc.* **153** C229–34

[149] Ozgit-akgun C, Donmez I, Alevli M and Biyikli N 2012 Self-limiting low-temperature growth of crystalline AlN thin films by plasma-enhanced atomic layer deposition *Thin Solid Films* **520** 2750–5

[150] Altuntas H, Bayrak T, Kizir S, Haider A and Biyikli N 2016 Electrical conduction and dielectric relaxation properties of AlN thin films grown by hollow-cathode plasma-assisted atomic layer deposition *Semicond. Sci. Technol.* **31** 075003

[151] Sadeghpour S, Ceyssens F and Puers R 2016 Crystalline growth of AlN thin films by atomic layer deposition *J. Phys.: Conf. Ser.* **757** 012003

[152] Motamedi P and Cadien K 2015 Structural and optical characterization of low-temperature ALD crystalline AlN *J. Cryst. Growth* **421** 45–52

[153] Tarala V, Ambartsumov M, Altakhov A, Martens V and Shevchenko M 2016 Growing c-axis oriented aluminum nitride films by plasma-enhanced atomic layer deposition at low temperatures *J. Cryst. Growth* **455** 157–60

[154] Ozgit-Akgun C, Goldenberg E, Bolat S, Tekcan B, Kayaci F, Uyar T, Okyay A K and Biyikli N 2015 Low-temperature hollow cathode plasma-assisted atomic layer deposition of crystalline III-nitride thin films and nanostructures *Phys. Status Solidi* **12** 394–8

[155] Haider A, Kizir S, Ozgit-Akgun C, Goldenberg E, Leghari S A, Okyay A K and Biyikli N 2015 Low-temperature grown wurtzite $In_xGa_{1-x}N$ thin films via hollow cathode plasma-assisted atomic layer deposition *J. Mater. Chem.* C **3** 9620–30

[156] Haider A, Kizir S, Ozgit-Akgun C, Okyay A K and Biyikli N 2016 Low-temperature sequential pulsed chemical vapor deposition of ternary $B_xGa_{1-x}N$ and $B_xIn_{1-x}N$ thin film alloys *J. Vac. Sci. Technol.* A **34** 01A123

[157] Haider A, Kizir S and Biyikli N 2016 Low-temperature self-limiting atomic layer deposition of wurtzite InN on Si(100) *AIP Adv.* **6** 045203

[158] Nepal N, Mahadik N A, Nyakiti L O, Qadri S B, Mehl M J, Hite J K and Eddy C R 2013 Epitaxial growth of cubic and hexagonal InN thin films via plasma-assisted atomic layer epitaxy *Cryst. Growth Des.* **13** 1485–90

[159] Mårlid B, Ottosson M, Pettersson U, Larsson K and Carlsson J O 2002 Atomic layer deposition of BN thin films *Thin Solid Films* **402** 167–71

[160] Ferguson J D, Weimer A W and George S M 2002 Atomic layer deposition of boron nitride using sequential exposures of BCl3 and NH3 *Thin Solid Films* **413** 16–25

[161] Olander J, Ottosson L M, Heszler P, Carlsson J-O and Larsson K M E 2005 Laser-assisted atomic layer deposition of boron nitride thin films *Chem. Vapor Depos.* **11** 330–7

[162] Haider A, Ozgit-Akgun C, Goldenberg E, Okyay A K and Biyikli N 2014 Low-temperature deposition of hexagonal boron nitride via sequential injection of triethylboron and N_2/H_2 plasma *J. Am. Ceram. Soc.* **97** 4052–9

[163] Driver M S, Beatty J D, Olanipekun O, Reid K, Rath A, Voyles P M and Kelber J A 2016 Atomic layer epitaxy of h-BN(0001) multilayers on Co(0001) and molecular beam epitaxy growth of graphene on h-BN(0001)/Co(0001) *Langmuir* **32** 2601–7

[164] Jones J, Beauclair B, Olanipekun O, Lightbourne S, Zhang M, Pollok B, Pilli A and Kelber J 2017 Atomic layer deposition of h-BN (0001) on RuO_2(110)/Ru (0001) *J. Vac. Sci. Technol.* A **35** 01B139

[165] Suntola T and Antson J 1975 *US Patent* 4,058,430

[166] Ihanus J, Lankinen M P, Kemell M, Ritala M and Leskelä M 2005 Aging of electroluminescent ZnS:Mn thin films deposited by atomic layer deposition processes *J. Appl. Phys.* **98** 113526

[167] Yoo D, Heo S C, Choi M S, Kim D and Chung C 2013 Influence of different annealing ambients on the properties of zinc sulfide prepared by atomic layer deposition *Japan. J. Appl. Phys.* **52** 10MB19

[168] MacK J F, Van Stockum P B, Yemane Y T, Logar M, Iwadate H and Prinz F B 2012 Observing the nucleation phase of atomic layer deposition *in situ Chem. Mater.* **24** 4357–62

[169] Bakke J R, Tanskanen J T, Hägglund C, Pakkanen T A and Bent S F 2012 Growth characteristics, material properties, and optical properties of zinc oxysulfide films deposited by atomic layer deposition *J. Vac. Sci. Technol.* A **30** 01A135

[170] Tanskanen J T, Bakke J R, Bent S F and Pakkanen T A 2010 ALD growth characteristics of ZnS films deposited from organozinc and hydrogen sulfide precursors *Langmuir* **26** 11899–906

[171] Bakke J R, King J S, Jung H J, Sinclair R and Bent S F 2010 Atomic layer deposition of ZnS via *in situ* production of H_2S *Thin Solid Films* **518** 5400–8

[172] Kim Y S and Yun S J 2004 Studies on polycrystalline ZnS thin films grown by atomic layer deposition for electroluminescent applications *Appl. Surf. Sci.* **229** 105–11

[173] Stuyven G, De Visschere P, Hikavyy A and Neyts K 2002 Atomic layer deposition of ZnS thin films based on diethyl zinc and hydrogen sulfide *J. Cryst. Growth* **234** 690–8

[174] Dasgupta N P, Meng X, Elam J W and Martinson A B F 2015 Atomic layer deposition of metal sulfide materials *Acc. Chem. Res.* **48** 341–8

[175] Short A, Jewell L, Doshay S, Church C, Keiber T, Bridges F, Carter S and Alers G 2013 Atomic layer deposition of zinc sulfide with $Zn(TMHD)_2$ *J. Vac. Sci. Technol.* A **31** 01A138

[176] Tadokoro O, Ohta S-I, Ishiguro T, Ichinose Y, Kobayashi S and Yamamoto N 1993 Growth and characterization of CdS epilayers on (100)GaAs by atomic layer epitaxy *J. Cryst. Growth* **130** 29–36

[177] Luo Y, Han M, Slater D A and Osgood R M Jr 2000 Studies of heteroepitaxial growth of thin II–VI semiconductor layers by sequential ultrahigh vacuum dosing *J. Vac. Sci. Technol.* A **18** 438–49

[178] Bakke J R, Jung H J, Tanskanen J T, Sinclair R and Bent S F 2010 Atomic layer deposition of CdS films *Chem. Mater.* **22** 4669–78

[179] Schneider N, Lincot D and Donsanti F 2016 Atomic layer deposition of copper sulfide thin films *Thin Solid Films* **600** 103–8

[180] Short A, Jewell L, Bielecki A, Keiber T, Bridges F, Carter S and Alers G 2014 Structure in multilayer films of zinc sulfide and copper sulfide via atomic layer deposition *J. Vac. Sci. Technol.* A **32** 01A125

[181] Martinson A B F, Riha S C, Thimsen E, Elam J W and Pellin M J 2013 Structural, optical, and electronic stability of copper sulfide thin films grown by atomic layer deposition *Energy Environ. Sci.* **6** 1868–78

[182] Martinson A B F, Elam J W and Pellin M J 2009 Atomic layer deposition of Cu_2S for future application in photovoltaics *Appl. Phys. Lett.* **94** 123107

[183] Reijnen L, Meester B, Goossens A and Schoonman J 2003 Atomic layer deposition of Cu_xS for solar energy conversion *Chem. Vapor Depos.* **9** 15–20

[184] Johansson J, Kostamo J, Karppinen M and Niinistö L 2002 Growth of conductive copper sulfide thin films by atomic layer deposition *J. Mater. Chem.* **12** 1022–6

[185] Dasgupta N P, Lee W and Prinz F B 2009 Atomic layer deposition of lead sulfide thin films for quantum confinement *Chem. Mater.* **21** 3973–8

[186] Dasgupta N P, Walch S P and Prinz F 2008 Fabrication and characterization of lead sulfide thin films by atomic layer deposition *ECS Trans.* **16** 29–36

[187] Lee W, Dasgupta N P, Trejo O, Lee J R, Hwang J, Usui T and Prinz F B 2010 Area-selective atomic layer deposition of lead sulfide: nanoscale patterning and DFT simulations *Langmuir* **26** 6845–52

[188] Kim J Y and George S M 2010 Tin monosulfide thin films grown by atomic layer deposition using tin 2,4-pentanedionate and hydrogen sulfide *J. Phys. Chem.* **114** 17597–603

[189] Sinsermsuksakul P, Heo J, Noh W, Hock A S and Gordon R G 2011 Atomic layer deposition of tin monosulfide thin films *Adv. Energy Mater.* **1** 1116–25

[190] Ham G, Shin S, Park J, Choi H, Kim J, Lee Y-A, Seo H and Jeon H 2013 Tuning the electronic structure of tin sulfides grown by atomic layer deposition *ACS Appl. Mater. Interfaces* **5** 8889–96

[191] McCarthy R F, Weimer M S, Emery J D, Hock A S and Martinson A B F 2014 Oxygen-free atomic layer deposition of indium sulfide *ACS Appl. Mater. Interfaces* **6** 12137–45

[192] Yousfi E B, Weinberger B, Donsanti F, Cowache P and Lincot D 2001 Atomic layer deposition of zinc oxide and indium sulfide layers for Cu (In,Ga)Se_2 thin-film solar cells *Thin Solid Films* **387** 29–32

[193] Meng X, Libera J A, Fister T T, Zhou H, Hedlund J K, Fenter P and Elam J W 2014 Atomic layer deposition of gallium sulfide films using hexakis(dimethylamido) digallium and hydrogen sulfide *Chem. Mater.* **26** 1029–39

[194] Pore V, Hatanpää T, Ritala M and Leskela M 2009 Atomic layer deposition of metal tellurides and selenides using alkylsilyl compounds of tellurium and selenium *J. Am. Chem. Soc.* **131** 3478–80

[195] Kopalko K, Godlewski M, Guziewicz E, Łusakowska E, Paszkowicz W, Domagała J, Dynowska E, Szczerbakow A, Wójcik A and Phillips M R 2004 Monocrystalline thin films of ZnSe and ZnO grown by atomic layer epitaxy *Vacuum* **74** 269–72

[196] Guziewicz E, Godlewski M, Kopalko K, Łusakowska E, Dynowska E, Guziewicz M, Godlewski M M and Phillips M 2004 Atomic layer deposition of thin films of ZnSe—structural and optical characterization *Thin Solid Films* **446** 172–7

[197] Ezhovskii Y K 2014 Atomic-layer deposition of cadmium chalcogenides on silicon *Russ. J. Phys. Chem.* A **88** 1580–4

[198] Sarnet T, Hatanpää T, Laitinen M, Sajavaara T, Mizohata K, Ritala M and Leskelä M 2016 Alkylsilyl compounds as enablers of atomic layer deposition: analysis of $(Et_3Si)_3$ as through the GaAs process *J. Mater. Chem.* C **4** 449–54

[199] Matsuyama M, Sugahara S, Ikeda K, Uchida Y and Matsumura M 2000 Hetero atomic-layer epitaxy of Ge on Si (100) *Japan. J. Appl. Phys.* **39** 2536–40

[200] Sugahara S, Uchida Y, Kitamura T, Nagai T, Matsuyama M, Hattori T and Matsumura M 1997 A proposed atomic-layer-deposition of germanium on Si surface *Japan. J. Appl. Phys.* **36** 1609–13

[201] Chiang C M, Rowe J E, Malic R A, Sen A, Steigerwald M L and Mills A P 1996 A new CVD reaction for atomic layer deposition of silicon *Appl. Surf. Sci.* **107** 189–96

[202] Yokoyama S, Ohba K and Nakajima A 2001 Self-limiting atomic-layer deposition of Si on SiO_2 by alternate supply of Si_2H_6 and $SiCl_4$ *Appl. Phys. Lett.* **79** 617–9

[203] Winter C, Sun J, Savithra L, Kalutarage L, Knisley T and Saly M 2016 Low temperature, thermal atomic layer deposition of elemental germanium films. Selective growth on platinum substrates *ALD 2016 Conf. Abstract* https://happen.conference-services.net/resources/2074/4959/pdf/ALDep2016_0270.pdf

[204] Sang B, Yamada A and Konagai M 1997 Growth of boron-doped ZnO thin films by atomic layer deposition *Sol. Energy Mater. Sol. Cells* **49** 19–26

[205] Lin M-C, Chang Y-J, Chen M-J and Chu C-J 2011 Characteristics of Zr-doped ZnO thin films grown by atomic layer deposition *J. Electrochem. Soc.* **158** D395–8

[206] Cheng Y-C 2011 Effects of post-deposition rapid thermal annealing on aluminum-doped ZnO thin films grown by atomic layer deposition *Appl. Surf. Sci.* **258** 604–7

[207] Dhakal T, Vanhart D, Christian R, Nandur A, Sharma A and Westgate C R 2012 Growth morphology and electrical/optical properties of Al-doped ZnO thin films grown by atomic layer deposition *J. Vac. Sci. Technol.* A **30** 021202

[208] Qian K-J, Chen S, Zhu B, Chen L, Ding S-J, Lu H-L, Sun Q-Q, Zhang D W and Chen Z 2012 Atomic layer deposition of ZnO on thermal SiO_2 and Si surfaces using N_2-diluted diethylzinc and H_2O_2 precursors *Appl. Surf. Sci.* **258** 4657–66

[209] Genevee P, Donsanti F, Renou G and Lincot D 2013 Study of the aluminum doping of zinc oxide films prepared by atomic layer deposition at low temperature *Appl. Surf. Sci.* **264** 464–9

[210] Baji Z, Lábadi Z, Molnár G, Pécz B, Vad K, Horváth Z E, Szabó P J, Nagata T and Volk J 2014 Highly conductive epitaxial ZnO layers deposited by atomic layer deposition *Thin Solid Films* **562** 485–9

[211] Choi N-J, Kim K-W, Son H-S and Lee S-N 2014 Optical and electrical characterization of AZO films grown on c-plane sapphire substrates by atomic layer deposition *Electron. Mater. Lett.* **10** 259–62

[212] Choi N-J, Son H-S, Choi H-J, Kim K-K and Lee S-N 2014 Comparative studies of nonpolar (10-10) ZnO films grown by using atomic layer deposition and radio-frequency magnetron sputtering *J. Korean Phys. Soc.* **65** 417–20

[213] Kolkovsky V, Snigurenko D, Jakiela R and Guziewicz E 2014 Electrical and structural characterization of nitrogen doped ZnO layers grown at low temperature by atomic layer deposition *Semicond. Sci. Technol.* **29** 085006

[214] Särkijärvi S, Sintonen S, Tuomisto F, Bosund M, Suihkonen S and Lipsanen H 2014 Effect of growth temperature on the epitaxial growth of ZnO on GaN by ALD *J. Cryst. Growth* **398** 18–22

[215] Snigurenko D *et al* 2014 XPS study of arsenic doped ZnO grown by atomic layer deposition *J. Alloys Compd.* **582** 594–7

[216] Zhang Y, Lu H-L, Geng Y, Sun Q-Q, Ding S-J and Zhang D W 2014 Impact of rapid thermal annealing on structural and electrical properties of ZnO thin films grown atomic layer deposition on GaAs substrates *Vacuum* **103** 1–4

[217] Akopyan I K *et al* 2015 Photoluminescence spectra of thin Zno films grown by ALD technology *Phys. Solid State* **57** 1865–9

[218] Kumar A, Kumar P, Kumar K, Singh T, Singh R, Asokan K and Kanjilal D 2015 Role of growth temperature on the structural, optical and electrical properties of ZnO thin films *J. Alloys Compd.* **649** 1205–9

[219] Wang A, Chen T, Lu S, Wu Z, Li Y, Chen H and Wang Y 2015 Effects of doping and annealing on properties of ZnO films grown by atomic layer deposition *Nanoscale Res. Lett.* **10** 75

[220] Iqbal J, Jilani A, Ziaul Hassan P M, Rafique S, Jafer R and Alghamdi A A 2016 ALD grown nanostructured ZnO thin films: Effect of substrate temperature on thickness and energy band gap *J. King Saud Univ., Eng. Sci.* **28** 347–54

[221] Vceh M, Chen H-C, Chen M-J, Yang J-R and Shiojiri M 2010 Structure and electro-optical properties of thin films grown by alternate atomic layer deposition of ZnO and Al_2O_3 on the sapphire substrate *Mater. Trans.* **51** 219–26

[222] Haider A, Deminskyi P, Khan T M, Eren H and Biyikli N 2016 Area-selective atomic layer deposition using inductively coupled plasma polymerized fluorocarbon layer: a case study for metal-oxides *J. Phys. Chem.* C **120** 26393–401

[223] Dasgupta N P, Neubert S, Lee W, Trejo O, Lee J R and Prinz F B 2010 Atomic layer deposition of Al-doped ZnO films: Effect of grain orientation on conductivity *Chem. Mater.* **22** 4769–75

[224] Lee D-J, Kim H-M, Kwon J-Y, Choi H, Kim S-H and Kim K-B 2011 Structural and electrical properties of atomic layer deposited Al-doped ZnO films *Adv. Funct. Mater.* **21** 448–55

[225] Lee D-J, Kwon J-Y, Kim S-H, Kim H-M and Kim K-B 2011 Effect of Al distribution on carrier generation of atomic layer deposited Al-doped ZnO films *J. Electrochem. Soc.* **158** D277–81

[226] Baji Z, Lábadi Z, Horváth Z E and Bársony I 2012 Structure and morphology of aluminium doped zinc-oxide layers prepared by atomic layer deposition *Thin Solid Films* **520** 4703–6

[227] Frölich A and Wegener M 2011 Spectroscopic characterization of highly doped ZnO films grown by atomic-layer deposition for three-dimensional infrared metamaterials *Opt. Mater. Express* **1** 883–9

[228] Haider A, Yilmaz M, Deminskyi P, Eren H and Biyikli N 2016 Nanoscale selective area atomic layer deposition of TiO_2 using e-beam patterned polymers *RSC Adv.* **6** 106109–19

[229] Tao Q, Overhage K, Jursich G and Takoudis C 2012 On the initial growth of atomic layer deposited TiO_2 films on silicon and copper surfaces *Thin Solid Films* **520** 6752–6

[230] Aarik J, Arroval T, Aarik L, Rammula R, Kasikov A, Mändar H, Hudec B, Hušeková K and Fröhlich K 2013 Atomic layer deposition of rutile-phase TiO_2 on RuO_2 from $TiCl_4$ and O_3: growth of high-permittivity dielectrics with low leakage current *J. Cryst. Growth* **382** 61–6

[231] Aarik L, Arroval T, Rammula R, Mändar H, Sammelselg V and Aarik J 2013 Atomic layer deposition of TiO_2 from $TiCl_4$ and O_3 *Thin Solid Films* **542** 100–7

[232] Lee J, Lee S J, Han W B, Jeon H, Park J, Jang W, Yoon C S and Jeon H 2013 Deposition temperature dependence of titanium oxide thin films grown by remote-plasma atomic layer deposition *Phys. Status Solidi* a **210** 276–84

[233] Theirich D, Muller R, Zilberberg K, Trost S, Behrendt A and Riedl T 2013 Atmospheric pressure plasma ALD of titanium oxide *Chem. Vapor Depos.* **19** 167–73

[234] Zhao C, Hedhili M N, Li J, Wang Q, Yang Y, Chen L and Li L 2013 Growth and characterization of titanium oxide by plasma enhanced atomic layer deposition *Thin Solid Films* **542** 38–44

[235] Strobel A, Schnabel H-D, Reinhold U, Rauer S and Neidhardt A 2016 Room temperature plasma enhanced atomic layer deposition for TiO_2 and WO_3 films *J. Vac. Sci. Technol.* A **34** 01A118

[236] Jin C, Liu B, Lei Z and Sun J 2015 Structure and photoluminescence of the TiO_2 films grown by atomic layer deposition using tetrakis-dimethylamino titanium and ozone *Nanoscale Res. Lett.* **10** 95

[237] Ratzsch S, Kley E-B, Tünnermann A and Szeghalmi A 2015 Influence of the oxygen plasma parameters on the atomic layer deposition of titanium dioxide *Nanotechnology* **26** 024003

[238] Chiappim W, Testoni G E, Moraes R S, Pessoa R S, Sagas J C, Origo F D, Vieira L and MacIel H S 2016 Structural, morphological, and optical properties of TiO_2 thin films grown by atomic layer deposition on fluorine doped tin oxide conductive glass *Vacuum* **123** 91–102

[239] Gebhard M, Mitschker F, Wiesing M, Giner I, Torun B, de los Arcos T, Awakowicz P, Grundmeier G and Devi A 2016 An efficient PE-ALD process for TiO_2 thin films employing a new Ti-precursor *J. Mater. Chem.* C **4** 1057–65

[240] Shan F K, Liu G X, Lee W J, Lee G H, Kim I S and Shin B C 2005 Structural, electrical, and optical properties of transparent gallium oxide thin films grown by plasma-enhanced atomic layer deposition *J. Appl. Phys.* **98** 023504

[241] Shan F K, Liu G X, Lee W J, Lee G H, Kim I S and Shin B C 2006 Ga_2O_3 thin film deposited by atomic layer deposition with high plasma power *Integr. Ferroelectr.* **80** 197–206

[242] Liu G X, Shan F K, Lee W J, Kim S C, Kim H S and Cho C R 2007 Growth temperature dependence of Ga_2O_3 thin films deposited by plasma enhanced atomic layer deposition *Integr. Ferroelectr.* **94** 11–20

[243] Comstock D J and Elam J W 2012 Atomic layer deposition of Ga_2O_3 films using trimethylgallium and ozone *Chem. Mater.* **24** 4011–8

[244] Chandiran A K, Tetreault N, Humphry-baker R, Kessler F, Barano E, Yi C, Nazeeruddin M K and Grätzel M 2012 Sub-nanometer Ga_2O_3 tunnelling layer by atomic layer deposition to achieve 1.1 V open- circuit potential in dye-sensitized solar cells *Nano Lett.* **12** 3941–7

[245] Allen T G and Cuevas A 2014 Electronic passivation of silicon surfaces by thin films of atomic layer deposited gallium oxide *Appl. Phys. Lett.* **105** 031601

[246] Ramachandran R K, Dendooven J and Detavernier C 2014 Plasma enhanced atomic layer deposition of Fe_2O_3 thin films *J. Mater. Chem.* A **2** 10662–7

[247] Altuntas H, Donmez I, Ozgit-Akgun C and Biyikli N 2014 Effect of postdeposition annealing on the electrical properties of β-Ga_2O_3 thin films grown on p-Si by plasma-enhanced atomic layer deposition *J. Vac. Sci. Technol.* A **32** 041504

[248] Boschi F, Bosi M, Berzina T, Buffagni E, Ferrari C and Fornari R 2016 Hetero-epitaxy of ε-Ga_2O_3 layers by MOCVD and ALD *J. Cryst. Growth* **443** 25–30

[249] Shih H-Y, Chu F-C, Das A, Lee C-Y, Chen M-J and Lin R-M 2016 Atomic layer deposition of gallium oxide films as gate dielectrics in AlGaN/GaN metal-oxide-semiconductor high-electron-mobility transistors *Nanoscale Res. Lett.* **11** 235

[250] Jeong B-S, Norton D P, Budai J D and Jellison G E 2004 Epitaxial growth of anatase by reactive sputter deposition using water vapor as the oxidant *Thin Solid Films* **446** 18–22

[251] Gebhard M, Hellwig M, Parala H, Xu K, Winter M and Devi A 2014 Indium-tris-guanidinates: a promising class of precursors for water assisted atomic layer deposition of In_2O_3 thin films *Dalton Trans.* **43** 937–40

[252] Macco B, Wu Y, Vanhemel D and Kessels W M M 2014 High mobility In_2O_3:H transparent conductive oxides prepared by atomic layer deposition and solid phase crystallization *Phys. Status Solidi* **8** 987–90

[253] Macco B, Knoops H C M and Kessels W M M 2015 Electron scattering and doping mechanisms in solid-phase-crystallized In_2O_3:H prepared by atomic layer deposition *ACS Appl. Mater. Interfaces* **7** 16723–9

[254] Maeng W J, Choi D, Park J and Park J-S 2015 Atomic layer deposition of highly conductive indium oxide using a liquid precursor and water oxidant *Ceram. Int.* **41** 10782–7

[255] Kim D, Nam T, Park J, Gatineau J and Kim H 2015 Growth characteristics and properties of indium oxide and indium-doped zinc oxide by atomic layer deposition *Thin Solid Films* **587** 83–7

[256] Kim H Y *et al* 2016 Low-temperature growth of indium oxide thin film by plasma-enhanced atomic layer deposition using liquid dimethyl (N-ethoxy-2,2-dimethylpropanamido) indium for high-mobility thin film transistor application *ACS Appl. Mater. Interfaces* **8** 26924–31

[257] Mane A U, Allen A J, Kanjolia R K and Elam J W 2016 Indium oxide thin films by atomic layer deposition using trimethylindium and ozone *J. Phys. Chem.* C **120** 9874–83

[258] Yang T S, Cho W, Kim M, An K-S, Chung T-M, Kim C G and Kim Y 2005 Atomic layer deposition of nickel oxide films using $Ni(dmamp)_2$ and water *J. Vac. Sci. Technol.* A **23** 1238

[259] Lu H L, Scarel G, Wiemer C, Perego M, Spiga S, Fanciulli M and Pavia G 2008 Atomic layer deposition of NiO films on Si(100) using cyclopentadienyl-type compounds and ozone as precursors *J. Electrochem. Soc.* **155** H807–11

[260] Lindahl E, Lu J, Ottosson M and Carlsson J-O 2009 Epitaxial NiO (100) and NiO (111) films grown by atomic layer deposition *J. Cryst. Growth* **311** 4082–8

[261] Lindahl E, Ottosson M and Carlsson J O 2009 Atomic layer deposition of NiO by the $Ni(thd)_2/H_2O$ precursor combination *Chem. Vapor Depos.* **15** 186–91

[262] Bachmann J, Zolotaryov A, Albrecht O, Goetze S, Berger A, Hesse D, Novikov D and Nielsch K 2011 Stoichiometry of nickel oxide films prepared by ALD *Chem. Vapor Depos.* **17** 177–80

[263] Song S J, Lee S W, Kim G H, Seok J Y, Yoon K J, Yoon J H, Hwang C S, Gatineau J and Ko C 2012 Substrate dependent growth behaviors of plasma-enhanced atomic layer deposited nickel oxide films for resistive switching application *Chem. Mater.* **24** 4675–85

[264] Thimsen E, Martinson A B F, Elam W and Pellin M J 2012 Energy levels, electronic properties, and rectification in ultrathin p—NiO films synthesized by atomic layer deposition *J. Phys. Chem.* C **116** 16830–40

[265] Hsu C-C, Su H-W, Hou C-H, Shyue J-J and Tsai F-Y 2015 Atomic layer deposition of NiO hole-transporting layers for polymer solar cells *Nanotechnology* **26** 385201

[266] Nardi K L, Yang N, Dickens C F, Strickler A L and Bent S F 2015 Creating highly active atomic layer deposited NiO electrocatalysts for the oxygen evolution reaction *Adv. Energy Mater.* **5** 1500412

[267] Shen Y D, Li Y W, Li W M, Zhang J Z, Hu Z G and Chu J H 2012 Growth of Bi_2O_3 ultrathin films by atomic layer deposition *J. Phys. Chem.* C **116** 3449–56

[268] Tsuchiya H, Akamatsu M, Ishida M and Hasegawa F 1996 Layer-by-layer growth of GaN on GaAs substrates by alternate supply of $GaCl_3$ and NH_3 *Japan. J. Appl. Phys.* **35** L748–50

[269] Haider A, Kizir S, Alevli M, Gungor N, Deminskyi P, Tsymbalenko O, Leghari S A and Biyikli N 2016 Effect of substrate temperature and Ga source precursor on growth and material properties of GaN grown by hollow cathode plasma assisted atomic layer deposition *2016 IEEE 36th Int. Conf. Electron. Nanotechnology, ELNANO 2016* pp 132–4

[270] Motamedi P and Cadien K 2015 Structure–property relationship and interfacial phenomena in GaN grown on C-plane sapphire via plasma-enhanced atomic layer deposition *RSC Adv.* **5** 57865–74

[271] Shih H-Y, Lin M-C, Chen L-Y and Chen M-J 2015 Uniform GaN thin films grown on (100) silicon by remote plasma atomic layer deposition *Nanotechnology* **26** 014002

[272] Acharya A R, Thoms B D, Nepal N and Eddy C R 2015 Surface structure and surface kinetics of InN grown by plasma-assisted atomic layer epitaxy: a HREELS study *J. Vac. Sci. Technol.* A **33** 021401

[273] Consiglio S, Clark R D, O'Meara D, Wajda C, Tapily K and Leusink G J 2016 Comparison of B_2O_3 and BN deposited by atomic layer deposition for forming ultrashallow dopant regions by solid state diffusion *J. Vac. Sci. Technol.* A **34** 01A102

[274] Snure M, Paduano Q, Hamilton M, Shoaf J and Matthew Mann J 2014 Optical characterization of nanocrystalline boron nitride thin films grown by atomic layer deposition *Thin Solid Films* **571** 51–5

[275] Goerke S, Ziegler M, Ihring A, Dellith J, Undisz A, Diegel M, Anders S, Huebner U, Rettenmayr M and Meyer H-G 2015 Atomic layer deposition of AlN for thin membranes using trimethylaluminum and H_2/N_2 plasma *Appl. Surf. Sci.* **338** 35–41

[276] Nepal N, Goswami R, Qadri S B, Mahadik N A, Kub F J and Eddy C R 2014 Growth of AlN/Pt heterostructures on amorphous substrates at low temperatures via atomic layer epitaxy *Scr. Mater.* **93** 44–7

[277] Dendooven J, Deduytsche D, Musschoot J, Vanmeirhaeghe R L and Detavernier C 2010 Conformality of Al_2O_3 and AlN deposited by plasma-enhanced atomic layer deposition *J. Electrochem. Soc.* **157** G111–6

[278] Ezhovskii Y K and Zakharova N V 2016 Atomic layer deposition of zinc sulfide nanolayers on monocrystalline silicon substrates *Russ. J. Phys. Chem.* A **90** 647–51

[279] Sinsermsuksakul P, Chakraborty R, Kim S B, Heald S M, Buonassisi T and Gordon R G 2012 Antimony-doped Tin(II) sulfide thin films *Chem. Mater.* **24** 4556–62

[280] Zhang K, Pillai A D R, Bollenbach K, Nminibapiel D, Cao W, Baumgart H, Scherer T, Chakravadhanula V S K, Kübel C and Kochergin V 2014 Atomic layer deposition of nanolaminate structures of alternating PbTe and PbSe thermoelectric films *ECS J. Solid State Sci. Technol.* **3** P207–12

[281] Takemura Y, Nakanishi H, Konagai M and Takahashi K 1991 Self-limiting growth in atomic layer epitaxy of ZnTe *Japan. J. Appl. Phys.* **30** L246–8

[282] Sarnet T, Hatanpää T, Puukilainen E, Mattinen M, Vehkamäki M, Mizohata K, Ritala M and Leskela M 2014 Atomic layer deposition and characterization of Bi_2Te_3 thin films *J. Phys. Chem.* A **119** 2298–306

[283] Kente T and Mhlanga S D 2016 Gallium nitride nanostructures: synthesis, characterization and applications *J. Cryst. Growth* **444** 55–72
[284] Haider A, Ozgit-Akgun C, Kayaci F, Okyay A K, Uyar T and Biyikli N 2014 Fabrication of AlN/BN bishell hollow nanofibers by electrospinning and atomic layer deposition *Apl. Mater.* **2** 096109
[285] Ozgit-Akgun C, Kayaci F, Vempati S, Haider A, Celebioglu A, Goldenberg E, Kizir S, Uyar T and Biyikli N 2015 Fabrication of flexible polymer–GaN core–shell nanofibers by the combination of electrospinning and hollow cathode plasma-assisted atomic layer deposition *J. Mater. Chem.* C **3** 5199–206
[286] Koester R, Hwang J S, Durand C, Dang D L S and Eymery J 2010 Self-assembled growth of catalyst-free GaN wires by metal-organic vapour phase epitaxy *Nanotechnology* **21** 015602
[287] Lin Y T, Yeh T W, Nakajima Y and Dapkus P D 2014 Catalyst-free GaN nanorods synthesized by selective area growth *Adv. Funct. Mater.* **24** 3162–71
[288] Brennan T P, Ardalan P, Lee H-B-R, Bakke J R, Ding I-K, McGehee M D and Bent S F 2011 Atomic layer deposition of CdS quantum dots for solid-state quantum dot sensitized solar cells *Adv. Energy Mater.* **1** 1169–75
[289] Brennan T P, Trejo O, Roelofs K E, Xu J, Prinz F B and Bent S F 2013 Efficiency enhancement of solid-state PbS quantum dot-sensitized solar cells with Al_2O_3 barrier layer *J. Mater. Chem.* A **1** 7566–71
[290] Dasgupta N P, Jung H J, Trejo O, McDowell M T, Hryciw A, Brongersma M, Sinclair R and Prinz F B 2011 Atomic layer deposition of lead sulfide quantum dots on nanowire surfaces *Nano Lett.* **11** 934–40
[291] Pourret A, Guyot-Sionnest P and Elam J W 2009 Atomic layer deposition of ZnO in quantum dot thin films *Adv. Mater.* **21** 232–5
[292] Wu M K, Shih Y T, Chen M J, Yang J R and Shiojiri M 2009 ZnO quantum dots embedded in a SiO_2 nanoparticle layer grown by atomic layer deposition *Phys. Status Solidi* **3** 88–90
[293] Huang S-H, Liao S-Y, Wang C-C, Kei C-C, Gan J Y and Perng T P 2016 Direct formation of anatase TiO_2 nanoparticles on carbon nanotubes by atomic layer deposition and their photocatalytic properties *Nanotechnology* **27** 405702
[294] Deng S, Verbruggen S W, He Z, Cott D J, Vereecken P M, Martens J A, Bals S, Lenaerts S and Detavernier C 2014 Atomic layer deposition-based synthesis of photoactive TiO_2 nanoparticle chains by using carbon nanotubes as sacrificial templates *RSC Adv.* **4** 11648–53
[295] Kayaci F, Ozgit-Akgun C, Biyikli N and Uyar T 2013 Surface-decorated ZnO nanoparticles and ZnO nanocoating on electrospun polymeric nanofibers by atomic layer deposition for flexible photocatalytic nanofibrous membranes *RSC Adv.* **3** 6817–20
[296] Drozd V E, Nikiforova I O, Bogevolnov V B, Yafyasov A M, Filatova E O and Papazoglou D 2009 ALD synthesis of SnSe layers and nanostructures *J. Phys. D: Appl. Phys.* **42** 125306
[297] Suresh V, Huang M S, Srinivasan M P, Guan C, Fan H J and Krishnamoorthy S 2012 Robust, high-density zinc oxide nanoarrays by nanoimprint lithography-assisted area-selective atomic layer deposition *J. Phys. Chem.* C **116** 23729–34
[298] Park J Y, Choi S-W and Kim S S 2010 A synthesis and sensing application of hollow ZnO nanofibers with uniform wall thicknesses grown using polymer templates *Nanotechnology* **21** 475601
[299] Cho S, Kim D-H, Lee B-S, Jung J, Yu W-R, Hong S-H and Lee S 2012 Ethanol sensors based on ZnO nanotubes with controllable wall thickness via atomic layer deposition, an O_2 plasma process and an annealing process *Sensors Actuators* B **162** 300–6
[300] Gong B, Peng Q, Na J S and Parsons G N 2011 Highly active photocatalytic ZnO nanocrystalline rods supported on polymer fiber mats: synthesis using atomic layer deposition and hydrothermal crystal growth *Appl. Catal.* A **407** 211–6
[301] Fang X, Li S, Wang X, Fang F, Chu X, Wei Z, Li J, Chen X and Wang F 2012 The growth and photocatalytic property of ZnO nanofibers synthesized by atom layer deposition using PVP nanofibers as templates *Appl. Surf. Sci.* **263** 14–7
[302] Kayaci F, Ozgit-akgun C, Donmez I, Biyikli N and Uyar T 2012 Polymer-inorganic core–shell nano fibers by electrospinning and atomic layer deposition: flexible nylon-ZnO core–shell nano fiber mats and their photocatalytic activity *ACS Appl. Mater. Interfaces* **4** 6185–94
[303] Pinna N, Hochepied J-F, Niederberger M and Gregg M 2009 Chemistry and physics of metal oxide nanostructures *Phys. Chem. Chem. Phys.* **11** 3607
[304] Wu M-K, Chen M-J, Tsai F-Y, Yang J-R and Shiojiri M 2010 Fabrication of ZnO nanopillars by atomic layer deposition *Mater. Trans.* **51** 253–5
[305] Elam J W, Routkevitch D, Mardilovich P P and George S M 2003 Conformal coating on ultrahigh-aspect-ratio nanopores of anodic alumina by atomic layer deposition *Chem. Mater.* **15** 3507–17
[306] Bae C, Zierold R, Moreno J M M, Kim H, Shin H, Bachmann J and Nielsch K 2012 Multisegmented nanotubes by surface-selective atomic layer deposition *J. Mater. Chem.* C **1** 621–5
[307] Subannajui K, Güder F, Danhof J, Menzel A, Yang Y, Kirste L, Wang C, Cimalla V, Schwarz U and Zacharias M 2012 An advanced fabrication method of highly ordered ZnO nanowire arrays on silicon substrates by atomic layer deposition *Nanotechnology* **23** 235607
[308] Chang Y-H, Wang S-M, Liu C-M and Chen C 2010 Fabrication and characteristics of self-aligned ZnO nanotube and nanorod arrays on Si substrates by atomic layer deposition *J. Electrochem. Soc.* **157** K236–41
[309] Sultan S M, Sun K, Clark O D, Masaud T B, Fang Q, Gunn R, Partridge J, Allen M W, Ashburn P and Chong H M H 2012 Electrical characteristics of top-down ZnO nanowire transistors using remote plasma ALD *IEEE Electron Device Lett.* **33** 203–5
[310] Norek M, Łuka G, Godlewski M, Płociński T, Michalska-Domańska M and Stępniowski W J 2013 Plasmonic enhancement of blue emission from ZnO nanorods grown on the anodic aluminum oxide (AAO) template *Appl. Phys.* A **111** 265–71
[311] Ra H W, Choi K S, Kim J H, Hahn Y B and Im Y H 2008 Fabrication of ZnO nanowires using nanoscale spacer lithography for gas sensors *Small* **4** 1105–9
[312] Lim Y T, Son J Y and Rhee J-S 2013 Vertical ZnO nanorod array as an effective hydrogen gas sensor *Ceram. Int.* **39** 887–90
[313] Altuntas S, Buyukserin F, Haider A, Altinok B, Biyikli N and Aslim B 2016 Protein-releasing conductive anodized alumina membranes for nerve-interface materials *Mater. Sci. Eng.* C **67** 590–8
[314] Ras R H A, Sahramo E, Malm J, Raula J and Karppinen M 2008 Blocking the lateral film growth at the nanoscale in area-selective atomic layer deposition *J. Am. Chem. Soc.* **130** 11252–3
[315] Malm J, Sahramo E, Karppinen M and Ras R H A 2010 Photo-controlled wettability switching by conformal coating of nanoscale topographies with ultrathin oxide films *Chem. Mater.* **22** 3349–52

[316] Korhonen J T, Hiekkataipale P, Malm J, Karppinen M, Ikkala O and Ras R H A 2011 Inorganic hollow nanotube aerogels by atomic layer deposition onto native nanocellulose templates *ACS Nano* **5** 1967–74
[317] Garifullin R, Eren H, Ulusoy T G, Okyay A K, Biyikli N and Guler M O 2016 Self-assembled peptide nanofiber templated ALD growth of TiO_2 and ZnO semiconductor nanonetworks *Phys. Status Solidi* **213** 3238–44
[318] Ceylan H, Ozgit-Akgun C, Erkal T S, Donmez I, Garifullin R, Tekinay A B, Usta H, Biyikli N and Guler M O 2013 Size-controlled conformal nanofabrication of biotemplated three-dimensional TiO_2 and ZnO nanonetworks *Sci. Rep.* **3** 2306
[319] Solis-Pomar F, Matinez E, Melendrez M F and Perez-Tijerina E 2011 Growth of vertically aligned ZnO nanorods using textured ZnO films *Nanoscale Res. Lett.* **6** 524
[320] Meléndrez M F, Hanks K, Leonard-Deepak F, Solis-Pomar F, Martinez-Guerra E, Pérez-Tijerina E and José-Yacaman M 2012 Growth of aligned ZnO nanorods on transparent electrodes by hybrid methods *J. Mater. Sci.* **47** 2025–32
[321] Solís-Pomar F, Martínez E, Meléndrez M F and Pérez-Tijerina E 2011 Growth of vertically aligned ZnO nanorods using textured ZnO films *Nanoscale Res. Lett.* **6** 524
[322] Li Q, Kumar V, Li Y, Zhang H, Marks T J and Chang R P H 2005 Fabrication of ZnO nanorods and nanotubes in aqueous solutions *Chem. Mater.* **17** 1001–6
[323] Ding J, Liu Y, Tan C and Yuan N 2012 Investigations into the impact of various substrates and ZnO ultra thin seed layers prepared by atomic layer deposition on growth of ZnO nanowire array *Nanoscale Res. Lett.* **7** 368
[324] Baek S-H, Noh B-Y, Park I-K and Kim J H 2012 Fabrication and characterization of silicon wire solar cells having ZnO nanorod antireflection coating on Al-doped ZnO seed layer *Nanoscale Res. Lett.* **7** 29
[325] Kayaci F, Vempati S, Ozgit-Akgun C, Biyikli N and Uyar T 2014 Enhanced photocatalytic activity of homoassembled ZnO nanostructures on electrospun polymeric nanofibers: a combination of atomic layer deposition and hydrothermal growth *Appl. Catal.* B **156–157** 173–83
[326] Lee J, Ju H, Kwang Lee J, Sung H S and Lee J 2010 Electrochemistry communications atomic layer deposition of TiO_2 nanotubes and its improved electrostatic capacitance *Electrochem. Commun.* **12** 210–2
[327] Meng X, Banis M N, Geng D, Li X, Zhang Y, Li R, Abou-Rachid H and Sun X 2013 Controllable atomic layer deposition of one-dimensional nanotubular TiO_2 *Appl. Surf. Sci.* **266** 132–40
[328] Liang Y-C, Wang C-C, Kei C-C, Hsueh Y-C, Cho W-H and Perng T-P 2011 Photocatalysis of Ag-loaded TiO_2 nanotube arrays formed by atomic layer deposition *J. Phys. Chem.* C **115** 9498–502
[329] Jukk K, Kongi N, Tarre A, Rosental A, Treshchalov A B, Kozlova J, Ritslaid P, Matisen L, Sammelselg V and Tammeveski K 2014 Electrochemical oxygen reduction behaviour of platinum nanoparticles supported on multi-walled carbon nanotube/titanium dioxide composites *J. Electroanal. Chem.* **735** 68–76
[330] Ng C J W, Gao H and Tan T T Y 2008 Atomic layer deposition of TiO_2 nanostructures for self-cleaning applications *Nanotechnology* **19** 445604
[331] Meng X, Zhang Y, Sun S, Li R and Sun X 2011 Three growth modes and mechanisms for highly structure-tunable SnO_2 nanotube arrays of template-directed atomic layer deposition *J. Mater. Chem.* **21** 12321–30
[332] Marichy C, Donato N, Willinger M G, Latino M, Karpinsky D, Yu S H, Neri G and Pinna N 2011 Tin dioxide sensing layer grown on tubular nanostructures by a non-aqueous atomic layer deposition process *Adv. Funct. Mater.* **21** 658–66
[333] Ozgit-Akgun C, Kayaci F, Donmez I, Uyar T and Biyikli N 2013 Template-based synthesis of aluminum nitride hollow nanofibers via plasma-enhanced atomic layer deposition *J. Am. Ceram. Soc.* **96** 916–22
[334] Farhangfar S, Yang R B, Pelletier M and Nielsch K 2009 Atomic layer deposition of ZnS nanotubes *Nanotechnology* **20** 325602
[335] Meng X, Riha S C, Libera J A, Wu Q, Wang H H, Martinson A B F and Elam J W 2015 Tunable core–shell single-walled carbon nanotube-Cu_2S networked nanocomposites as high-performance cathodes for lithium-ion batteries *J. Power Sources* **280** 621–9
[336] Meng X *et al* 2014 Gallium sulfide-single-walled carbon nanotube composites: high-performance anodes for lithium-ion batteries *Adv. Funct. Mater.* **24** 5435–42
[337] Zhang Y, Liu M, Ren W and Ye Z G 2015 Well-ordered ZnO nanotube arrays and networks grown by atomic layer deposition *Appl. Surf. Sci.* **340** 120–5
[338] Kim H W, Shim S H and Lee J W 2007 Growth of MgO thin films with subsequent fabrication of ZnO rods: structural and photoluminescence properties *Thin Solid Films* **515** 6433–7
[339] Chaaya A A, Bechelany M, Balme S and Miele P 2014 ZnO 1D nanostructures designed by combining atomic layer deposition and electrospinning for UV sensor applications *J. Mater. Chem.* A **2** 20650–8
[340] Kemell M, Härkönen E, Pore V, Ritala M and Leskela M 2009 Ta_2O_5- and TiO_2- based nanostructures made by atomic layer deposition *Nanotechnology* **21** 035301
[341] Shi J, Sun C, Starr M B and Wang X 2011 Growth of titanium dioxide nanorods in 3D-confined spaces *Nano Lett.* **11** 624–31
[342] Pallister P J, Buttera S C and Barry S T 2015 Self-seeding gallium oxide nanowire growth by pulsed chemical vapor deposition *Phys. Status Solidi* a **212** 1514–8
[343] Meng X, Zhong Y, Sun Y, Banis M N, Li R and Sun X 2011 Nitrogen-doped carbon nanotubes coated by atomic layer deposited SnO_2 with controlled morphology and phase *Carbon* **49** 1133–44
[344] Marichy C, Russo P A, Latino M, Tessonnier J P, Willinger M G, Donato N, Neri G and Pinna N 2013 Tin dioxide-carbon heterostructures applied to gas sensing: structure-dependent properties and general sensing mechanism *J. Phys. Chem.* C **117** 19729–39
[345] Cadot S *et al* 2016 A novel 2-step ALD route to ultra-thin MoS_2 films on SiO_2 through a surface organometallic intermediate *Nanoscale* **9** 538–46
[346] Jang Y, Yeo S, Lee H B R, Kim H and Kim S H 2016 Wafer-scale, conformal and direct growth of MoS_2 thin films by atomic layer deposition *Appl. Surf. Sci.* **365** 160–5
[347] Browning R, Padigi P, Solanki R, Tweet D J, Schuele P and Evans D 2015 Atomic layer deposition of MoS_2 thin films *Mater. Res. Express* **2** 035006
[348] Kim Y *et al* 2016 Self-limiting layer synthesis of transition metal dichalcogenides *Sci. Rep.* **6** 18754
[349] Scharf T W, Diercks D R, Gorman B P, Prasad S V and Dugger M T 2009 Atomic layer deposition of tungsten disulphide solid lubricant nanocomposite coatings on rolling element bearings *Tribol. Trans.* **52** 284–92
[350] Scharf T W, Prasad S V, Dugger M T, Kotula P G, Goeke R S and Grubbs R K 2006 Growth, structure, and tribological behavior of atomic layer-deposited tungsten disulphide solid lubricant coatings with applications to MEMS *Acta Mater.* **54** 4731–43
[351] Song J *et al* 2013 Layer-controlled wafer-scale and conformal synthesis of tungsten disulfide nanosheets using atomic layer deposition *ACS Nano* **7** 11333–40

[352] Ko K Y *et al* 2016 Improvement of gas-sensing performance of large-area tungsten disulfide nanosheets by surface functionalization *ACS Nano* **10** 9287–96

[353] Zhang Y, Ren W, Jiang Z, Yang S, Jing W, Shi P, Wu X and Ye Z G 2014 Low-temperature remote plasma-enhanced atomic layer deposition of graphene and characterization of its atomic-level structure *J. Mater. Chem.* C **2** 7570–4

[354] Nandi D K, Sen U K, Choudhury D, Mitra S and Sarkar S K 2014 Atomic layer deposited MoS_2 as a carbon and binder free anode in Li-ion battery *Electrochim. Acta* **146** 706–13

[355] Valdivia A, Tweet D J and Conley J F Jr 2016 Atomic layer deposition of two dimensional MoS_2 on 150 mm substrates *J. Vac. Sci. Technol.* A **34** 021515

[356] Kwon D H, Jin Z, Shin S, Lee W-S and Min Y-S 2016 Comprehensive study on atomic layer deposition of molybdenum sulfide for electrochemical hydrogen evolution *Nanoscale* **8** 7180–8

[357] Li N, Feng L, Su J, Zeng W and Liu Z 2016 Optical and electrical properties of Al:WS2 films prepared by atomic layer deposition and vulcanization *RSC Adv.* **6** 64879–84

[358] Chang Y-M, Kao P-H, Liu M-C, Lin C-M, Lee H-Y and Juang J-Y 2012 Fabrication and optoelectronic properties of core–shell biomimetic ZnO/Si nanoball arrays *RSC Adv.* **2** 11089–94

[359] King D M, Li J, Liang X, Johnson S I, Channel M M and Weimer A W 2009 Crystal phase evolution in quantum confined ZnO domains on particles via atomic layer deposition *Cryst. Growth Des.* **9** 2828–34

[360] King D M, Johnson S I, Li J, Du X, Liang X and Weimer A W 2009 Atomic layer deposition of quantum-confined ZnO nanostructures *Nanotechnology* **20** 195401

[361] Libera J A, Elam J W and Pellin M J 2008 Conformal ZnO coatings on high surface area silica gel using atomic layer deposition *Thin Solid Films* **516** 6158–66

[362] King D M, Liang X, Carney C S, Hakim L F, Li P and Weimer A W 2008 Atomic layer deposition of UV-absorbing ZnO films on SiO_2 and TiO_2 nanoparticles using a fluidized bed reactor *Adv. Funct. Mater.* **18** 607–15

[363] King D M, Liang X, Li P and Weimer A W 2008 Low-temperature atomic layer deposition of ZnO films on particles in a fluidized bed reactor *Thin Solid Films* **516** 8517–23

[364] Rauwel E, Galeckas A, Rauwel P, Nilsen O, Walmsley J C, Rytter E and Fjellwag H ALD applied to conformal coating of nanoporous γ-alumina: spinel formation and luminescence induced by europium doping *J. Electrochem. Soc.* **159** P45–9

[365] Kim H W, Shim S H and Lee J W 2008 Variation of ZnO shell thickness and its effects on the characteristics of coaxial nanowires *Nanotechnology* **19** 145601

[366] Dobrokhotov V *et al* 2012 ZnO coated nanospring-based chemiresistors *J. Appl. Phys.* **111** 044311

[367] Chang Y-M, Jian S-R, Lee H-Y, Lin C-M and Juang J-Y 2010 Enhanced visible photoluminescence from ultrathin ZnO films grown on Si-nanowires by atomic layer deposition *Nanotechnology* **21** 385705

[368] Dobrokhotov V *et al* 2012 Toward the nanospring-based artificial olfactory system for trace-detection of flammable and explosive vapors *Sensors Actuators* B **168** 138–48

[369] Li H H, Yang C E, Kei C C, Su C Y, Dai W S, Tseng J K, Yang P Y, Chou J C and Cheng H C 2013 Coaxial-structured ZnO/silicon nanowires extended-gate field-effect transistor as pH sensor *Thin Solid Films* **529** 173–6

[370] Chang Y M, Shieh J, Chu P Y, Lee H Y, Lin C M and Juang J Y 2011 Enhanced free exciton and direct band-edge emissions at room temperature in ultrathin ZnO films grown on Si nanopillars by atomic layer deposition *ACS Appl. Mater. Interfaces* **3** 4415–9

[371] Chang Y M, Liu M C, Kao P H, Lin C M, Lee H Y and Juang J Y 2012 Field emission in vertically aligned ZnO/Si-nanopillars with ultra low turn-on field *ACS Appl. Mater. Interfaces* **4** 1411–6

[372] Han H C *et al* 2013 High K nanophase zinc oxide on biomimetic silicon nanotip array as supercapacitors *Nano Lett.* **13** 1422–8

[373] Choi S-W, Park J Y and Kim S S 2009 Synthesis of SnO_2–ZnO core–shell nanofibers via a novel two-step process and their gas sensing properties *Nanotechnology* **20** 465603

[374] Park S, An S, Ko H, Jin C and Lee C 2013 Enhanced NO_2 sensing properties of Zn_2SnO_4-core/ZnO-shell nanorod sensors *Ceram. Int.* **39** 3539–45

[375] Kim H, Jin C, Park S and Lee C 2012 Enhanced H_2S gas sensing properties of multiple-networked Pd-doped SnO_2-core/ZnO-shell nanorod sensors *Mater. Res. Bull.* **47** 2708–12

[376] Jin C, Kim H, Ryu H Y, Kim H W and Lee C 2011 Subwavelength optical resonant cavity-induced enhancement of the near-band-edge emission from ZnO-core/SnO_2-shell nanorods *J. Phys. Chem.* C **115** 8513–8

[377] Kayaci F, Vempati S, Ozgit-Akgun C, Donmez I, Biyikli N and Uyar T 2014 Selective isolation of the electron or hole in photocatalysis: ZnO–TiO_2 and TiO_2–ZnO core–shell structured heterojunction nanofibers via electrospinning and atomic layer deposition *Nanoscale* **6** 5735–45

[378] Wang H-B, Ma F, Li Q-Q, Dong C-Z, Ma D-Y, Wang H-T and Xu K-W 2013 Synthesis and stress relaxation of ZnO/Al-doped ZnO core–shell nanowires *Nanoscale* **5** 2857–63

[379] Peng Q, Sun X Y, Spagnola J C, Saquing C, Khan S A, Spontak R J and Parsons G N 2009 Bi-directional kirkendall effect in coaxial microtube nanolaminate assemblies fabricated by atomic layer deposition *ACS Nano* **3** 546–54

[380] Alessandri I, Zucca M, Ferroni M, Bontempi E and Depero L E 2009 Growing ZnO nanocrystals on polystyrene nanospheres by extra-low-temperature atomic layer deposition *Cryst. Growth Des.* **9** 1258–9

[381] Park J Y, Choi S W, Lee J W, Lee C and Kim S S 2009 Synthesis and gas sensing properties of TiO_2–ZnO core–shell nanofibers *J. Am. Ceram. Soc.* **92** 2551–4

[382] Janik E, Wachnicka A, Guziewicz E, Godlewski M, Kret S, Zaleszczyk W, Dynowska E, Presz A, Karczewski G and Wojtowicz T 2010 ZnTe–ZnO core–shell radial heterostructures grown by the combination of molecular beam epitaxy and atomic layer deposition *Nanotechnology* **21** 015302

[383] Park S, Jun J, Kim H W and Lee C 2009 Preparation of one dimensional Bi_2O_3-core/ZnO-shell structures by thermal evaporation and atomic layer deposition *Solid State Commun.* **149** 315–8

[384] Clavel G, Marichy C, Willinger M G, Ravaine S, Zitoun D and Pinna N 2010 $CoFe_2O_4$–TiO_2 and $CoFe_2O_4$–ZnO thin film nanostructures elaborated from colloidal chemistry and atomic layer deposition *Langmuir* **26** 18400–7

[385] Sun W-C, Yeh Y-C, Ko C-T, He J-H and Chen M-J 2011 Improved characteristics of near-band-edge and deep-level emissions from ZnO nanorod arrays by atomic-layer-deposited Al_2O_3 and ZnO shell layers *Nanoscale Res. Lett.* **6** 556

[386] Pan K-Y, Lin Y-H, Lee P-S, Wu J-M and Shih H C 2012 Synthesis of SnO_2–ZnO core–shell nanowires and their optoelectronic properties *J. Nanomater.* **2012** 279245

[387] Solanki R, Huo J, Freeouf J L and Miner B 2002 Atomic layer deposition of ZnSe/CdSe superlattice nanowires *Appl. Phys. Lett.* **81** 3864–6

[388] Ferguson J D, Weimer A W and George S M 2005 Surface chemistry and infrared absorbance changes during ZnO atomic layer deposition on ZrO_2 and $BaTiO_3$ particles *J. Vac. Sci. Technol.* A **23** 118–25

[389] Gas K *et al* 2011 Selected optical properties of core/shell ZnMnTe/ZnO nanowire structures *Phys. Status Solidi Basic Res.* **248** 1592–5

[390] Karlsson M, Jogi I, Eriksson S K, Rensmo H, Boman M, Boschloo G and Hagfeldt A 2013 Dye-sensitized solar cells employing a SnO_2–TiO_2 core–shell structure made by atomic layer deposition *Chimia* **67** 142–8

[391] Zhang Z, Patterson M, Ren M, Wang Y, Flake J C, Sprunger P T and Kurtz R L 2013 Atomic layer deposition of ZnO on Cu-nanoclusters for methanol synthesis *J. Vac. Sci. Technol.* A **31** 01A144

[392] Kim M, Lee J, Lee S, Seo S, Bae C and Shin H 2015 Nanotubular heterostructure of tin dioxide/titanium dioxide as a binder-free anode in lithium-ion batteries *ChemSusChem* **8** 2363–71

[393] Zhang Y, Lu H-L, Wang T, Ren Q-H, Gu Y-Z, Li D-H and Zhang D W 2015 Facile synthesis and enhanced luminescent properties of ZnO/HfO_2 core–shell nanowires *Nanoscale* **7** 15462–8

[394] Lung C M, Wang W C, Chen C H, Chen L Y and Chen M J 2016 ZnO/Al_2O_3 core/shell nanorods array as excellent anti-reflection layers on silicon solar cells *Mater. Chem. Phys.* **180** 195–202

[395] Mirzaei A, Park S, Kheel H, Sun G J, Lee S and Lee C 2016 ZnO-capped nanorod gas sensors *Ceram. Int.* **42** 6187–97

[396] Torrisi G, Di Mauro A, Scuderi M, Nicotra G and Impellizzeri G 2016 Atomic layer deposition of ZnO/TiO_2 multilayers: towards the understanding of Ti-doping in ZnO thin films *RSC Adv.* **6** 88886–95

[397] Bolat S, Tekcan B, Ozgit-Akgun C, Biyikli N and Okyay A K 2015 Electronic and optical device applications of hollow cathode plasma assisted atomic layer deposition based GaN thin films *J. Vac. Sci. Technol.* A **33** 01A143

[398] Bolat S, Ozgit-Akgun C, Tekcan B, Biyikli N and Okyay A K 2014 Low temperature thin film transistors with hollow cathode plasma-assisted atomic layer deposition based GaN channels *Appl. Phys. Lett.* **104** 243505

[399] Lin Y Y, Hsu C C, Tseng M H, Shyue J J and Tsai F Y 2015 Stable and high-performance flexible ZnO thin-film transistors by atomic layer deposition *ACS Appl. Mater. Interfaces* **7** 22610–7

[400] Yang J, Park J K, Kim S, Choi W, Lee S and Kim H 2012 Atomic-layer-deposited ZnO thin-film transistors with various gate dielectrics *Phys. Status Solidi Appl. Mater. Sci.* **209** 2087–90

[401] Bolat S, Sisman Z and Okyay A K 2016 Demonstration of flexible thin film transistors with GaN channels *Appl. Phys. Lett.* **109** 233504

[402] Snyder M Q, Trebukhova S A, Ravdel B, Wheeler M C, DiCarlo J, Tripp C P and DeSisto W J 2007 Synthesis and characterization of atomic layer deposited titanium nitride thin films on lithium titanate spinel powder as a lithium-ion battery anode *J. Power Sources* **165** 379–85

[403] Meng X, Geng D, Liu J, Banis M N, Zhang Y, Li R and Sun X 2010 Non-aqueous approach to synthesize amorphous/crystalline metal oxide-graphene nanosheet hybrid composites *J. Phys. Chem.* C **114** 18330–7

[404] Cheah S K *et al* 2009 Self-supported three-dimensional nanoelectrodes for microbattery applications *Nano Lett.* **9** 3230–3

[405] Kim S W, Han T H, Kim J, Gwon H, Moon H S, Kang S W, Kim S O and Kang K 2009 Fabrication and electrochemical characterization of TiO_2 three-dimensional nanonetwork based on peptide assembly *ACS Nano* **3** 1085–90

[406] Li M, Li X, Li W, Meng X, Yu Y and Sun X 2015 Atomic layer deposition derived amorphous TiO_2 thin film decorating graphene nanosheets with superior rate capability *Electrochem. Commun.* **57** 43–7

[407] Wang X, Fan L, Gong D, Zhu J, Zhang Q and Lu B 2016 Core–shell Ge@Graphene@TiO_2 nanofibers as a high-capacity and cycle-stable anode for lithium and sodium ion battery *Adv. Funct. Mater.* **26** 1104–11

[408] Tian M, Wang W, Liu Y, Jungjohann K L, Thomas Harris C, Lee Y C and Yang R 2015 A three-dimensional carbon nano-network for high performance lithium ion batteries *Nano Energy* **11** 500–9

[409] Bai Y *et al* 2016 Core–shell Si@TiO_2 nanosphere anode by atomic layer deposition for Li-ion batteries *J. Power Sources* **308** 75–82

[410] Wang X H, Guan C, Sun L M, Susantyoko R A, Fan H J and Zhang Q 2015 Highly stable and flexible Li-ion battery anodes based on TiO_2 coated 3D carbon nanostructures *J. Mater. Chem.* A **3** 15394–8

[411] Charlton M R, Dylla A G and Stevenson K J 2015 Direct evidence of a chemical conversion mechanism of atomic layer deposited TiO_2 anodes during lithiation using $LiPF_6$ salt *J. Phys. Chem.* C **119** 28285–91

[412] Hong K J and Kim S O 2016 Atomic layer deposition assisted sacrificial template synthesis of mesoporous TiO_2 electrode for high performance lithium ion battery anodes *Energy Storage Mater.* **2** 27–34

[413] Ye J, Baumgaertel A C, Wang Y M, Biener J and Biener M M 2015 Structural optimization of 3D porous electrodes for high-rate performance lithium ion batteries *Nano Lett.* **9** 2194–202

[414] Xie M, Sun X, Zhou C, Cavanagh A S, Sun H, Hu T, Wang G, Lian J and George S M 2015 Amorphous ultrathin TiO_2 atomic layer deposition films on carbon nanotubes as anodes for lithium ion batteries *J. Electrochem. Soc.* **162** A974–81

[415] Liang Z, Zheng G, Li W, Seh Z W, Yao H, Yan K, Kong D and Cui Y 2014 Sulfur cathodes with hydrogen reduced titanium dioxide inverse opal structure *ACS Nano* **8** 5249–56

[416] Knoops H C M, Baggetto L, Langereis E, van de Sanden M C M, Klootwijk J H, Roozeboom F, Niessen R A H, Notten P H L and Kessels W M M 2007 Deposition of TiN and TaN by remote plasma ALD for Cu and Li diffusion barrier applications *ECS Trans.* **155** G287–94

[417] Baggetto L, Oudenhoven J F M, van Dongen T, Klootwijk J H, Mulder M, Niessen R A H, de Croon M H J M and Notten P H L 2009 On the electrochemistry of an anode stack for all-solid-state 3D-integrated batteries *J. Power Sources* **189** 402–10

[418] Baggetto L, Knoops H C M, Niessen R A H, Kessels W M M and Notten P H L 2010 3D negative electrode stacks for integrated all-solid-state lithium-ion microbatteries *J. Mater. Chem.* **20** 3703–8

[419] Badot J C, Ribes S, Yousfi E B, Viver V, Pereira-Ramos J P, Baffier N and Lincot D 2000 Atomic layer epitaxy of vanadium oxide thin films and electrochemical behavior in presence of lithium ions *Electrochem. Solid State Lett.* **3** 485–8

[420] Donders M E, Knoops H C M, Kessels W M M and Notten P H L 2012 Co_3O_4 as anode material for thin film micro-batteries prepared by remote plasma atomic layer deposition *J. Power Sources* **203** 72–7

[421] Zhang P, Tachikawa T, Fujitsuka M and Majima T 2016 Atomic layer deposition-confined nonstoichiometric TiO_2 nanocrystals with tunneling effects for solar driven hydrogen evolution *J. Phys. Chem. Lett.* **7** 1173–9

[422] Kim M W *et al* 2017 Nanotextured cupric oxide nanofibers coated with atomic layer deposited ZnO–TiO_2 as highly efficient photocathodes *Appl. Catal.* B **201** 479–85

[423] Levchuk I, Guillard C, Dappozze F, Parola S, Leonard D and Sillanpää M 2016 Photocatalytic activity of TiO_2 films immobilized on aluminum foam by atomic layer deposition technique *J. Photochem. Photobiol.* A **328** 16–23

[424] Edy R, Zhao Y, Huang G S, Shi J J, Zhang J, Solovev A A and Mei Y 2016 TiO_2 nanosheets synthesized by atomic layer deposition for photocatalysis *Prog. Nat. Sci. Mater. Int.* **26** 493–7

[425] Di Mauro A, Cantarella M, Nicotra G, Privitera V and Impellizzeri G 2016 Low temperature atomic layer deposition of ZnO: applications in photocatalysis *Appl. Catal.* B **196** 68–76

[426] Nagy D, Firkala T, Drotár E, Szegedi Á, László K and Szilágyi I M 2016 Photocatalytic WO_3/TiO_2 nanowires: WO_3 polymorphs influencing the atomic layer deposition of TiO_2 *RSC Adv.* **6** 95369–77

[427] Singh R, Bapat R, Qin L, Feng H and Polshettiwar V 2016 Atomic layer deposited (ALD) TiO_2 on fibrous nano-silica (KCC-1) for photocatalysis: nanoparticle formation and size quantization effect *ACS Catal.* **6** 2770–84

[428] Hendricks O L, Scheuermann A G, Schmidt M, Hurley P K, McIntyre P C and Chidsey C E D 2016 Isolating the photovoltaic junction: atomic layer deposited TiO_2–RuO_2 alloy Schottky contacts for silicon photoanodes *ACS Appl. Mater. Interfaces* **8** 23763–73

[429] Pan S, Zhao Y, Huang G, Wang J, Baunack S, Gemming T, Li M, Zheng L, Schmidt O G and Mei Y 2015 Highly photocatalytic TiO_2 interconnected porous powder fabricated by sponge-templated atomic layer deposition *Nanotechnology* **26** 364001

[430] Zhang Y, Creatore M, Ma Q, El A, Gao L, Verheijen M A, Verhoeven M W G M T and Hensen E J M 2015 Nitrogen-doping of bulk and nanotubular TiO_2 photocatalysts by plasma-assisted atomic layer deposition *Appl. Surf. Sci.* **330** 476–86

[431] Lin Y, Zhou S, Liu X, Sheehan S and Wang D 2009 TiO_2/$TiSi_2$ heterostructures for high-efficiency photoelectrochemical H_2O splitting *J. Am. Chem. Soc.* **131** 2772–3

[432] Zhu W, Liu X, Liu H, Tong D, Yang J and Peng J 2010 Coaxial heterogeneous structure of TiO_2 nanotube arrays with CdS as a superthin coating synthesized via modified electrochemical atomic layer deposition *J. Am. Chem. Soc.* **132** 12619–26

[433] Lin Y, Zhou S, Sheehan W and Wang D 2011 Nanonet-based hematite heteronanostructures for efficient solar water splitting *J. Am. Chem. Soc.* **133** 2398–401

[434] Paracchino A, Laporte V, Sivula K, Grätzel M and Thimsen E 2011 Highly active oxide photocathode for photoelectrochemical water reduction *Nat. Mater.* **10** 456–61

[435] Hoex B, Heil S B S, Langereis E, Van De Banden M C M and Kessels W M M 2006 Ultralow surface recombination of c-Si substrates passivated by plasma-assisted atomic layer deposited Al_2O_3 *Appl. Phys. Lett.* **89** 042112

[436] Martinson A B F, Elam J W, Hupp J T and Pellin M J 2007 ZnO nanotube based dye-sensitized solar cells *Nano Lett.* **7** 2183–7

[437] Martinson A B F, Elam J W, Liu J, Pellin M J, Marks T J and Hupp J T 2008 Radial electron collection in dye-sensitized solar cells *Nano Lett.* **8** 2862–6

[438] Hamann T W, Martinson A B F, Elam J W, Pellin M J and Hupp J T 2008 Aerogel templated ZnO dye-sensitized solar cells *Adv. Mater.* **20** 1560–4

[439] Foong T R B, Shen Y, Hu X and Sellinger A 2010 Template-directed liquid ALD growth of TiO_2 nanotube arrays: properties and potential in photovoltaic devices *Adv. Funct. Mater.* **20** 1390–6

[440] Chandiran A K, Yella A, Mayer M T and Gao P 2014 Sub-nanometer conformal TiO_2 blocking layer for high efficiency solid-state perovskite absorber solar cells *Adv. Mater.* **26** 4309–12

[441] Mali S S, Shim C S, Park H K, Heo J, Patil P S and Hong C K 2015 Ultrathin atomic layer deposited TiO_2 for surface passivation of hydrothermally grown 1D TiO_2 nanorod arrays for efficient solid-state perovskite solar cells *Chem. Mater.* **27** 1541–51

[442] Haider A, Cansizoglu H, Cansizoglu M F, Karabacak T, Okyay A K and Biyikli N 2015 Enhanced photoresponse of conformal TiO_2/Ag nanorod array-based Schottky photodiodes fabricated via successive glancing angle and atomic layer deposition *J. Vac. Sci. Technol.* A **33** 01A110

[443] Cao Y, Deng S, Hu Q, Zhong Q, Luo Q-P, Yuan L and Zhou J 2015 Three-dimensional ZnO porous films for self-cleaning ultraviolet photodetectors *RSC Adv.* **5** 85969–73

[444] Liang Y-C and Liao W-K 2014 Annealing induced solid-state structure dependent performance of ultraviolet photodetectors made from binary oxide-based nanocomposites *RSC Adv.* **4** 19482–7

[445] Shao D, Sun H, Xin G, Lian J and Sawyer S 2014 High quality ZnO–TiO_2 core–shell nanowires for efficient ultraviolet sensing *Appl. Surf. Sci.* **314** 872–6

[446] Bang S, Lee S, Ko Y, Park J, Shin S, Seo H and Jeon H 2012 Photocurrent detection of chemically tuned hierarchical ZnO nanostructures grown on seed layers formed by atomic layer deposition *Nanoscale Res. Lett.* **7** 290

[447] Katoch A, Kim J-H and Kim S S 2014 TiO_2/ZnO inner/outer double-layer hollow fibers for improved detection of reducing gases *ACS Appl. Mater. interfaces* **6** 21494–9

[448] Zhao X, Shi W, Mu H, Xie H and Liu F 2016 Templated bicontinuous Tin oxide thin film fabrication and the NO_2 gas sensing *J. Alloys Compd.* **659** 60–5

[449] Park S, Ko H, Lee S, Kim H and Lee C 2014 Light-activated gas sensing of Bi_2O_3-core/ZnO-shell nanobelt gas sensors *Thin Solid Films* **570** 298–302

[450] Park S, Ko H, Kim S and Lee C 2014 Role of the interfaces in multiple networked one-dimensional core–shell nanostructured gas sensors *ACS Appl. Mater. Interfaces* **6** 9595–600

[451] Park S, Kim S, Ko H and Lee C 2014 Light-enhanced gas sensing of ZnS-core/ZnO-shell nanowires at room temperature *J. Electroceramics* **33** 75–81

[452] Marichy C, Donato N, Latino M, Georg Willinger M, Tessonnier J-P, Neri G and Pinna N 2015 Gas sensing properties and p-type response of ALD TiO_2 coated carbon nanotubes *Nanotechnology* **26** 024004

[453] Kim J H and Kim S S 2015 Realization of ppb-scale toluene-sensing abilities with Pt-functionalized SnO_2–ZnO core–shell nanowires *ACS Appl. Mater. Interfaces* **7** 17199–208

[454] Clavijo W P, Atkinson G M, Castano C E and Pestov D 2016 Novel low-temperature fabrication process for integrated high-aspect ratio zinc oxide nanowire sensors *J. Vac. Sci. Technol.* B **34** 022203

[455] Ansari L, Fagas G, Colinge J P and Greer J C 2012 A proposed confinement modulated gap nanowire transistor based on a metal (Tin) *Nano Lett.* **12** 2222–7